SINGLE PION PRODUCTION IN INTERMEDIATE ENERGY RANGE K^+P REACTIONS

by

Graham Thompson

A thesis submitted for the degree of
Doctor of Philosophy of the University of London

Department of Physics
Imperial College
London S.W.7.

December 1970

CONTENTS

A B S T R A C T

An experiment in the British National Hydrogen Bubble Chamber (1.5 m) with positive incident K mesons at momenta 2.11, 2.31, 2.53 and 2.72 GeV/c is described, together with techniques of film analysis involving an automatic measuring machine (H.P.D.). Methods of selecting three body final states, resolving ambiguities and calculating contamination yield partial cross-sections for the channels involving single pion production.

A maximum likelihood program for fitting effective masses on the Dalitz plot is discussed, the resulting resonance parameters giving quasi two body cross-sections.

Using two different computational methods, the production angular distributions of the $\Delta(1236)$ and $K^*(892)$ are expanded into Legendre polynomial series, whose coefficients are combined with other published data in the 1 to 3 GeV/c range in a search for possible effects of an exotic resonance as suggested by total K^+P cross-section counter experiments.

The peripheral part of the resonance production is studied in the context of the one meson exchange model. Differential cross-sections are presented with computed slopes and intercepts, and the variations of density matrix elements are compared to the Stodolsky-Sakurai ρ exchange model for Δ production and the Dass and Frogatt Regge pole model for K^* production.

LIST OF TABLES

LIST OF DIAGRAMS

LIST OF DIAGRAMS CONTINUED

It is well known that when you do anything, unless you understand its actual circumstances, its nature and its relations to other things, you will not know the laws governing it, or know how to do it, or be able to do it well.

"Problems in China's Revolutionary War" (1936)
from "Quotations from Chairman Mao Tse-Tung" P.210.

CHAPTER 1

INTRODUCTION

In the early summer of 1967, an experiment was proposed[1] for a million picture bubble chamber survey of the K^+ - nucleon system in the momentum range 2 to 2.5 GeV/c. Previous studies had already been made in the T=1 K^+P system at single energies around the proposed range[2,3,4,5] and at higher energies results were just being published from the CERN-Brussels collaboration.[6] For the most part these were with quite low statistics, and in the mixed T=0 T=1 K^+N system there was very little work.[7,8] Accordingly, the proposed experiment was planned to be carried out principally in deuterium but with a series of "control" exposures made in hydrogen at broadly similar energies.

Originally, the experiment was proposed jointly by Imperial College and Westfield College of London, who already had close ties on other work. About the same time a similar proposal for a slightly lower energy was entered by the French group C.E.N. (Saclay). A three-way collaboration was thus constructed, and eventually the film was divided equally between the participants. At a later stage Collège de France joined the other groups, and helped measure the French film.

Interest had recently been focussed on the K^+N systems because of the observations of Cool et al[9] and Abrams et al[10] of a peak at $E^* = 1.9$ GeV and bumps, at 2.2 GeV and 2.5 GeV, in the total cross-sections of K^+P reactions, and similar, but more pronounced, behaviour of $\sigma_{tot}(K^+N)$. Much

more violent structure in the K^- - nucleon total cross-sections had long since been confirmed as s-channel resonances (the Y_1^*'s and Y_0^*'s). In the K^+ system the bumps were very much smaller being 1 mb for the peak and ~ 0.2 mb above background for the two bumps, as opposed to the K^- peaks of almost 20 mb, but if they could be given the same interpretation it meant that positive strangeness (S=1) baryonic (B=1) resonances, the Z^*, were being formed.[11]

Although there is no known selection rules which forbid the formation of such particles, they would be members of SU(3) $[27]$ multiplets (for the Z_1^*) or $[\overline{10}]$ multiplet (for the Z_0^*), whereas it would appear that every other particle discovered so far is a member of the singlet, octet or decuplet $[\underline{10}]$. Such structures would have to be composed of four quarks and an anti-quark (e.g. $pnnn\bar{\lambda}$) and would be fatal to the simple quark model which sees all particles being built up from three quark (baryon) or two quark (meson) states with increasing relative angular momentum rather than the composite quark model which sees all quarks in a relative S-state, the total spin of the particle being built up from the spin $\frac{1}{2}$ of the quarks.

From the unitarity limit for a partial wave given by $\sigma^{\text{res.}}_{\text{tot.}} = 4\pi.\lambda\!\!\!^{-2} . (J+\frac{1}{2})x$ it is clear that even taking the spin of such resonances as $J=\frac{1}{2}$ they are highly inelastic. In the case of the bump near 2.5 GeV/c $(J+\frac{1}{2})x = 0.04$ giving elasticity $x<0.08$.

For this reason it is clear that searches for such states are best carried out using production experiments rather than formation experiments. Half of the total inelastic

cross-section at the energies used lies in the three body final state and the majority of this thesis will be concerned with these channels.

Early on in the search for exotic resonances the work at UCRL, Berkeley[12] confirmed that the first peak in the T=1 cross-section could be explained by the violent, but non-resonant, onset of $K\Delta$ production after its threshold at 1050 MeV/c, and its subsequent fall-off coupled with the regular fall in the elastic cross-section.

At the present state of understanding of K^+P interactions, there are three major fields of interest. In the low momentum region, up to 2 GeV/c, there is a small enough number of contributing partial waves to make phase shift analysis a powerful technique. Lea, Martin and Oades[13] presented evidence for resonant-like behaviour in the $P\frac{1}{2}$ wave at about the position of the second bump but later polarisation work by Andersson[14] favoured a non-resonant solution. However, more recent work at Argonne[15] now suggests a solution involving the $P\frac{3}{2}$ wave in resonance.

In the higher momentum region, above 3 GeV/c, the Regge pole mechanism has given a comprehensive representation of the phenomena, both in the elastic[16] and inelastic channels.[17]

This leaves an intermediate momentum region where the experiments now discussed were performed and where there must be a merging of the two previous approaches at some level, bearing in mind the requirements of duality. This means that the standard methods of analysis in these areas may be of limited applicability. Despite this, chapter 5 contains a

Legendre polynomial analysis of the $K\Delta$ and K^*N states and there has been some attempt at identifying effects on certain polynomials as caused by certain partial wave amplitudes. On the other hand in chapters 6 and 7, slopes for partial differential cross-sections are computed and there are comparisons to a one meson exchange model and a Regge pole model. It is to be hoped that fully dual models like the Veneziano will soon complement our knowledge of this area of K^+P scattering.

In the thesis which follows, chapter 2 concerns the data processing, chapter 3 the selection of three body events and later chapters their analysis. The author was concerned with the experiment from its proposal, but much of the work described in the next two chapters was not entirely his. All the analysis from chapter 4 onwards was, however, his direct responsibility.

CHAPTER 2

EXPERIMENTAL SYSTEM

2.1 Beam and Bubble Chamber

The K9 beam at the Rutherford High Energy Laboratory, on which the experiment was run, was designed to be a general purpose beam line capable of delivering up to 5×10^{11}, 8 GeV/c protons, $\sim 10^2$ 2 to 3 GeV/c positive kaons and $\sim 10^3$ 1 to 5 GeV/c pions when on full beam. In practice, with the two extracted beams X1 and X2 sharing the spill, and X1, the beam which feeds K9 only working at a maximum efficiency of 25-30%, it was extremely difficult getting an optimum twenty kaons per pulse. The author assisted in the first tuning of this beam for general purposes in the late summer of 1967.

The layout of the beam components may be seen from Fig. (1). X1 delivered the extracted beam on to a 1.5 x 2.0 x 10 cm. copper target at the head of K9. M104 selected the required angle of beam but in this case was switched off as 0^o emergence was being used. The collimators CH1 and CV1 served to define the acceptance of the beam line in the horizontal and vertical planes respectively. The first stage of the beam consisted in the bending pair M106 and M204 alternated with the quadropole triplet Q112, Q116, Q110 to produce a momentum dispersed image at CH2. The width of the jaws of this collimator thus defined the momentum bite and in this case, in order to get sufficient flux, was set to 1% $\Delta p/p$.

Just before this first horizontal focus there was

K 9 BEAM

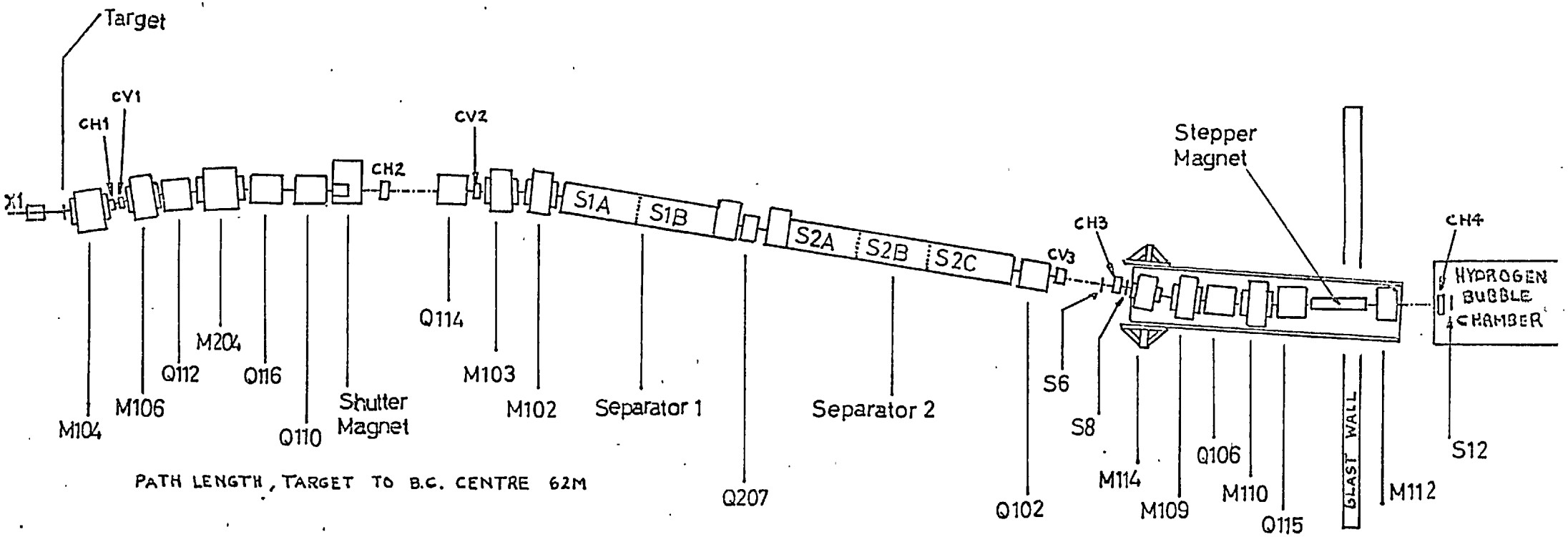

PATH LENGTH, TARGET TO B.C. CENTRE 62M

Main Components:
- 8 Quadrupoles (Q)
- 9 Bending Magnets (M)
- 5 Separator Tanks
- 6 Collimators (C)

a shutter magnet capable of deflecting the beam after a required number of particles had passed through the scintillator, S12, in front of the bubble chamber. Coupled with a further trigger which suppressed the flash when less than a given number of particles had passed through S12, this meant that despite large variations in the efficiency of the beam line and the effect of Poisson statistics a roughly constant number of ten to twelve kaons were obtained on each frame.

The second stage of the beam was essentially momentum recombination in the horizontal plane via the bending magnets M103 and M102 coupled with two stages of electrostatic mass separation in the vertical plane. As can be seen from the diagram there are in all five separator tanks totalling a distance of 17 m. Of all the components of the beam line these separators were the most sensitive and provided the biggest limitation on conditions. Operating on a sharp peak of maintainable high tension voltage vs. nitrogen pressure they were often prone to sparking, ruining a number of frames before the magnet and H.T. power could be re-established. Also difficulty with "conditioning" meant that frequently the separators were not working at full field (500 kv. over a 10 cm. gap) and hence separation curves were very sensitive to slight voltage variation.

In Fig. (2) examples of the actual experimental separation curves are given at the two extremes of the operating momenta; 2.1 GeV/c, where flux was a problem, and 2.7 GeV/c, where separation was difficult. These show numbers of counts recorded on the final scintillator, S12, normalised

Fig. 2 SEPARATION CURVES

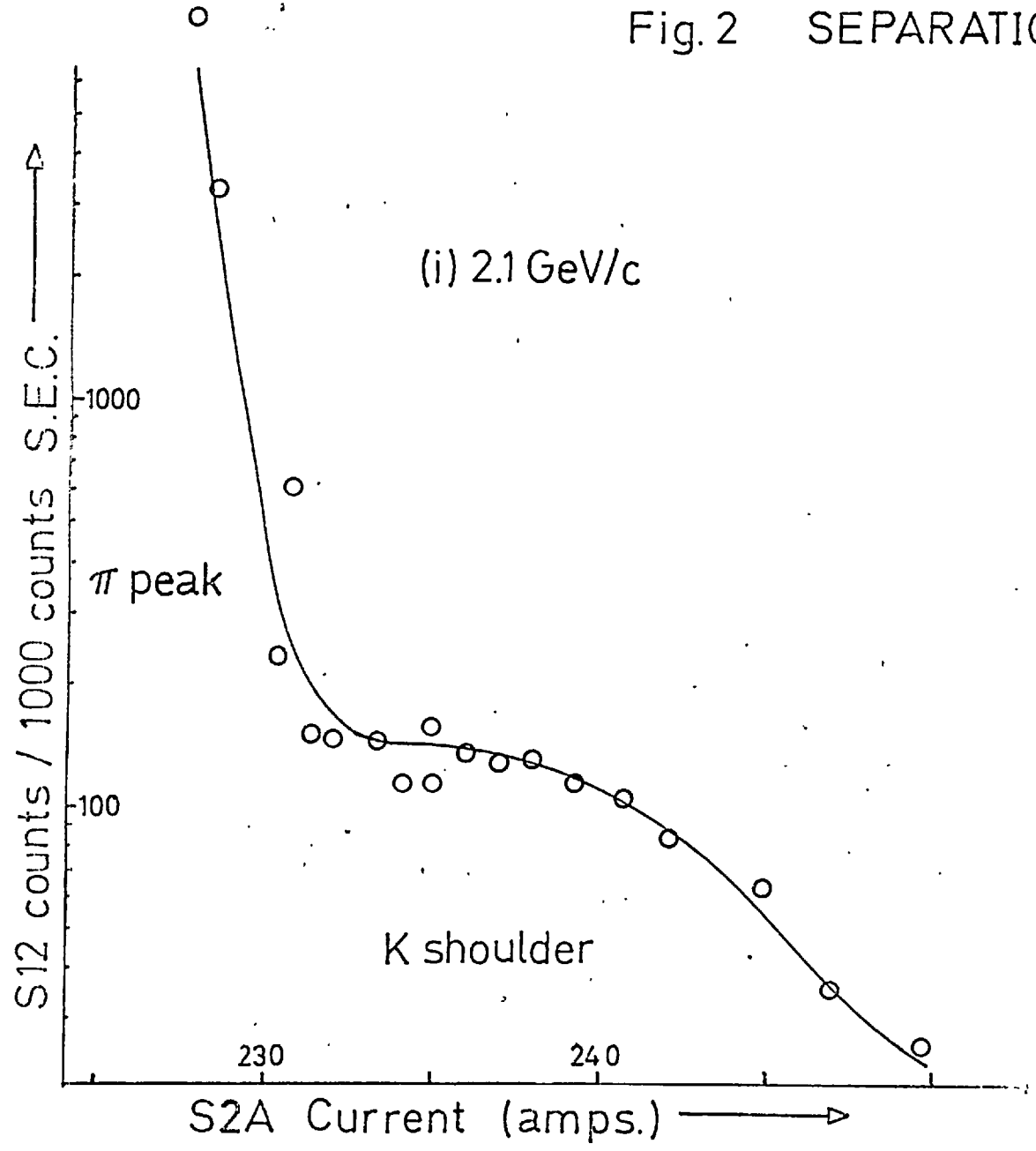

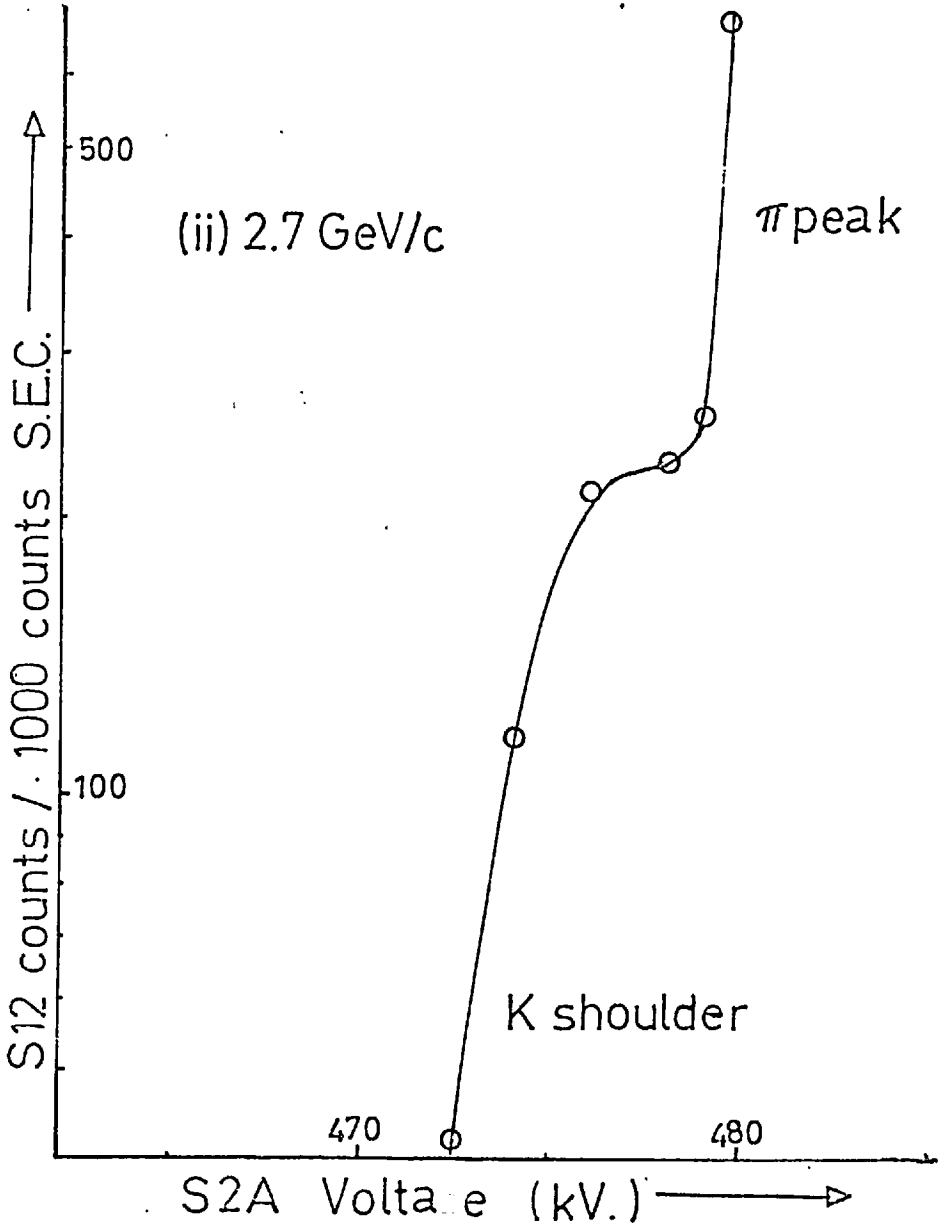

against 1000 counts at the secondary emission chamber, placed near the target of K9, whilst varying respectively current and voltage on the second separator, the two techniques available. Some exposures were attempted at 2.9 GeV/c but this film was so badly pion contaminated that it was discarded.

The third stage of the beam was merely to provide final horizontal and vertical steering of the beam into the bubble chamber. An interesting feature was the stepper magnet. This was designed to give regular kicks to individual particles on a non-dispersed beam ray such that a clearly separated, but well collimated, set of beam tracks could be received in the bubble chamber.(36) In the event the "spill" was so peaked that trouble was experienced with timing. Many particles fell into the same stepped channel, thus causing the measuring difficulty of overlapping beam tracks. Conversely the tightly-constrained beam parameters meant that editing of variables could be used when beam tracks were not successfully measured.

The bubble chamber used was the 1.5 m. British National Bubble Chamber which had only recently been moved from CERN. The large interaction space was sufficient to define a fiducial volume such that an average of one event of interest per two frames could almost be maintained. Exposures were produced on 35 mm. film but resolution was good enough to produce no problems for automatic measuring

The first data-taking run was in February of 1968 but because of beam line failures and a bubble chamber breakdown, the four thousand pictures obtained at 2.2 GeV/c

were used only for setting up scanning criteria and for establishing constants for automatic measuring. A large quantity of film was taken in March when the Imperial College allocation alone totalled 36,000 frames, largely at 2.5 and 2.7 GeV/c with some at 2.9 GeV/c, later abandoned.

A further large-scale picture-taking run took place in June-July of 1968 when some further 40,000 frames total were taken at each of 2.1 and 2.3 GeV/c.

2.2 Film Analysis

The general flow of the experiment processing, as used at Imperial College, can be seen in Fig. (3) where the symbols are generally self-explanatory forms of intermediate computer storage and the names are those of the programs used.

The analysis of the film started with two independently made scans for all topologies of events other than the simple one prong of K meson decay. It was calculated that individually these scans were of the order of 94% efficient, in so far as all events can be said to be equally observable. By combining them in a check scan an efficiency better than 99% could be achieved.

The film was then transferred to a pre-digitising table where rough co-ordinates on each of three views of two fiducial marks, the vertex and two further points on each track were fed either directly on to magnetic tape, when a computer controlled on-line checking procedure was in use, or indirectly via paper-tape. When processed through the CERN program MIST[37] this tape became a guiding reference for

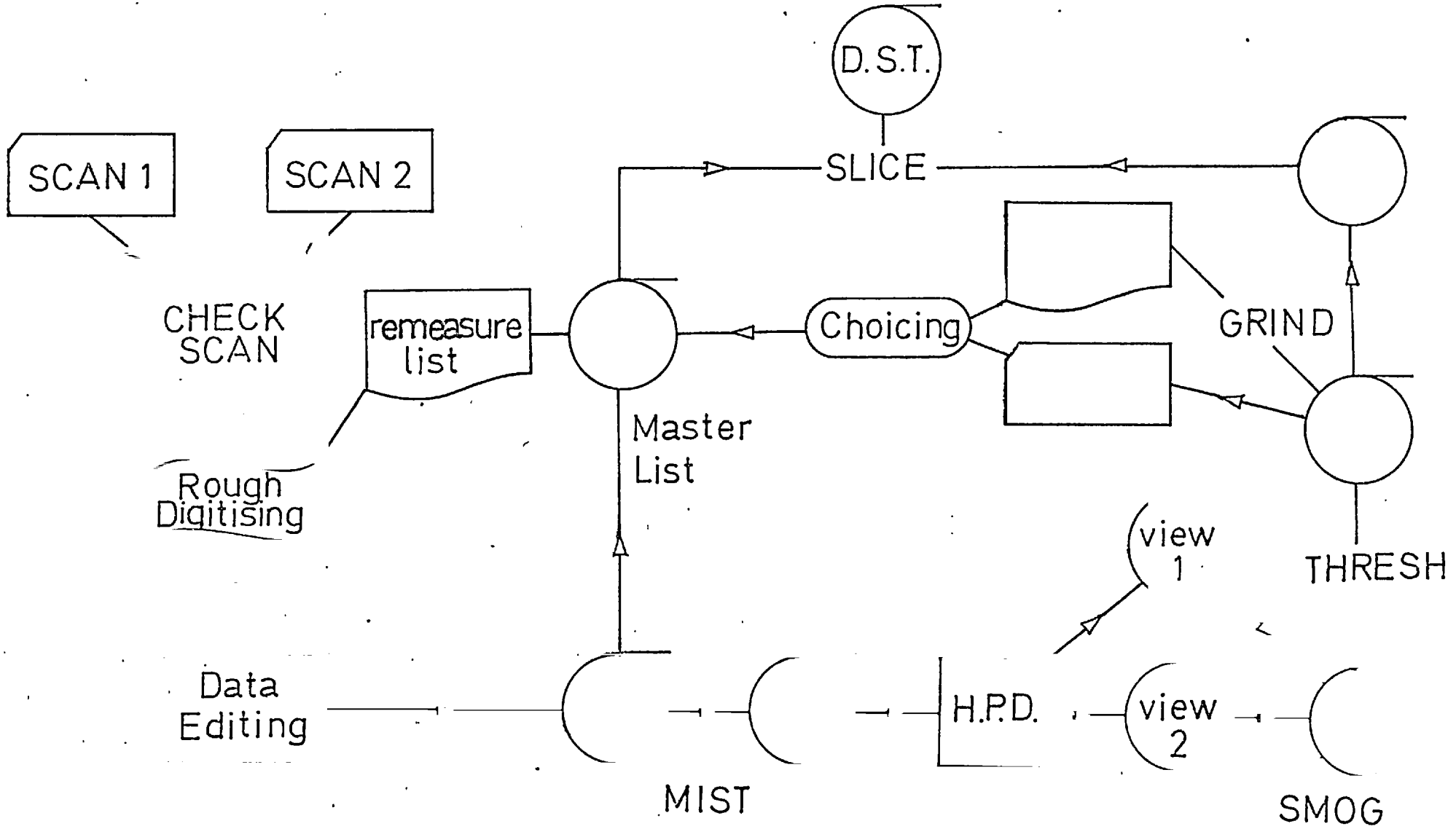

Fig. 3 EVENT PROCESSING

the accurate measuring machine.

This was the first experiment undertaken using the Imperial College automatic film measuring machine. This is an H.P.D. of Sogénique manufacture, similar to the so-called H.P.D.2 at CERN, which utilises a "flying-spot" of focussed light made mechanically by a crossed coincidence of a series of rotating optical fibres with one stationary fibre. The clamped film also moves in a calibrated fashion such that the whole frame is covered by a raster-like scan. Occlusion of the light-source to a photo-electric cell on the other side of the film causes a co-ordinate-pair digitization to be delivered to the controlling computer, the PDP-6, equivalent to the position of the bubble or "blob" which caused it.

The rough co-ordinates on the MIST tape defined wide annular "roads" which form the sensitive areas, in which the H.P.D. digitisings were processed. The Imperial College film at 2.1 GeV/c and most of the Westfield College film, measured with the same device, was processed using an on-line C.R.T. "light-pen" patching method of badly defined roads. This considerably improved the efficiency of the system. In slices of 32 scan lines (about 2 mm. on film), a histogramming technique produced a representative "master point". Between five and twenty of these points per track, together with accurate fiducial measurements were fed through the view-merging program SMOG to form the input data to THRESH. This latter program performed a stereo reconstruction of each track in purely geometric terms so that at the output stage the helix which each track describes in the magnetic field of the bubble chamber was parametrised by its curvature, dip-angle (Λ)

and the angle to the x-axis which the projection of the track makes at the vertex (ϕ). From a reconstruction of the intersection of the tracks the three-dimensional vertex co-ordinate sequence (X,Y,Z) may be found.

It is to be noted that the version of THRESH used could not give a mass-dependent correction for the slowing-down of the track. A histogram of the average residual per track of the distance of each master point from the reconstructed helix peaked at 3μ. Within this accuracy a mass-dependent correction would certainly be valuable. Indeed, an examination of the variation of the residual along the track gave direct evidence of the spiral rather than circular nature of the track. When, at a later stage of the experiment, conventional (I.E.P.) measuring machines were used for remeasures, the residual peaked at $7\text{-}8\mu$.

GRIND took the geometric quantities and attempted a series of kinematic fits by assuming mass assignments to the tracks in line with certain pre-arranged hypotheses for the event. The constraint equations of conservation of energy and momentum in three directions were satisfied and for each fit a χ^2 was calculated, and, with the number of degrees of constraint, this was converted to a confidence level for this fit having this χ^2 or greater. Only confidence levels of $\geqslant 0.25\%$ were accepted. Theory shows that a histogram of such confidence levels should be flat. By experiment, there was a slight upward gradient indicating an over-estimate of the errors involved. This was not serious as no fits were lost; however, there was also a small peak in the smallest bin suggesting that the fit-acceptance level had been set

rather low and there was a slight contamination from other fits. Throughout, stretch functions on the three geometric quantities had distributions with a mean close to zero and standard deviation ~ 1, for all classes of tracks.

It was the author's responsibility to establish versions of THRESH and GRIND compatible with the H.P.D. and I.E.P. programs to work on the same PDP-6 computer, where all processing was done "off-line". All the English events were passed through the same reconstruction programs.

As an interesting diversion at this point and as an example of some of the difficulties encountered in interpreting events it is instructive to consider the event shown in Fig. (4). The two prong neutral decay (or V^o) clearly present failed coplanarity checks to associate it with the production vertex. The usual $K^o \rightarrow \pi^+\pi^-$ decay fit also failed but a $\Lambda^o \rightarrow p\pi^-$ decay fit was completely successful and was further corroborated by a four constraint fit to the elastic pion scattering seen on one secondary. At this point the one prong secondary at the centre of the picture was noted and it was realised that the correct hypothesis for the event was

$$K^+p \longrightarrow K^o\, p\pi^+\pi^o$$

$$K^o \longrightarrow \overline{K}^o$$

$$\overline{K}^o p \longrightarrow \Lambda^o\pi^+\pi^o$$

$$\downarrow p\pi^-$$

On a remeasurement this was fitted. It will be noted that this sequence of events involves a transition from an S=1 K^o to an S=-1 $\overline{K}^o$. Although this is at first sight surprising, it can be shown that this is quite in accord with the laws of

Fig. 4. Event displaying $K^0 \rightarrow \overline{K^0}$ transition.

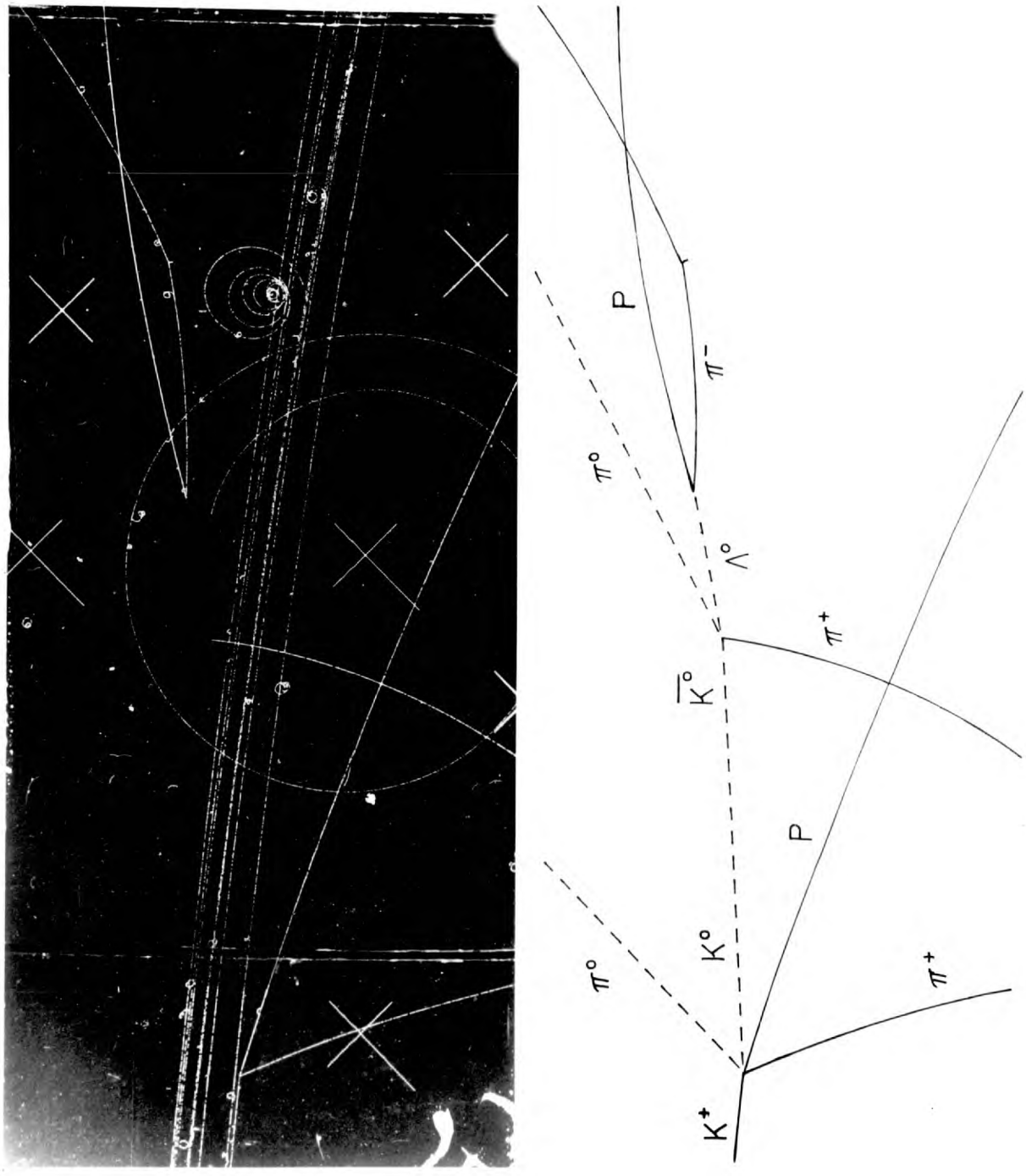

quantum mechanics. Immediately after the strong primary interaction the K^o is defined as having S=1. Neglecting for the moment the small effect of CP non-conservation, its wave function can also be described as being composed of equal parts of K_1^o and K_2^o components.

$$|K^o> = \frac{1}{\sqrt{2}} \left(|K_1^o> + |K_2^o> \right)$$

In travelling the 20 cm to the secondary interaction vertex the short-lived K_1^o component decays to ~1.5% of its previous strength so that we may now consider the particle to be almost entirely K_2^o, composed, in its turn, of equal parts of S=1 K^o and S= -1 $\overline{K}^o$:

$$|K_2^o> = \frac{1}{\sqrt{2}} \left(|K^o> + |\overline{K}^o> \right)$$

It is now not very surprising that the S=-1 component is selected by the next strong interaction to form the negative strangeness Λ^o.

As with all other events this event went through the process marked "choicing" on the chart, which consisted in a re-examination of the film with the output from GRIND so that cards representing fits not compatible with momentum/ionisation effects calculated, or momentum/range considerations could be rejected.

Also, suitable no-fit type of events, in which more than one unobserved neutral particle was produced were included, if the calculated missing-mass was correct for the hypothesis, competing on an equal level with one constraint fits. Because of the much smaller phase space allowed to the missing variables, one constraint fits were only allowed to compete against four constraint fits if their confidence level was

ten times greater. In practice this occurred extremely rarely.

The last program in the chain, SLICE, merely computed extra physical quantities from the basic four momenta of all particles and put all this information for the selected fits or no-fits on the data summary tape (D.S.T.), on which various statistics and fitting programs were run.

With all the difficulties involved in getting a new measuring system to operate, a considerable inefficiency was experienced, and because of this a "master-list" system was adopted. This consisted in a magnetic tape containing a short record of every event scanned, its measuring history and fit or fits eventually adopted for it. After each cycle through the chain of programs this tape could be up-dated from the cards selected at the choicing stage. The master-list could then be used by SLICE to pick off the required information from the GRIND tape, and also it could be used to create a complete remeasure list for the next cycle.

As can be seen from the figures of Table (1) the measuring efficiency appeared to be inversely dependent on the number of tracks in a given topology. Examination of the failing tracks at the choicing stage revealed no physical correlation between them, and the data from Westfield College, processed through the same system except for a small re-road-making loop for poorly rough-digitised events, was measured at a much greater success rate. For these reasons, and the fact that distributions of physical quantities compared with French data measured to 95% efficiency, were within statistical

errors, it appears that there is no gross physical bias even in the topological channels which fell to an overall efficiency of only 80-85%.

Table 1. Summary of Imperial College Data

Giving the number of events scanned and the measuring efficiency at each momentum in each of the major topology classifications.

Momentum (GeV/c)	2.11	2.31	2.53	2.72
Two Secondaries	5022 93%	3107 94%	2930 95%	3917 96%
Two Secondaries & associated V^0	560 89%	419 92%	407 91%	544 91%
Three Secondaries (τ)	283 84%	174 85%	187 90%	177 92%
Four Secondaries	662 90%	584 91%	555 93%	873 97%
All Topologies	6540 92%	4309 93%	4093 94%	5549 95%

Measuring efficiency here is defined as the percentage of events with acceptable fits/nofits to total events capable of being measured.

CHAPTER 3

3-BODY FINAL STATES

3.1 Final State Reactions

The final states whereby a single pion might be produced are limited in the doubly charged T=1 K^+P state to:

$$K^+P \rightarrow P\,K^0\pi^+ \quad - \quad (3.1)$$

$$K^+P \rightarrow P\,K^+\pi^0 \quad - \quad (3.2)$$

$$K^+P \rightarrow N\,K^+\pi^+ \quad - \quad (3.3)$$

For the most part these reactions give only one constraint kinematic fits because of the missing neutral, but where the decay mode $K^0 \rightarrow \pi^+\pi^-$ is seen, reaction (3.1) gives a highly constrained fit. This decay mode is readily distinguishable from $\Lambda^0 \rightarrow P\pi^-$ hence contamination from the reaction

$$K^+P \longrightarrow K^+\,K^+\Lambda^0 \quad - \quad (3.4)$$

can be safely considered to be non-existent. Only a few examples of reaction (3.4) were noted at the higher energies where phase space permits it. This then gives at least one well fitted, completely unambiguous channel on which to base cross-sections and with the help of which other ambiguities may be resolved.

3.2 Weighting Seen K^0 Events

In this final state, however, weights must be allotted to each event to allow for the possibility of similar events not having the K^0 decay mode observed as such, and hence being classed as a four prong event, if the decay took place very close to the vertex, or as the simple two prong variety of (3.1), if the decay took place outside the illuminated

region of the bubble chamber. This latter is referred to as the INLITE volume and, for these purposes, may be found by histogramming the co-ordinates of all V^o vertices which were observed. The potential length, P, of the K^o is then calculated as the distance from the primary interaction to the boundary of the INLITE volume along the direction of the K^o line of flight. The probability of a K^o not decaying in this distance is then $e^{-P/L}$, where L is the theoretical mean decay length for a K^o of this momentum.

For the other source of loss, a cut, C, is chosen as the minimum observable decay length projected on to the (X,Y) plane. If there were events with K^o's less than this distance they are then disregarded as the weighting would allow for them. Taking Cproj. as C projected on to the line of flight, $e^{-Cproj./L}$ is then the probability of the K^o surviving past the minimum observable decay length. $(e^{-Cproj./L} - e^{-P/L})$ is therefore the probability of a decay taking place and being seen and hence the required weight for each event is

$$\frac{1}{e^{-Cproj./L} - e^{-P/L}}$$

A rough approximation for C may be obtained from a histogram of observed projected decay lengths but to allow for the momentum spectrum of the K^o a better technique is to assume a series of values and then plot the resulting sum of the weights, disregarding cut events. At points where C has been over-estimated this plot flattens out at a value which is equal to the theoretical number of K^o's presumed to be present. At under-estimated values of C, events are not seen and this

quantity is smaller. This technique was used on the data at each momentum from each laboratory in the collaboration, and the values of C obtained varied from 2 to 6 mm. in space.

One method for checking the weighting procedure used is the self-consistency recalculation of the K^o life-time. Knowing the momentum of the seen K^o and its decay length, its life-time in its own rest system may be calculated, preferably in terms of the theoretical life-time, τ . If an exponential decay is then assumed with experimental life-time τ_e, then the number of K^o's, N, after a time $x\tau$ when there were N_o is $N = N_o e^{-x\tau/\tau_e}$ And the number decaying in an interval dx is

$$dN = - \frac{\tau}{\tau_e} N_o \cdot e^{-x\tau/\tau_e} \, dx$$

so, $\log_e \left(dN/dx\right) = \text{constant} - x\tau/\tau_e$

Hence a plot of $\log \left(dN/dx\right)$, where N is now the corrected, i.e. weighted, number of events, should give a straight line whose gradient is minus the ratio of the theoretical life-time to the experimentally measured life-time. Such a plot is shown in Fig. (5) made up from a sample of all K^o decays from all types of interaction at all momenta. The result of a straight line fit by the χ^2 method gave a gradient of -0.91 ± 0.05 corresponding to an experimentally observed K^o life-time of $(0.781 \pm .047) \times 10^{-10}$ Sec. An underestimate of C would have led to a depletion especially of the first point. Although this does occur slightly it is not to any serious extent.

3.3 Resolution of Ambiguities

The remaining reactions, (3.1) with the K^o unseen, (3.2) and (3.3) present rather greater problems. Having one

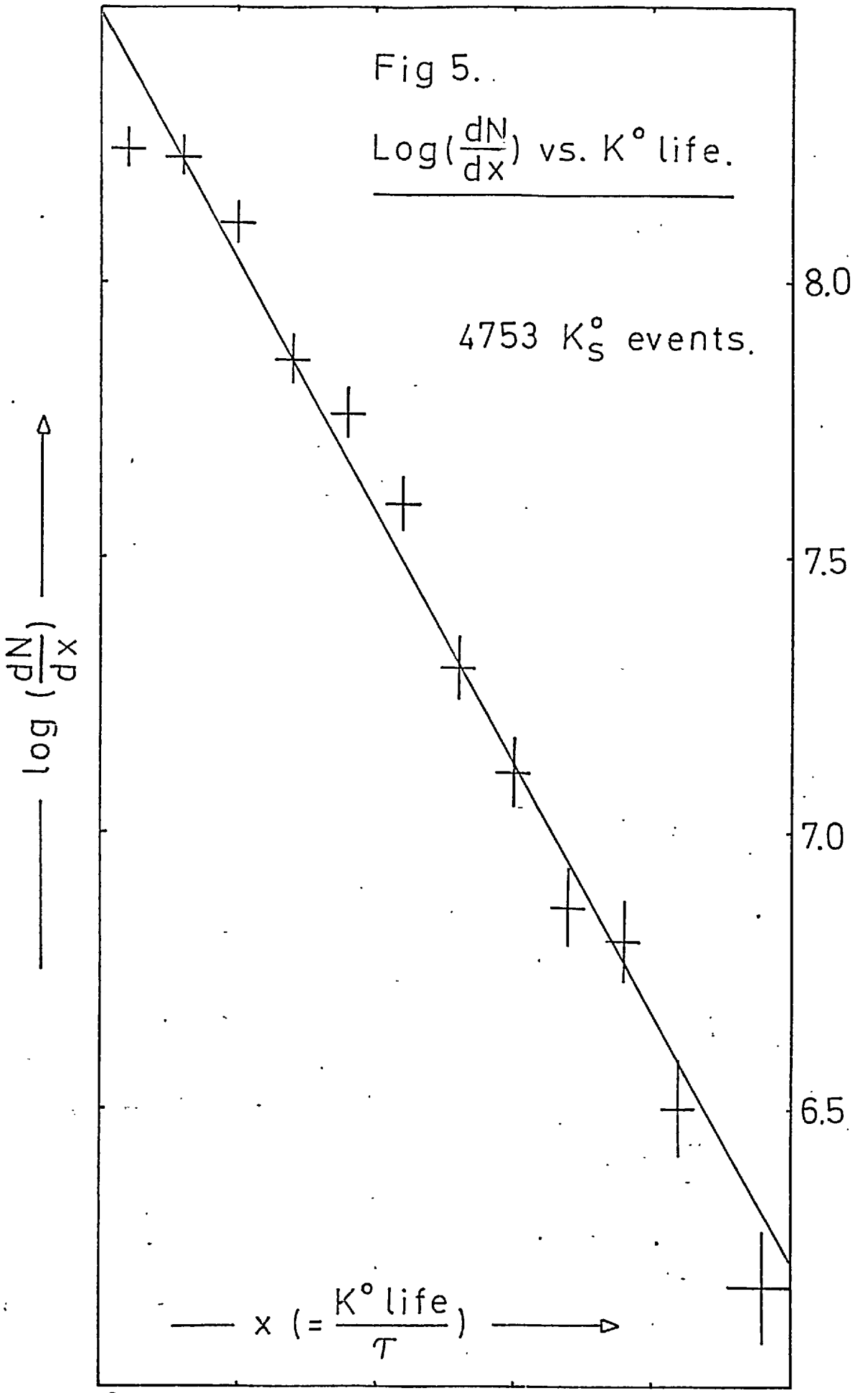
Fig 5.
Log(dN/dx) vs. K° life.
4753 K^0_S events.
log (dN/dx)
8.0
7.5
7.0
6.5
x (= K° life / τ)
0.0
1.0
2.0

missing neutral particle they fit with only one constraint. In practice GRIND was normally well able to fit two or even three of these reactions, or at least allow the NOFIT multi-neutral ease on examination of the missing-mass. Because of the ease with which fits could be obtained the χ^2 or resulting confidence level was not accepted as a sufficiently good selection criteria. This was justified at a later stage when a plot of the confidence level of one fit against the confidence level of an ambiguity, produced a more or less uniform scatter diagram with only a very small cluster near the axes. This left only momentum-range and ionisation considerations for effective criteria. Despite the large bubble chamber the former was only useful for tracks with momenta below 300 MeV/c and because of variable film quality, differentiation on the grounds of ionisation was only good for tracks less than 700 MeV/c (K/π ambiguity) or 1100 MeV/c (P/K ambiguity). An attempt at using the H.P.D. to supply ionisation information automatically was ruled somewhat premature at this stage.

After these conditions had been applied the numbers of events giving fits or nofits in the various two prong channels are shown in Tables 2a, 2b. Here, the diagonal elements give the number of events with uniquely chosen fits and the off-diagonal elements show the two-way ambiguous events. Three-way ambiguous events commonly represent some 1 to 3% of two prong events, depending on incident momentum and hence were disregarded, or classed as unmeasurable for the purposes of cross-sections. Tables 2a, 2b show the magnitude of the problem. Even if it were not for the kinematic

TABLE 2a Classification of Two Prong Events

2.11 GeV/c

10862 Uniquely Choiced Events
1629 2-way Ambiguous Events
62 3-way Ambiguous Events

Final State	PK^+	$PK^+\pi^o$	PK^+(MM)	$PK^o\pi^+$	$P\pi^+$(MM)	$NK^+\pi^+$	$K^+\pi^+$(MM)	$\pi^+\pi^+$(MM)
PK^+	5173/ 8	10	1	5	2	0	1	
$PK^+\pi^o$		1348/ 7	13	375	24	22	4	
PK^+(MM)			299/ 6	224	172	14	4	
$PK^o\pi^+$				1699/ 0	1	165	50	
$P\pi^+$(MM)					1050/ 2	251	91	
$NK^+\pi^+$						731/ 72	5	6
$K^+\pi^+$(MM)							374/ 5	81
$\pi^+\pi^+$(MM)								149/ 0

(MM), Missing Mass, Implies a multi-neutral hypothesis

2.31 GeV/c

7724 Uniquely Choiced Events
1319 2-way Ambiguous Events
60 3-way Ambiguous Events

Final State	PK^+	$PK^+\pi^o$	PK^+(MM)	$PK^o\pi^+$	$P\pi^+$(MM)	$NK^+\pi^+$	$K^+\pi^+$(MM)	$\pi^+\pi^+$(MM)
PK^+	3667/ 1	8	1	1	0	1	0	
$PK^+\pi^o$		906/ 8	8	386	22	18	1	
PK^+(MM)			216/ 1	128	151	29	3	
$PK^o\pi^+$				1209/ 1	0	137	40	
$P\pi^+$(MM)					849/ 0	155	66	
$NK^+\pi^+$						569/ 54	4	11
$K^+\pi^+$(MM)							279/ 8	72
$\pi^+\pi^+$(MM)								130/ 0

(MM), Missing Mass, Implies a multi-neutral hypothesis

TABLE 2b Classification of Two Prong Events

2.53 GeV/c

7269 Uniquely Choiced Events
1753 2-way Ambiguous Events
128 3-way Ambiguous Events

Final State	PK^+	$PK^+\pi^o$	PK^+(MM)	$PK^o\pi^+$	$P\pi^+$(MM)	$NK^+\pi^+$	$K^+\pi^+$(MM)	$\pi^+\pi^+$(MM)
PK^+	3580/ 3	19	1	1	1	3		
$PK^+\pi^o$		764/ 11	6	477	29	24	4	1
PK^+(MM)			203/ 0	146	547	56	12	0
$PK^o\pi^+$				1034/ 0	2	188	38	0
$P\pi^+$(MM)					769/ 0	164	96	0
$NK^+\pi^+$						459/ 72	3	8
$K^+\pi^+$(MM)							288/ 10	126
$\pi^+\pi^+$(MM)								157/ 0

(MM), Missing Mass, Implies a multi-neutral hypothesis

2.72 GeV/c

8500 Uniquely Choiced Events
2489 2-way Ambiguous Events
262 3-way Ambiguous Events

Final State	PK^+	$PK^+\pi^o$	PK^+(MM)	$PK^o\pi^+$	$P\pi^+$(MM)	$NK^+\pi^+$	$K^+\pi^+$(MM)	$\pi^+\pi^+$(MM)
PK^+	4003 3	35	4	2	1	0		
$PK^+\pi^o$		892/ 14	9	643	58	41	4	0
PK^+(MM)			229/ 6	163	323	90	16	0
$PK^o\pi^+$				1308/ 2	1	279	76	3
$P\pi^+$(MM)					981/ 1	213	142	1
$NK^+\pi^+$						478/ 88	10	27
$K^+\pi^+$(MM)							404/ 27	188
$\pi^+\pi^+$(MM)								187/ 0

(MM), Missing Mass, Implies a multi-neutral hypothesis

bias that could be introduced, the number of ambiguous events is such that they cannot be neglected. Although there are some ambiguous events almost everywhere they could be, the principal ambiguities cluster in the same places for every momentum. In the case of the $PK^{o}\pi^{+}$ channel the ambiguities come from $P^{+}K^{+}\pi^{o}$ and the equivalent multi-neutral channel and $NK^{+}\pi^{+}$ and its multi-neutral channel.

3.4 $PK^{o}\pi^{+}$ Ambiguities

At this stage, the behaviour of the $PK^{o}\pi^{+}$, seen K^{o}, events are most useful. Events which produce an S=1 K^{o} may be considered to be giving a K^{o}_{1} (with two pion decay mode) 50% of the time and a K^{o}_{2} (with three pion decay mode) for the remaining 50% of cases. With a decay length of some 343 metres per GeV/c the latter decay mode is almost never seen, and even when it is, the $\pi^{+}\pi^{-}\pi^{o}$ decay mode, 12.7% branching ratio, will seldon fit to $K^{o}\rightarrow\pi^{+}\pi^{-}$ without the other missing neutral pion. The remaining K^{o}_{1}'s decay either to $\pi^{+}\pi^{-}$ (68.4%) and are probably observed, or to $\pi^{o}\pi^{o}$ (31.6%) and are not observed. This gives a factor of 1.93 for the number of unseen K^{o} events there should be, more than the number of weighted seen K^{o} events in any kinematic region.

Of course, using this method some of the unseen K^{o} events are the very events for which the others are being weighted, so when both classes of events are being considered together, there only should be weights for the V^{o} events mis-classed as 4 prongs. This is, however, a negligible correction.

Looking at the difference between 1.93 times the weighted number of seen K^{o} events and the uniquely choiced

$PK^{o}\pi^{+}$ events, the kinematic regions to which the ambiguous events contribute are exposed. The situation is shown schematically in Fig. (6). A scatter plot of the laboratory momentum of the positive pion, P_{π}, against the neutral kaon, P_{K}, shows that the area of depletion of events is almost entirely in the region $P_{\pi} > 1000$ MeV/c, that is it probably results from an ionisation ambiguity of K/π. The same plots for the $PK^{+}\pi^{o}/PK^{o}\pi^{+}$ and PK^{+} (multi-neutral)$/PK^{o}\pi^{+}$ ambiguities show that this is exactly where they contribute, whereas the $NK^{+}\pi^{+}/PK^{o}\pi^{+}$ and $K^{+}\pi^{+}$ (multi-neutral)$/PK^{o}\pi^{+}$ ambiguities contribute chiefly to the area $P_{K} > 1000$ MeV/c, $P_{\pi} < 1000$ MeV/c and probably arise from a K/P ionisation ambiguity. The latter two cases thus may be universally resolved as not belonging to $PK^{o}\pi^{+}$ channels. Constant weights assumed for the other two ambiguous channels may be calculated by a least squares method such that the kinematic diagram is finally as predicted by the seen K^{o} events to within small errors.

In practice, this method gave an average weight for $PK^{o}\pi^{+}$ interpretation of 0.45 to all events from the $PK^{+}\pi^{o}$ ambiguity and 0.7 to those from the PK^{+} (multi-neutral) ambiguity.

A similar method, used originally by the French groups, involved five bin histograms of various physical quantities for the predicted $PK^{o}\pi^{+}$ behaviour, from weighted K^{o}_{1} events, for uniquely choiced $PK^{o}\pi^{+}$ events and for the events ambiguous with this channel. The fourteen physical quantities concerned were the cosine of the scattering angle in the centre of mass system (c.m.s.) and in the laboratory system for each of the three particles, the square of the effective masses for the three combinations of particles, the

Fig 6. $PK^{\circ}\pi^{+}$ Ambiguities.

Showing schematically the kinematic distribution of ambiguous events.

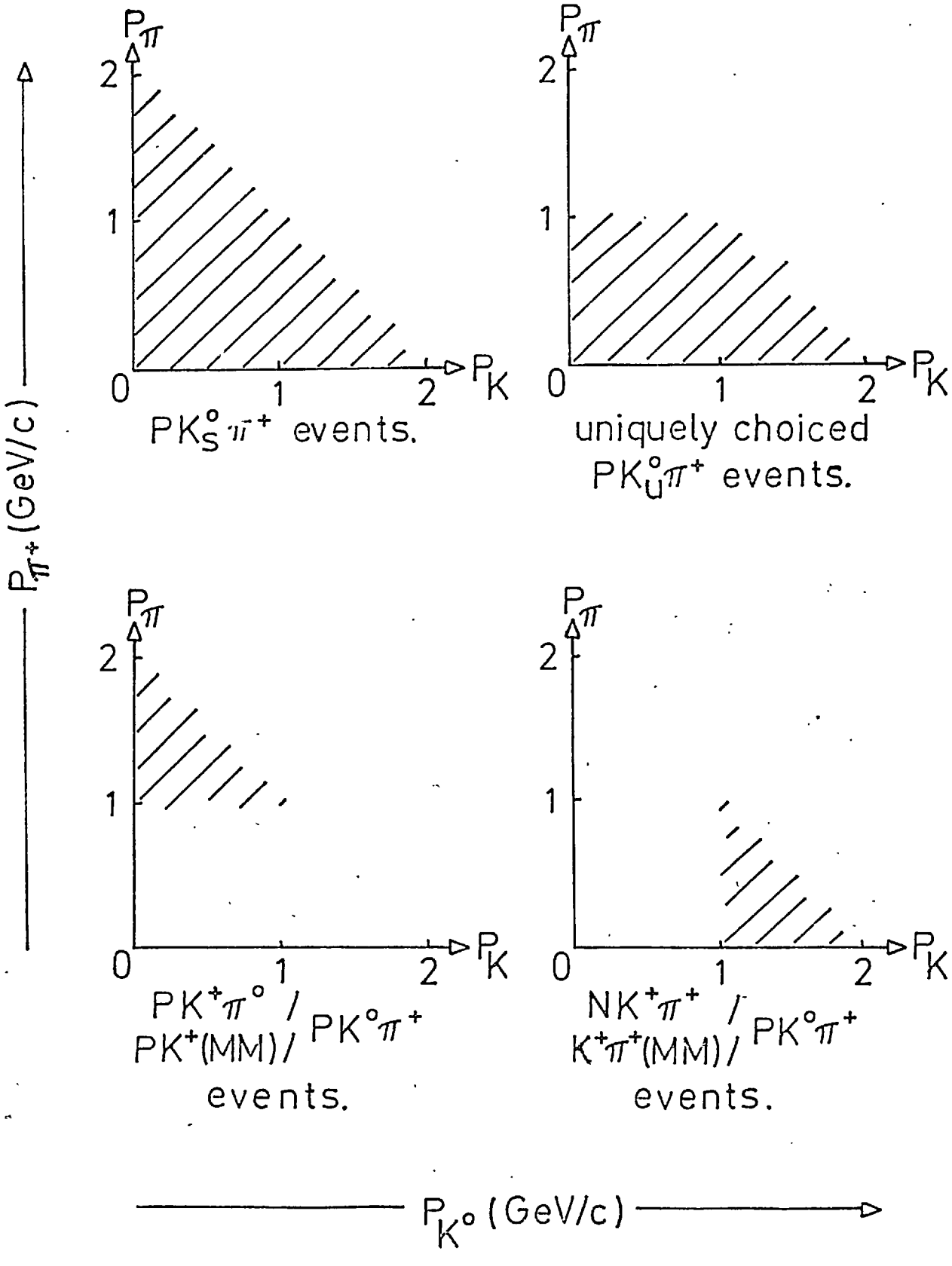

three missing momentum components and its magnitude in the c.m.s. for the K^o and the square of the missing mass for the neutral particle.

This procedure gave eight constraining bins where the uniquely choiced events already made up the predicted number. In this way the $NK^+\pi^+$ and $K^+\pi^+$ (multi-neutral) ambiguities were again ruled out. A process of averaging for the other bins gave the weight 0.61 to the $PK^+\pi^o$ ambiguity and 0.7 to the PK^+ (multi-neutral) ambiguity. These weights were finally adopted for all data.

Since the actual number of events of the final state $PK^o\pi^+$ were, by this method, being determined by the seen K^o decays, calculations of cross-sections were also determined purely by the seen K^o events instead of artificially reducing statistical errors by including all $PK^o\pi^+$ events.

3.5 Other Ambiguities

The resolution of the $PK^+\pi^o$ ambiguities was now made somewhat easier. Like all the other ambiguities the actual proportion of ambiguous events to uniquely choiced ones varied over a huge scale depending on the incident momentum and the laboratory where the data was prepared. At 2.1 GeV/c where somewhat slower tracks made ionisation decision equivalently easier this proportion fell to 27% in the French data. At 2.7 GeV/c for data from the English groups where, generally speaking, choicing decisions were not pushed quite so hard the proportion rose to 130%. Intermediate figures were obtained at the other momenta. Despite this variation it was once again possible to say that the proportion of these

ambiguities coming from a given channel was quite constant whatever the energy and wherever the film was analysed. This reflected the common kinematic origin of the ambiguity.

For example, the ambiguity arising from $PK^{o}\pi^{+}$ events, already dealt with, accounted for between 76 and 86% of all the $PK^{+}\pi^{o}$ ambiguities, under all circumstances. To maintain a normalized scheme the weight 1. - 0.61 = 0.39 was adopted for these events. The remaining 20% were spread over six other channels so a weight 0.5 for these other two-way ambiguities has been used.

The situation is similar though rather less well-constrained for final state $NK^{+}\pi^{+}$ and its ambiguities. Here, the already resolved $PK^{o}\pi^{+}$ ambiguities account for between 20% and 50% of all ambiguities the remainder coming largely from the $P\pi^{+}$ (multi-neutral) channel where the proton is fast enough to simulate a kaon. Overall, this reaction is not so important as the other two as isospin coefficients dictate that resonance production is very much lower than in the other reactions. Thus, weight 0.5 has been taken for the remaining ambiguities.

3.6 Contamination

After the above treatment of the ambiguity problem, cuts were imposed on the data so that a sample of events were obtained in a narrow band of incident beam momenta and from a well-defined rectangular parallelopiped of bubble chamber volume. As a fiducial volume had already been chosen for scanning purposes this did not lose many events. The data lost was ~ 10% but that left was then in a 60 MeV/c momentum region corresponding to a maximum spread of only 20 MeV in

E*, the centre of mass energy.

Looking at the numbers of events after these cuts, Table (3), it is possible to evaluate a contamination from other channels, because of ambiguities, based on the formula:

No. of contaminating events =

(1-w).(weighted no. of events - no. of unique events)

where w is the average weight applied to the ambiguities to bring the number of unique events up to the total weighted number of events. As some ambiguities are ruled out completely on kinematic grounds, they are not included in this calculation.

The contamination of, for example, the $PK^{o}\pi^{+}$ channel, by this method varies between 5 to 10% (see Table (3)) depending on momentum. Of course this is not to say that there is an extra error-bar ~ 10% to be inserted on every physical point computed. As will be shown the properties of the nucleon, kaon and pion in reactions (3.1) to (3.3), and even the multi-neutral cases, are very broadly similar.

Another source of error comes from contamination of the beam tracks in the bubble chamber. Separation curves indicated that there was a high percentage of background muons and a non-negligible number of pions too. Because of their lack of strong interactions the muons are of no concern but their presence does invalidate the use of beam track counts to compute cross-sections. Fortunately, there is available accurate measurements of total $K^{+}P$ cross-sections, σ_{Kt}, so contamination may be calculated from the number of three prong τ decays ($K^{+} \to \pi^{+}\pi^{+}\pi^{-}$) observed. (10)

TABLE 3.

Contamination of Data, Partial Cross-Sections

(Table concerns data after all cuts, see text)

2.11 GeV/c	$PK^o\pi^+$ ø	$PK^+\pi^o$	$NK^+\pi^+$
Uniquely Classified	1548	999	666
Weighted Number	1886	1238	1017
Ambiguity Contamination	6.4%	9.6%	13.1%
Cross-Section (mb)	4.00±0.21	1.76±0.19	1.29±0.14
Pion Contamination =			15 ± 4%

2.31 GeV/c	$PK^o\pi^+$ ø	$PK^+\pi^o$	$NK^+\pi^+$
Uniquely Classified	1039	774	486
Weighted Number	1290	886	717
Ambiguity Contamination	7.1%	6.9%	11.5%
Cross-Section (mb)	3.42±0.20	1.17±0.13	1.22±0.13
Pion Contamination =			9 ± 4%

2.53 GeV/c	$PK^o\pi^+$ ø	$PK^+\pi^o$	$NK^+\pi^+$
Uniquely Classified	935	619	412
Weighted Number	1235	809	711
Ambiguity Contamination	9.0%	13.5%	14.8%
Cross-Section (mb)	2.67±0.15	1.36±0.17	0.87±0.10
Pion Contamination =			1 ± 4%

2.72 GeV/c	$PK^o\pi^+$ ø	$PK^+\pi^o$	$NK^+\pi^+$
Uniquely Classified	1430	697	427
Weighted Number	1790	996	919
Ambiguity Contamination	5.3%	16.2%	17.8%
Cross-Section (mb)	2.77±0.17	1.10±0.12	1.01±0.11
Pion Contamination =			10 ± 4%

ø The Channel $PK^o\pi^+$ refers to unseen K^o's only for numbers of events but cross-sections are derived purely from numbers of seen K^o events.

The total interaction length of kaons in the scanned bubble chamber is

$$L_K = a\, N(\tau) \qquad \text{with} \qquad a = \frac{p}{m} \cdot \frac{ct}{f}$$

$N(\tau)$: estimated number of true τ decays

$$\left(= N_\tau + \frac{N_\tau}{(N_\tau + N_{N\tau})} \cdot N_R \right)$$

N_τ : Number of τ fits on the master-list

N_R : Number of non-fitting (unmeasurable etc.) three prong topologies on the master-list

$N_{N\tau}$: Number of above topologies fitting to other decay modes

p : beam momentum

m : mass of kaon[19] = 493.8 MeV/c^2

ct : mean-life of K^+ x velocity of light[19]

f : decay-fraction of $K^+ \rightarrow \pi^+\pi^+\pi^-$[19] = 5.57%

If we take the total number of events to be

$$N = N_E - N_{300} + N_P$$

N_E : estimated total number of events on the master-list, increased to allow for known scanning inefficiencies

N_{300} : Number of three prong topologies on the master-list

N_P : Number of unseen proton recoil type of events, estimated from elastic events scanning biases

then, $N = \beta (\sigma_{Kt} L_K + \sigma_{\pi t} L_\pi), \beta = \frac{A}{M} \cdot \rho$

A : Avogadro's number = 6.0222 x 10^{23} [19]

M : Atomic Mass of hydrogen = 1.007 [19]

ρ : Density of hydrogen in the chamber = 0.0597 c.g.s.

$\sigma_{\pi t}$: total pion cross-section at this energy[18]

Then the total interaction length of pions is

$$L_{\pi} = \frac{1}{\sigma_{\pi t}} \left(\frac{N}{\beta} - \sigma_{Kt} \cdot L_K \right)$$

From which the contamination of the beam is

$$C_{\pi} = \frac{L_{\pi}}{L_{\pi} + L_K}$$

Errors may be given by assuming Poisson type distributions in the number of observed events. The results of such calculations are shown in Table (3)

It may be noted that the answers are in some cases dangerously high. A more detailed analysis roll by roll revealed that there was some variation. By adopting a highest acceptable contamination cut off, it was possible to bring down the average but only at the cost of a large percentage of the data.

Pion contamination does not affect all reaction channels equally. For example, phase space only just allows the production of a pair of strange mesons in a four body final state π^+P interaction. It may be safely assumed that the final state $PK^o\pi^+$, seen K^o, is completely uncontaminated.

3.7 Partial Cross-Sections

If N_x is the total number of events estimated to be in the channel $K^+P \rightarrow X$ then the partial cross-section is σ_X where

$$N_X = \beta \sigma_X L_K = a \beta \sigma_X N(T)$$

or,

$$\sigma_x = \frac{N_x}{N(T)} \cdot \frac{1}{\alpha\beta}$$

To determine N_x, the weighted number of events seen on the D.S.T., N_{xs}, is used. The effect of the various momentum and fiducial volume cuts must also be allowed for, together with any bureaucratic losses, i.e. poor functioning of the SLICE program or tape errors and also the considerable measuring inefficiency. One overall scaling-factor may be used for all these losses, but as the measuring efficiency is topology dependent, so must be the scaling-factor. Clearly, the events lost through not observing short proton recoils do not affect any channels other than the elastic so we may write

$$\sigma_x = \frac{1}{N(T)} \cdot \frac{1}{\alpha\beta} \cdot \frac{N_T}{N_s} \cdot N_{xs}$$

N_T : Number of events of a given topology appearing on the master-list, weighted for scanning efficiency

N_S : Number of events of the same topology appearing on the D.S.T. after all cuts

In the $PK^o\pi^+$ channel only events with a seen K^o decay must be used for reasons given in section (3.3). The unseen K^o events are allowed for by multiplying by the further factor $(1 + 1.93) = 2.93$.

For the other channels the simple weighted number of events is used. Throughout, a normalized weighting system (i.e. $\sum_{\text{channels}} w_i = 1$) has been used so this is in order. Here, however, the effect of pion contamination must be allowed for

by calculating an event contamination:

$$F_{\pi} = \frac{\sigma_{\pi t} \; L_{\pi}}{\sigma_{Kt} \; L_K + \sigma_{\pi t} L_{\pi}}$$

N_{xs} is then reduced by the factor $(1 - E_{\pi})$ to get the true number of kaon events. Where the factor (N_T/N_s) is for two prongs, it is somewhat lower because of the better measuring efficiency. The results of calculations of partial cross-sections are given in Table (3) weighted for all three laboratories. The error-bars quoted arise purely from statistics.

CHAPTER 4

RESONANCE PRODUCTION

4.1 Dalitz Plots

The Dalitz plots of effective mass squared of (kaon - π) combination versus (nucleon - π) combination are shown at the four beam momenta for the three final states $PK^0\pi^+$, $PK^+\pi^0$ and $NK^+\pi^+$ in Fig. 7. The most obvious qualitative features are the strong $K^*(892)$ and $\Delta(1236)$ signals, especially in the $PK^0\pi^+$ channel. Starting from the pure T=1 K^+P state Clebsch-Gordan coefficients may be used to predict that these two resonances will be seen in the three channels in the ratios 2:1:0 and 9:2:1 respectively. This is why the $PK^0\pi^+$ channel is so important. The resonances produced there stand well clear of background. In the $NK^+\pi^+$ channel at the other extreme, the Δ^+ production is hardly noticeable and for most intents and purposes there is an evenly distributed Dalitz plot. Even at this early stage it can be seen that there is no clear evidence of interference, either positive or negative, between the K^* and Δ. The events in the cross-over region appear to be a direct sum of K^*, Δ and a small phase space contribution. More will be noted on this subject later, but the observation is interesting in view of the converse result found at energies closer to threshold,[20] where there appeared to be a momentum independent constant phase between the K^* and Δ Breit-Wigner amplitudes. A further qualitative note is that there seems to be no effect from the $K^*(1420)$ or the higher N^*'s. If there were a strong signal from a nucleon-kaon

Fig 7a. $PK^{\circ}\pi^{+}$ Dalitz Plots.

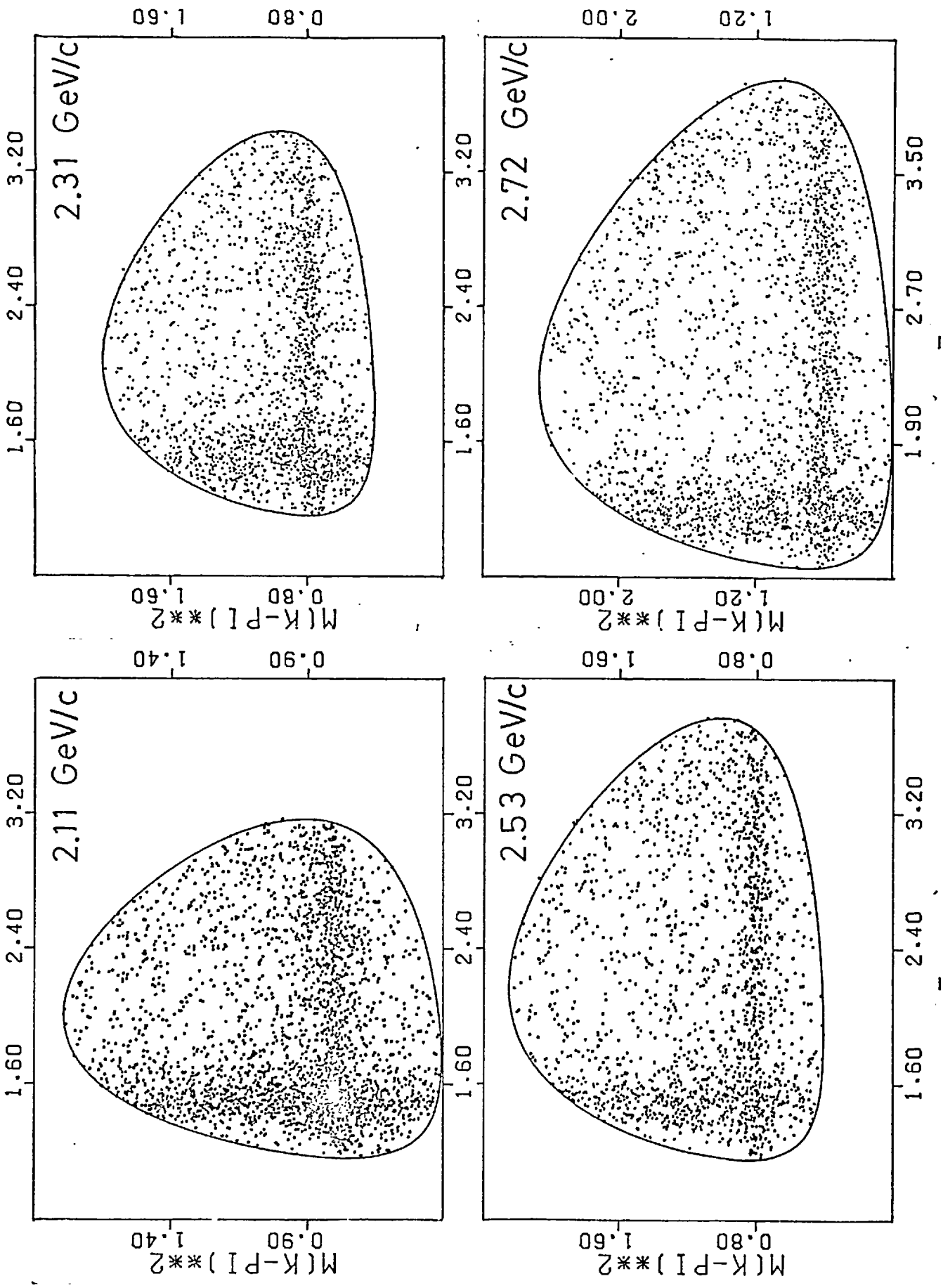

Fig 7b. $PK^{+}\pi^{\circ}$ Dalitz Plots.

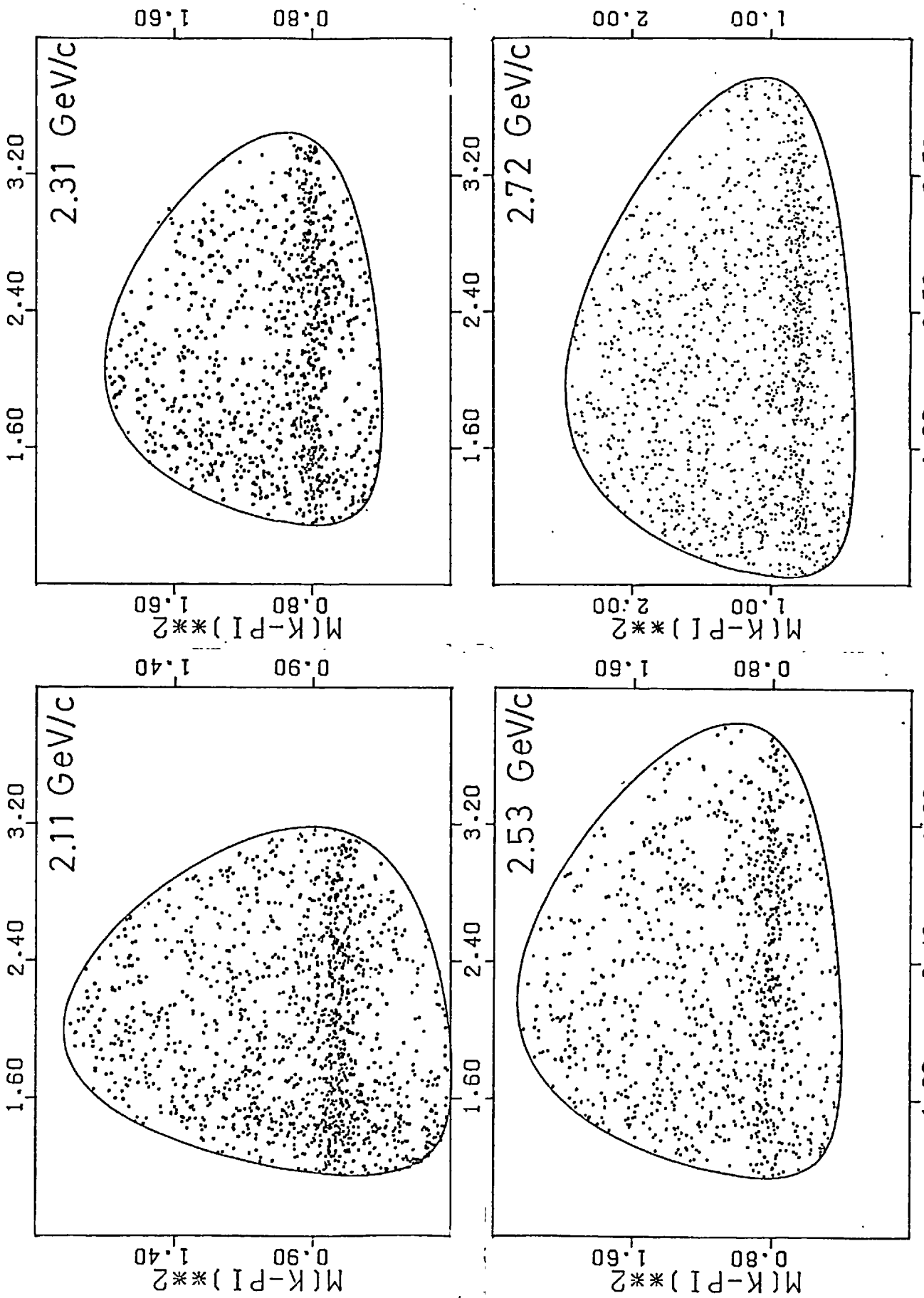

Fig 7c. $NK^+\pi^+$ Dalitz Plots.

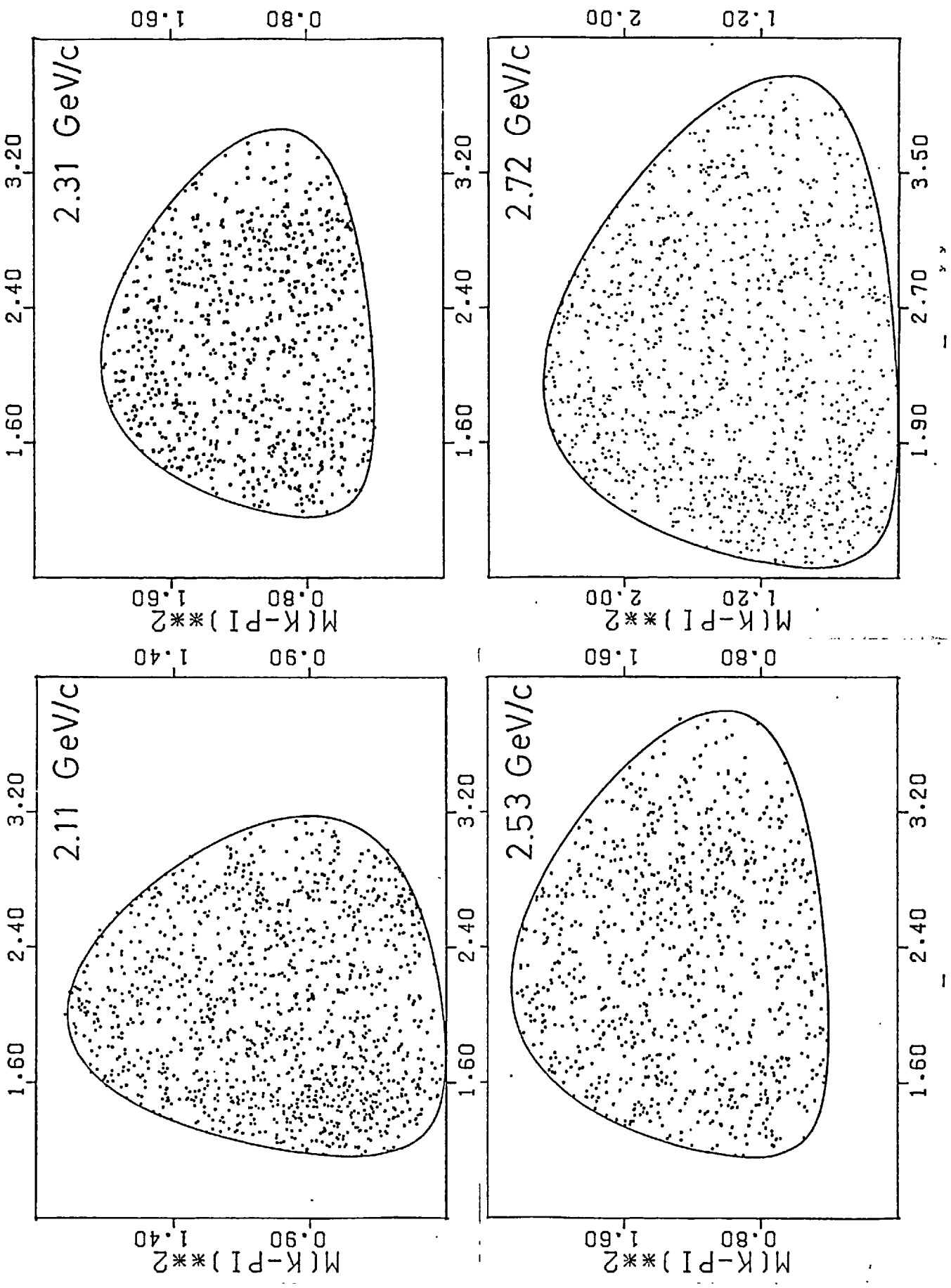

resonance, the exotic Z^*, there would be a diagonal band on the Dalitz plot. This is not observed.

4.2 Effective Mass Fitting

The Dalitz plots of each of the three reactions were fitted using a maximum likelihood method. For each event the following function was calculated:

$$\mathcal{L}_j = \sum_i \frac{a_i \cdot (BW)_i \cdot (PH)}{N} + \frac{1 - \sum_i a_i}{A} \quad - (4.1)$$

a_i : production intensity (fraction) of resonance i.

(BW) : Breit-Wigner function for resonance i.

(PH) : an inverse phase space term, to be discussed.

N : a normalization factor.

A : the area of the Dalitz plot.

This expression ignores interference between resonances.

The summation over i is a summation over contributions from the various quasi-two body resonance components. The second term represents phase space, the genuine three body state. The normalization factor consists in an integral over the plot,

$$N = \int\int BW(\omega_1) \cdot (PH) \quad d\omega_1^2 \quad d\omega_2^2 \quad - (4.2)$$

where ω_1 and ω_2 are effective masses. A is a special case of this as the area of the plot is given by

$$A = \int\int d\omega_1^2 \quad d\omega_2^2 \quad - (4.3)$$

These integrations were, in fact, carried out by a numerical method involving summation over small segments. Having obtained $\mathcal{L}_j$, the likelihood function to be maximised

is

$$L = \prod_j \mathcal{L}_j W_j$$

where W_j is the weight of event j as calculated via an ambiguity resolution or from a seen K^o decay. For convenience, the negative logarithm of L was minimised using the CERN optimising program MINUIT.

The Breit-Wigner expression was that used by Jackson[21]:

$$BW(\omega) = \frac{\pi^{-1}\,\omega_0\,\Gamma(\omega)}{(\omega_0^2 - \omega^2)^2 + \omega_0^2\Gamma^2(\omega)} \qquad -(4.4)$$

where ω_0 is defined as the mass of the resonance and $\Gamma(\omega)$ is the width (full width at half height) defined by an integration over a decay vertex amplitude V for the resonance as

$$\Gamma(\omega) = \frac{1}{32\pi^3} \cdot \frac{1}{2J+1} \sum \int |V|^2 \frac{q}{\omega}\, d\Omega_{12} \qquad -(4.5)$$

J is the angular momentum of the resonant state. q is the resonance-system momentum of either of the decay particles, the expression q/ω is the available phase space for a two body decay. The integration is over the decay angles of the two body phase space and the summation is over the spins of the resonance and decay particles.

If the two body decay of the resonance proceeds via a partial wave of orbital angular moment l the width may be parametrised as

$$\Gamma(\omega) = \Gamma_0 \left(\frac{q}{q_0}\right)^{2l+1} \cdot \frac{\rho(\omega)}{\rho(\omega_0)} \qquad -(4.6)$$

Γ_0, the width at $\omega = \omega_0$ is a constant to be fitted for. q_0 is the resonance system internal momentum q when $\omega = \omega_0$.

The second term is then an angular momentum barrier for the resonance decay. P wave decay was used for both K^* and Δ. The function $\rho(\omega)$ used was that as found from lowest order perturbation theory i.e.

(i) for $K^* \longrightarrow K\pi$ or $(1^-) \longrightarrow (0^-)\ (0^-)$

$$\rho(\omega) = \omega^{-1} \qquad -(4.7)$$

(ii) for $\Delta \longrightarrow P\pi$ or $(\frac{3}{2}^+) \longrightarrow (\frac{1}{2}^+)\ (0^-)$

$$\rho(\omega) = \frac{(\omega + M)^2 - m^2}{\omega^2} \qquad -(4.8)$$

where M is the mass of the $(\frac{1}{2}^+)$ particle (proton) and m that of the (0^-), (pion).

As such, this neglects the presence of any vertex form factor in the decay.

As is clearly implied, the Breit-Wigner expression as commonly used (4.4) explicitly contains a factor for the phase space decay of a resonance into two particles. This is quite correct when fitting effective-mass histograms, but in fitting the Dalitz plot where phase space is uniform only the square of the matrix element is wanted. This is given by dividing out the two body phase space from (BW) at every point on the Dalitz plot by introducing

$$\text{PH}\quad(\omega) = \frac{\omega}{q} \qquad -(4.9)$$

The complete expression should then be multiplied by the decay angular distribution $W(\cos\theta_d)$. The decay angle, θ_d, is defined as the angle, measured in the resonance system, made by the decaying pion from the resonance to the line of flight of the resonance in the centre of mass system:

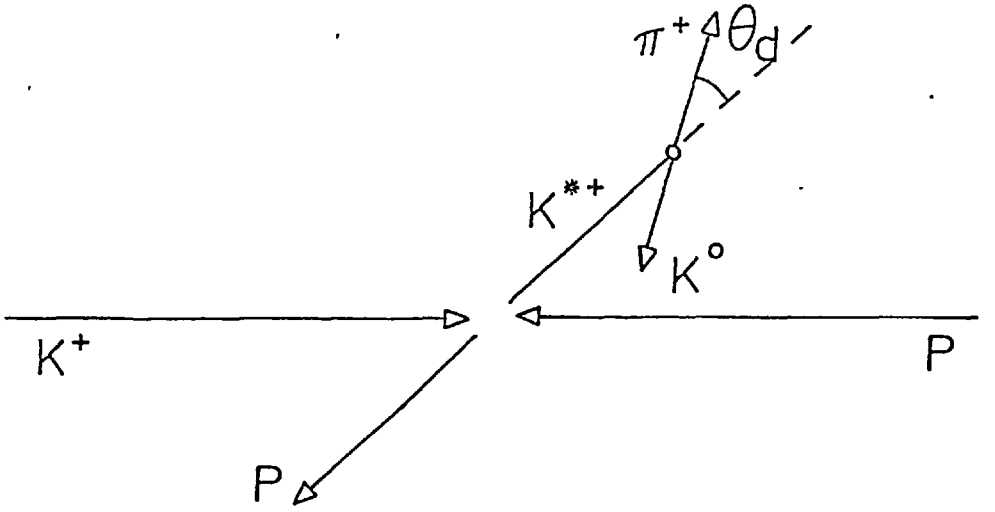

Fig. (8) shows, for a sample of events from the $PK^o\pi^+$ channel at 2.72 GeV/c, that the distribution of cos θ_d is almost isotropic. For this reason, the term $W(\cos\theta_d)$ has been ignored.

Jackson points out that the vector exchange model of Sakurai and Stodolsky[21] leads to a factor P^{*3}, P^* being the centre of mass system momentum of the resonance, as the phase space factor in differential cross-section predictions. An integration of $(BW(\omega) \times PH(\omega))$ over a strip of Dalitz plot gives the usual P^* phase space dependence so, following Bomse et al[3], an additional factor P^{*2} has been introduced to the (PH) factor at least for Δ production. In the case of the K^* there is evidence for both vector and pseudo-scalar exchange (see Chapter 7) and, although the former dominates, better likelihoods were obtained without the additional factor. Results are, therefore, quoted without this term in Table (4) where all the Dalitz plot fits are summarised. For the purposes of defining errors in the parameters in this table, a change $\delta(-\log_e L) = .5$ has been used. As may be seen from this summary, the results obtained show a K^* of rather

Fig. 8. Resonance Decay Distributions.

(a) Decay angle of π in K^* system.

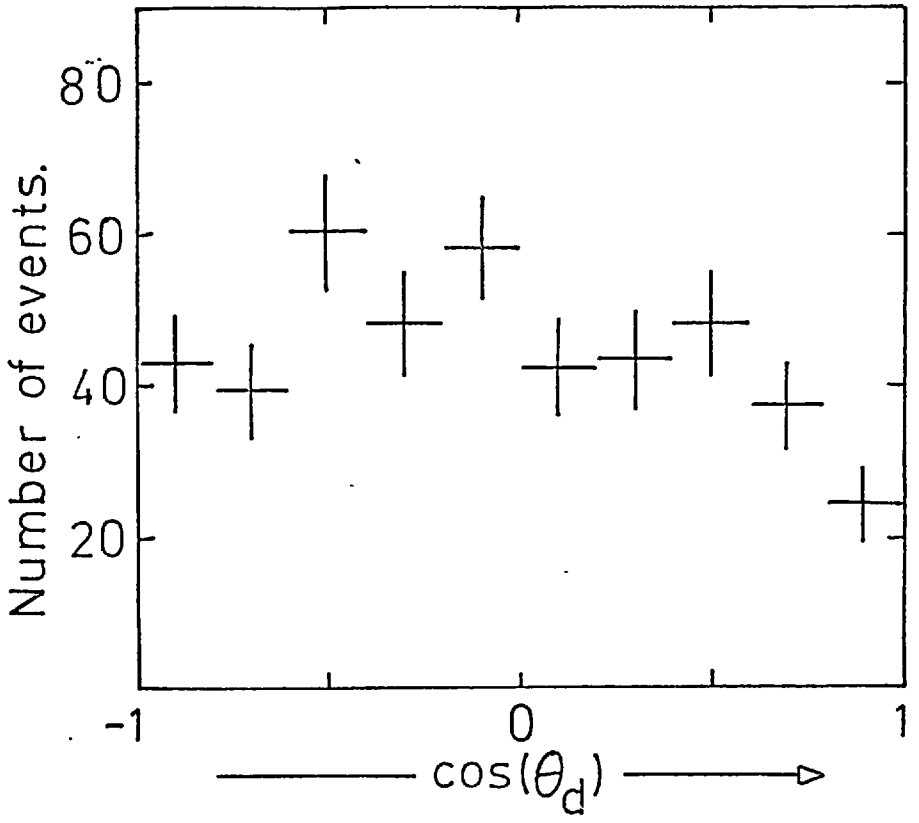

(b) Decay angle of π in Δ system.

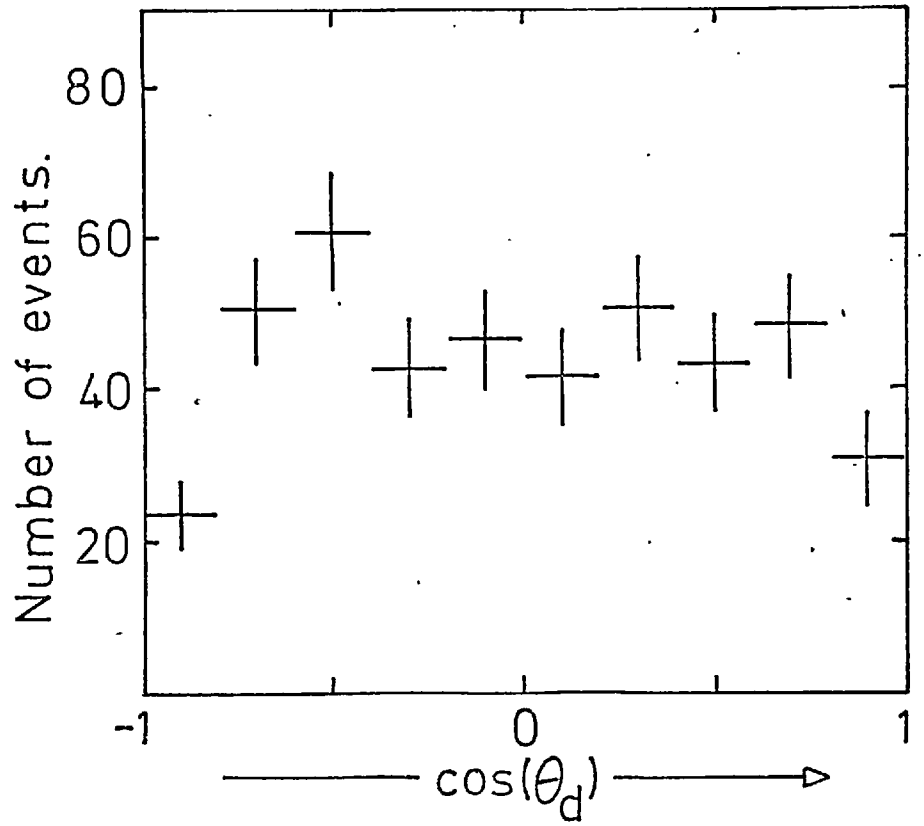

TABLE 4.

Summary of Results of Dalitz plot fits

"FIXED" implies that values from the current review of particle properties[19] have been imposed as the Δ signal is too small for a stable convergence. They are: Mass (Δ) = 1236.0 MeV/c^2; Width (Δ) = 120.0 MeV/c^2

Channel	P_{lab}	% K^*	Mass (K^*)	Width(K^*)	% Δ	Mass (Δ)	Width (Δ)	Events	-log L
$PK^0\pi^+$	2.11	40.1±2.0	902.4±1.7	67.6±5.9	36.6±1.5	1227.8±2.4	81.9± 8.2	2824	1355
	2.31	40.2±2.2	897.3±1.6	55.8±5.1	31.1±1.8	1228.9±4.2	106.9±16.3	1952	1485
	2.53	35.5±2.1	902.8±1.9	56.8±5.7	28.4±1.6	1227.9±3.3	86.0±11.8	1880	2031
	2.72	33.6±1.5	899.3±1.8	61.9±0.7	26.9±1.4	1224.0±2.9	82.8±10.7	2391	3188
$PK^+\pi^0$	2.11	38.4±2.4	901.2±1.7	47.8±4.8	16.5±1.9	FIXED		1471	1170
	2.31	38.7±2.8	896.0±2.3	55.1±6.8	13.7±2.1	FIXED		1093	1222
	2.53	34.0±2.3	899.6±2.9	61.9±7.9	10.5±1.9	FIXED		1067	1627
	2.72	28.6±1.9	896.4±0.2	55.1±1.6	8.0±1.6	FIXED		1406	2557
$NK^+\pi^+$	2.11	NO K^*			14.2±2.1	FIXED		1231	1194
	2.31				8.8±2.3	FIXED		847	1046
	2.53				6.3±2.0	FIXED		873	1360
	2.72				11.6±0.9	FIXED		1163	2080

higher mass than noted in the Rosenfeld tables[19] and a Δ somewhat light and narrow. Where noted fits were also tried fixing the masses and widths of the resonances at the above values and varying only the resonance fraction. This was especially necessary for the $PK^+\pi^o$ and $NK^+\pi^+$ channels where small signal to noise ratios for the resonances made fits somewhat unstable.

For a better comparison with the data these fits are projected out on to effective mass histograms for the three channels at four momenta Figs. (9a, b, c, d). Histograms of the error on effective masses show that the mass resolution of the experiment is ~ 10 MeV/c^2 for $(K\pi)$ masses and 10 to 20 MeV/c^2 for $(P\pi)$ masses from 1 constraint fits. Figs. (9a, b, c, d) display data in bins of 20 MeV/c^2. It is interesting to note that there was no appreciable improvement of mass resolution in data measured on the H.P.D., probably because of the gross effects of the imposition of external errors common in the CERN reconstruction programs.

4.3 Kappa Production

As has been noted, for the most part the effective mass histograms are consistent with no resonances other than the well-established $K^*(892)$ and $\Delta(1236)$. The 2.11 GeV/c raw data, however, shows a pronounced bump more than four standard deviations above phase space in the $PK^+\pi^o$ channel. On closer examination this same enhancement is present, to a lesser extent, in the same channel at the other momenta. This occurs at about 720 MeV/c^2 in the $(K^+\pi^o)$ spectrum where previous experiments[22] have reported production of a K-meson,

Fig 9a. 2.11 GeV/c mass histograms.

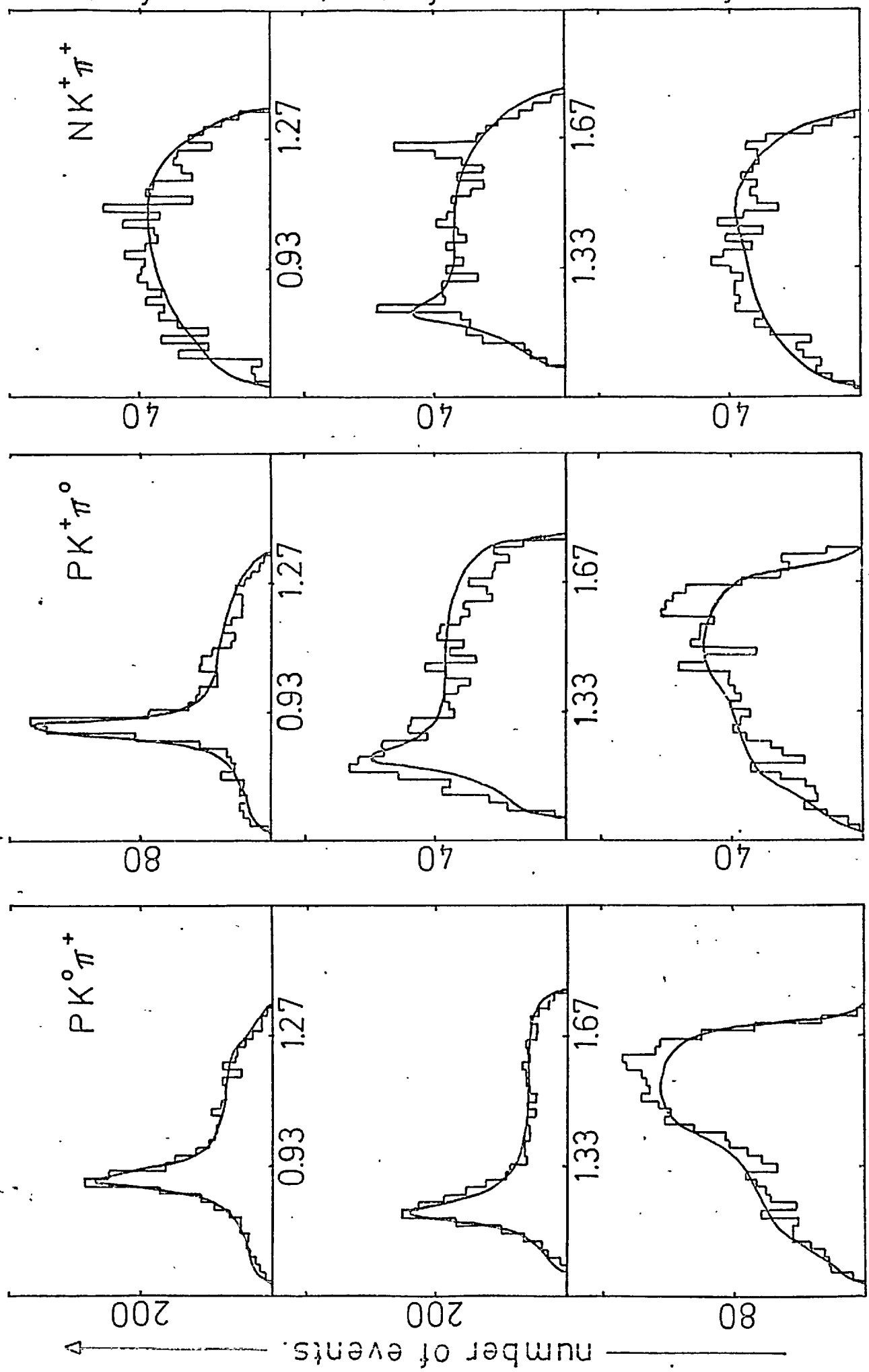

Fig 9b. 2.31 GeV/c mass histograms.

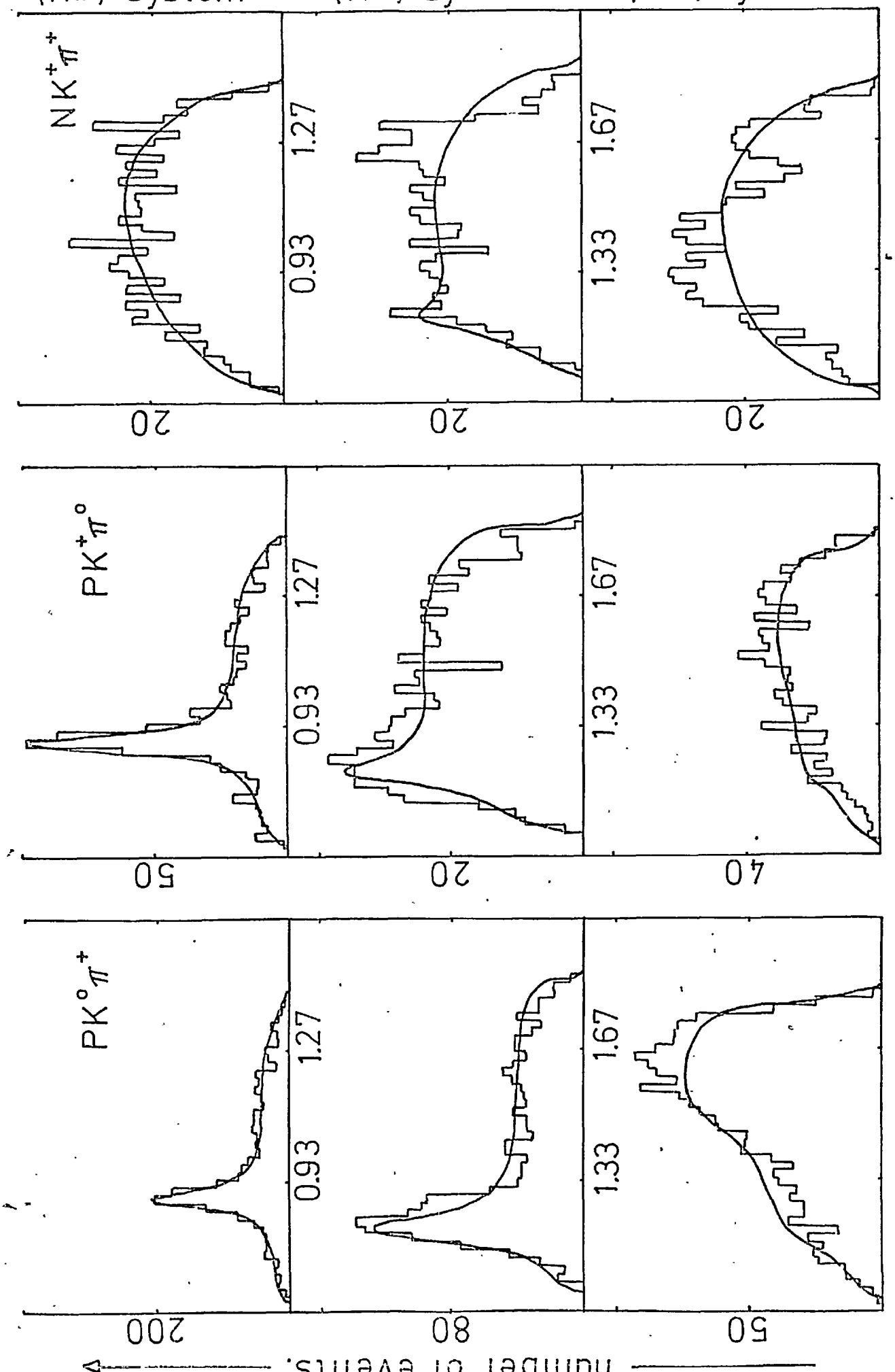

Fig 9c. 2.53 GeV/c mass histograms.

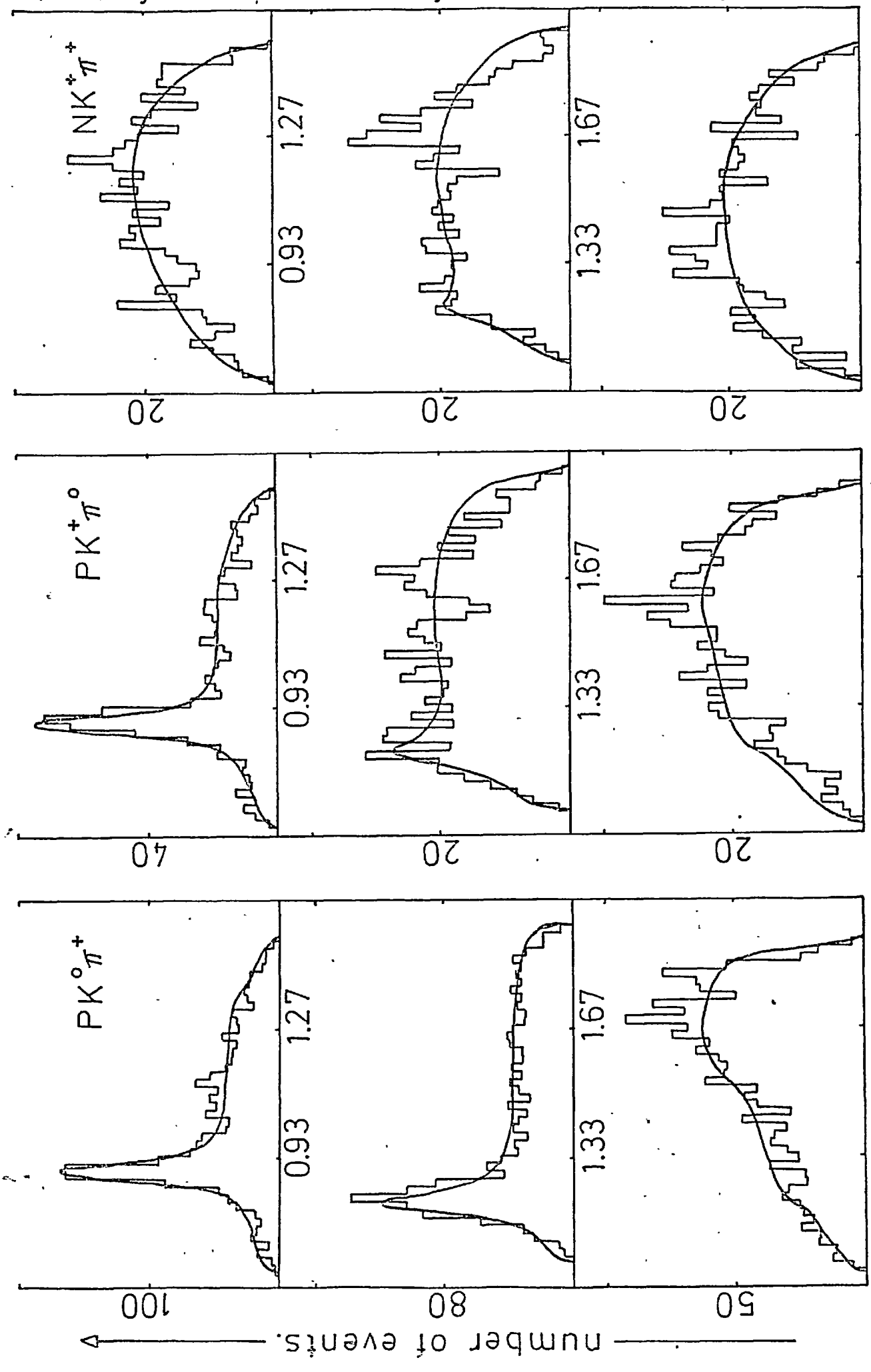

Fig 9d. 2.72 GeV/c mass histograms.

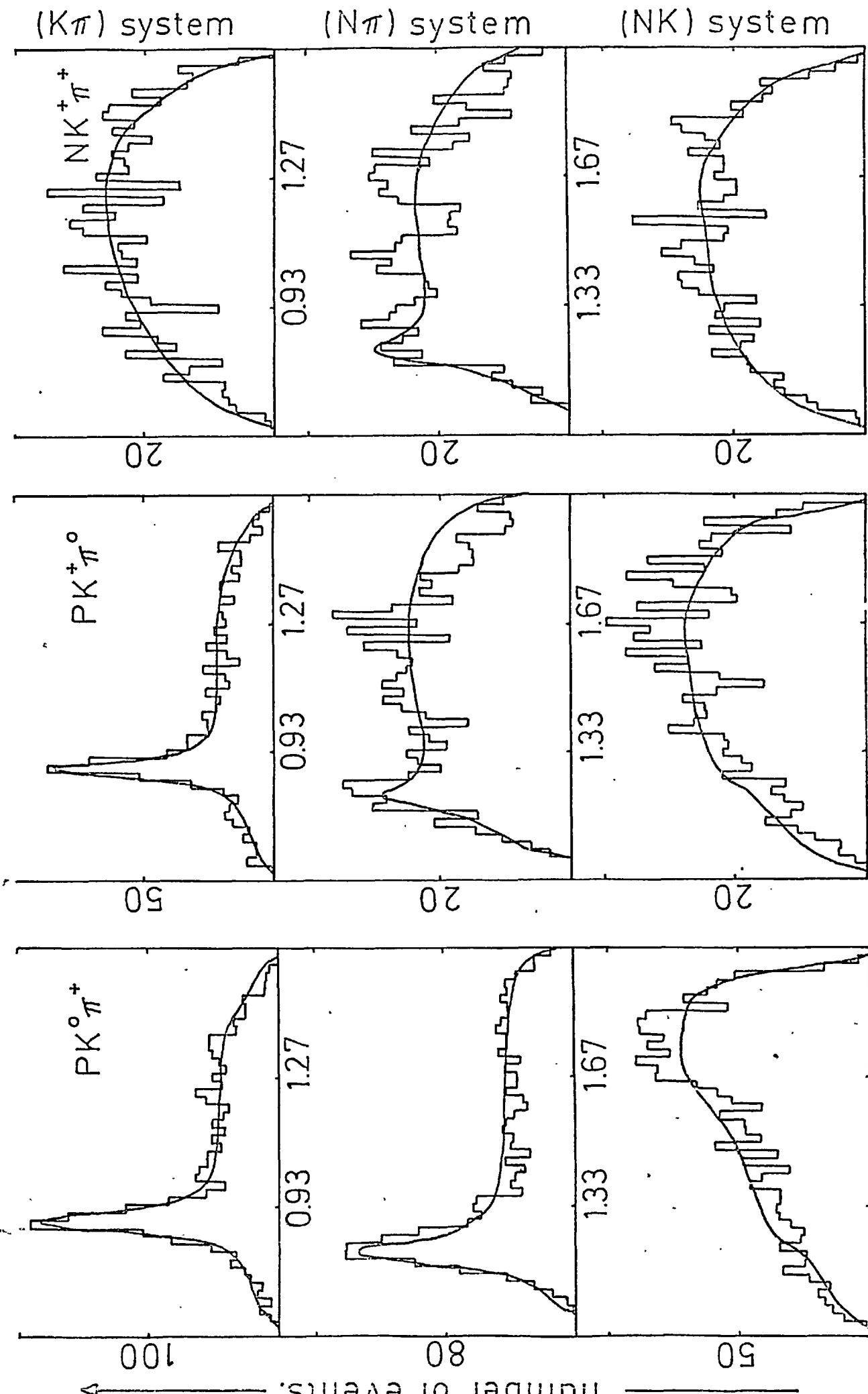

of width varying from 15 to 50 MeV/c^2. Indeed, when the possibility of such a resonance is allowed the fitting program converges with the parameters:

Mass $(K) = 697 \pm 6$ MeV/c^2

Width $(K) = 66 \pm 27$ MeV/c^2

Fraction $(K) = 11 \pm 2$ %

This is seen in Fig. (10a). More recently the K meson seems to have been largely discredited.[20,23] When the $PK^0\pi^+$ and $NK^+\pi^+$ states are examined it is seen that there is no sign of any such enhancement. The latter case merely indicates the iso-spin of any kappa would not permit a doubly charged state, but the former case is most suspicious as Clebsch-Gordan coefficients would rather tend to favour decay of a K^+ into $K^0\pi^+$ rather than $K^+\pi^0$, accepting a half-integral total iso-spin in order to get the z-component of the final state $= {}^1/2$. Because of this, all of the events in the K peak were examined at the output stage of the kinematics fitting program, GRIND. The vast majority of these fits were, in fact uniquely choiced confirming that the method of resolving ambiguities was not at fault. However, a large percentage of these events had failed an elastic 4 constraint fit purely by rejection of an over-large χ^2, i.e. as a result of the confidence-level cut at 0.25%. In all cases this fit was with the mass assignment of the charged tracks reversed. See Fig. (10b,c). At this stage it is instructive to investigate the effect this has on the fitting procedure. Most elastic events are strongly peaked in the forward direction i.e. they often resemble the topology of Fig. (10b) with the K^+ going essentially forward, little diverted from the original beam direction, and the hydrogen

Fig 10. Kappa Meson Production.

(a)

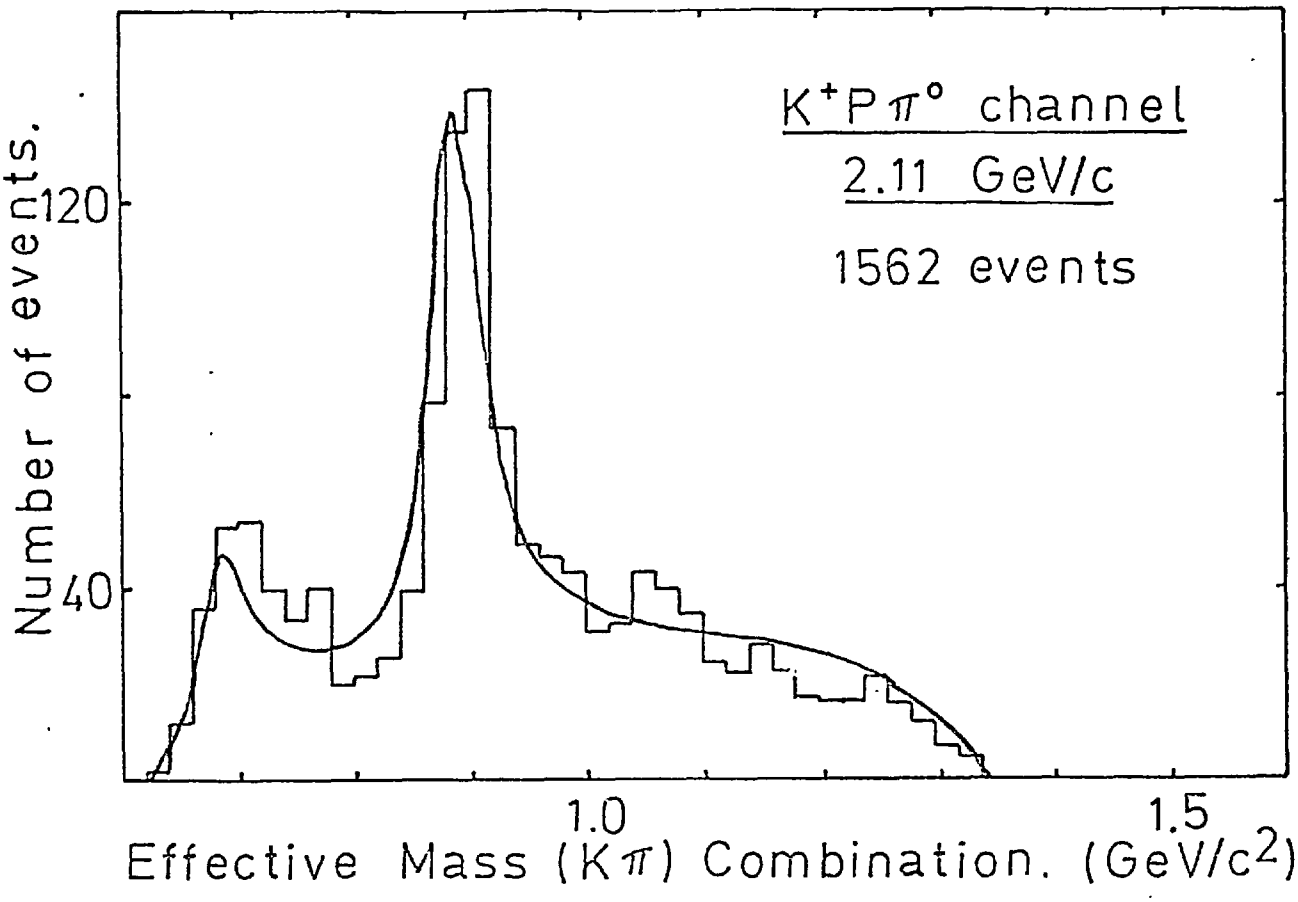

(b)

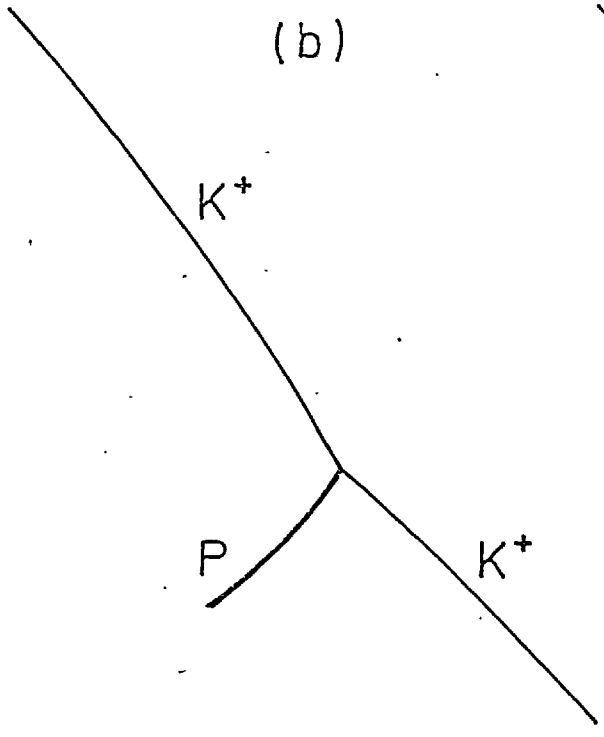

(c)

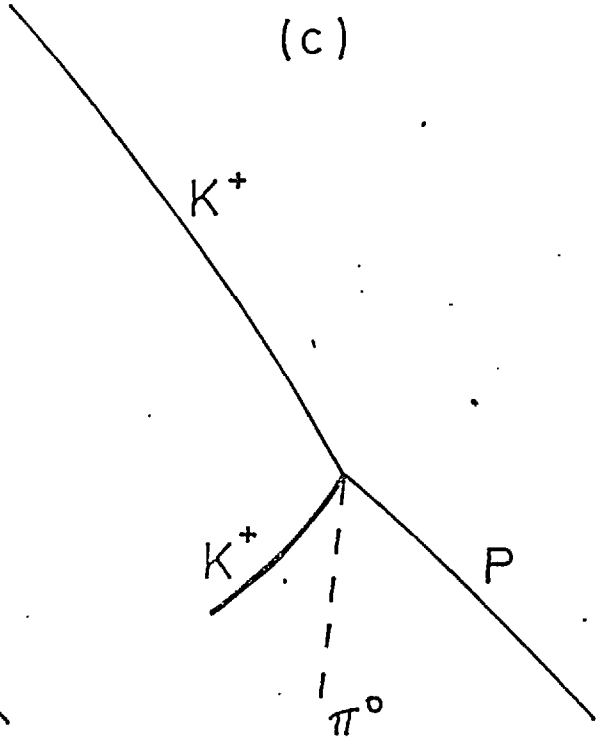

nucleus, the proton, recoiling slowly. The effect is similar though not so marked, in the three body case when an extra pion is produced. It is now possible to swop the mass assignments of the charged tracks to get the topology of Fig. (10c). If the forward going track has a momentum $>$ 1300 MeV/c and the other track has momentum $<$ 350 MeV/c these conditions are virtually indistinguishable on ionisation grounds. There would be a much smaller region of error if one of the tracks were a pion. In both cases the incoming energy of the incident kaon is the same, but replacing the higher momentum track with a heavier particle and vice versa has the net effect of increasing the available energy, and hence the missing mass squared, of the event. The extent of this effect can be seen by taking a typical case, i.e. a kaon of momentum $\sim$ 1500 MeV/c and a proton of momentum $\sim$ 350 MeV/c. The energy difference on opposite identification may be calculated using the relativistic energy, E, formula in terms of mass, m, and momentum, p, of a particle, $E = \sqrt{m^2 + p^2}$.

Energy difference in mistaking forward track:

$$= E_K - E_p = \sqrt{0.24 + 2.25} - \sqrt{0.88 + 2.25} = -0.19 \text{ GeV}$$

Energy difference in mistaking slow track :

$$= E_p - E_K = \sqrt{0.88 + 0.12} - \sqrt{0.24 + 0.12} = 0.40 \text{ GeV}$$

Net energy gain 0.21 GeV.

Thus, by miss-assigning masses there is an apparent energy, or missing mass gain of around 200 MeV. It would then be possible for the kinematics program to fit an extra π^0 particle (mass $\sim$ 140 MeV/c^2) of very low momentum. Again, with thoughts of the other two channels in mind it is

extremely unlikely for a situation to arise to generate sufficient missing mass to fit an extra K^o or neutron. The low energy π^o and the low momentum K^+ of the misidentified event would then tend together to make a low effective-mass enhancement, the kappa. This theory can be readily checked because of the peculiar attributes of the misidentified events. Indeed it was found that the events in the kappa enhancement accounted for unnaturally large bumps of forward going protons, slow moving kaons and practically stationary pions - in the centre of mass system these pions clustered in a very sharp peak of $\cos\theta^* \leqslant -0.92$, otherwise a quite uniform distribution. The final piece of evidence comes from histogramming the angle between the beam track and the normal to the plane of the charged particles, see Fig. (11). For genuine three body events this forms a normal distribution of half-width at half height of 0.25 radian about $\pi/2$. For elastic events the width is 0.02 radian and 80% of the kappa events lie in this region. With a series of tests based on coplanarity and the other properties, it is possible to exclude only the misidentified events with ~ 95% efficiency. This was then done to obtain the results of Table (4).

4.4 Quasi two body cross-sections

Using the results of Table (4) for the fractions of the resonances produced and those of Table (3) for the channel cross-sections, it is a simple matter to calculate the quasi two body cross-section results. This is done in Table (5).

Fig.11 Coplanarity Angle Histograms.

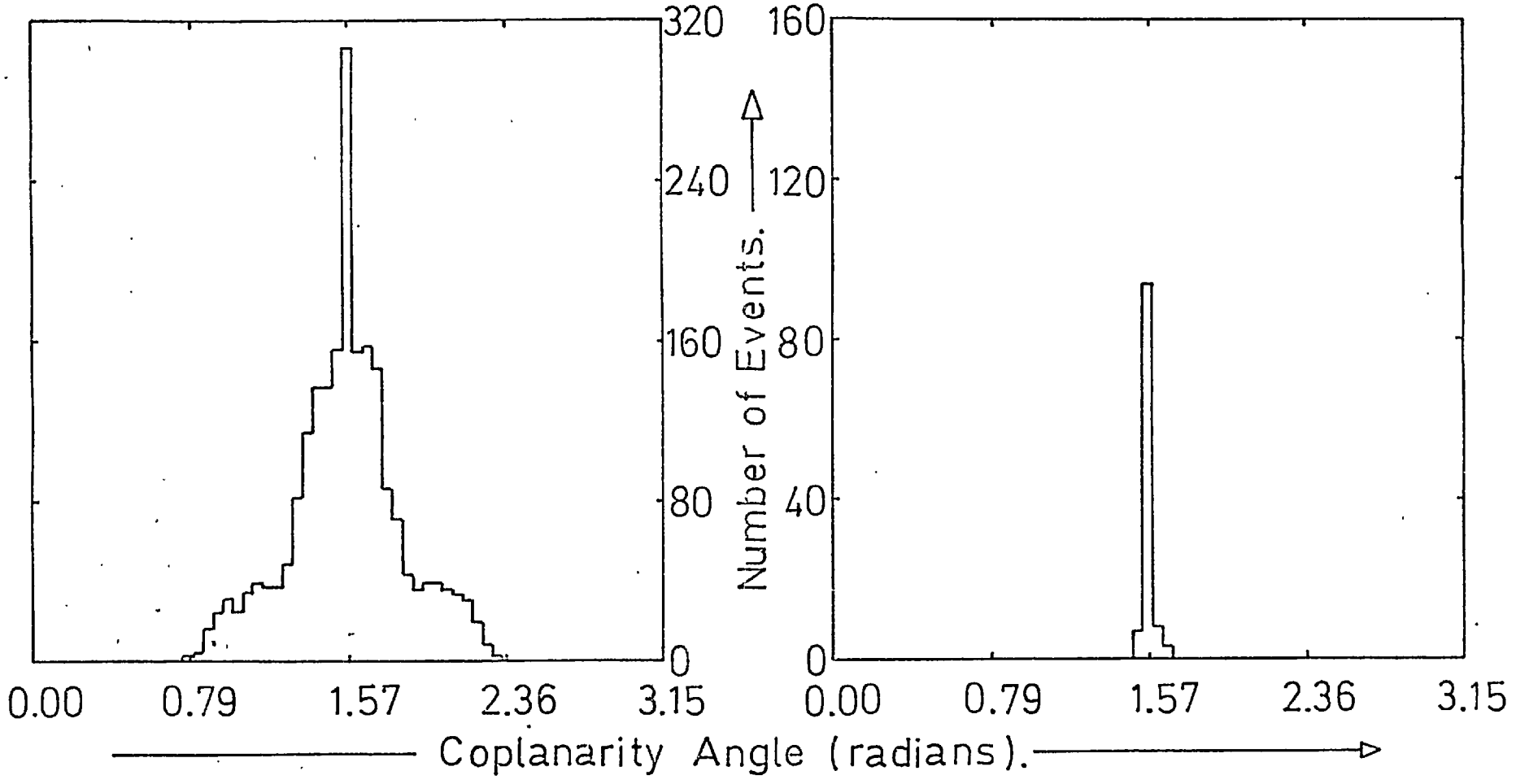

Sample of all 3-body events.

$0.66 < M(K^+\pi^0) < 0.76$, $K^+P\pi^0$ events.

TABLE 5. Quasi two body cross-sections

All cross-sections in mb. Total cross-sections derived from seen K^o (a) events only

K^*

$P_{lab.}$ (GeV/c)	2.11	2.31	2.53	2.72
(a) $\sigma_{K^{*+}\to K^o\pi^+}$	1.60±.16	1.37±.16	0.95±.11	0.93±.10
(b) $\sigma_{K^{*+}\to K^+\pi^o}$	0.68±.12	0.45±.08	0.46±.09	0.31±.05
2 x $(\frac{b}{a})$	0.84±.23	0.66±.20	0.98±.30	0.67±.20
$\sigma_{K^{*+}(total)}$	2.40±.24	2.06±.24	1.42±.17	1.39±.15

Δ

$P_{lab.}$ (GeV/c)	2.11	2.31	2.53	2.72
(a) $\sigma_{\Delta^{++}\to p\pi^+}$	1.47±.14	1.07±.13	0.76±.09	0.75±.08
(b) $\sigma_{\Delta^{+}\to p\pi^o}$	0.29±.06	0.16±.04	0.14±.04	0.09±.03
(c) $\sigma_{\Delta^{+}\to n\pi^+}$	0.18±.05	0.11±.04	0.05±.02	0.12±.02
9 x $(\frac{b}{a})$	1.77±.58	1.36±.52	1.69±.70	1.06±.44
9 x $(\frac{c}{a})$	1.12±.39	0.90±.44	0.65±.36	1.41±.42
$\sigma_{\Delta(total)}$	1.96±.18	1.43±.17	1.01±.12	0.99±.11

The errors quoted are compounded from the statistical error on the cross-sections and the fit errors on the resonance fractions. For these purposes masses and widths corresponding to the Rosenfeld tables [19] were assumed for the Δ, except for the $pK^o\pi^+$ final state.

The results of Table (5) are presented in a way which invites easy comparison with the Clebsch-Gordan coefficients predictions mentioned in (4.1). Within the large errors there is reasonable agreement. This forms in some way an independent check on the method of resolving ambiguities, though Sällström et al[24] point out that interference between the general $T = \frac{1}{2}$ $(K\pi)$ state and the $T = \frac{3}{2}$ $(K\pi)$ state can alter observed branching ratios. A similar situation can occur in the $(P\pi)$ state.

At 2.97 GeV/c they quote:

$$\frac{(K^{*} \rightarrow K^{+}\pi^{o})}{(K^{*} \rightarrow K^{o}\pi^{+})} = 0.43 \pm 0.11$$

$$\frac{(\Delta^{+} \rightarrow N\pi^{+})}{(\Delta^{+} \rightarrow P\pi^{o})} = 0.05 \pm 0.20$$

which agree, within errors, with the values given in Table (5).

The cross-sections as derived from this experiment are shown together with all other published data[33] in Fig. (12), for Δ production, and Fig. (13), for K^{*+} production. The behaviour of both is similar, viz. a swift rise after threshold and then a steady fall as the high energy region is approached. This energy dependence is commensurate with the Regge pole prediction as will be discussed in Chapters 6 and 7. Considering that the resonant cross-section for production of an exotic state is a fraction of a millibarn, the errors are rather too large to say whether or not such a state exists in either of these two inelastic channels. The peak in $K\Delta$ production together with processes occurring in other channels has been used[12] to explain the presence of the first, large, peak in total cross-section at $P_{lab.} = 1.25$ GeV/c.

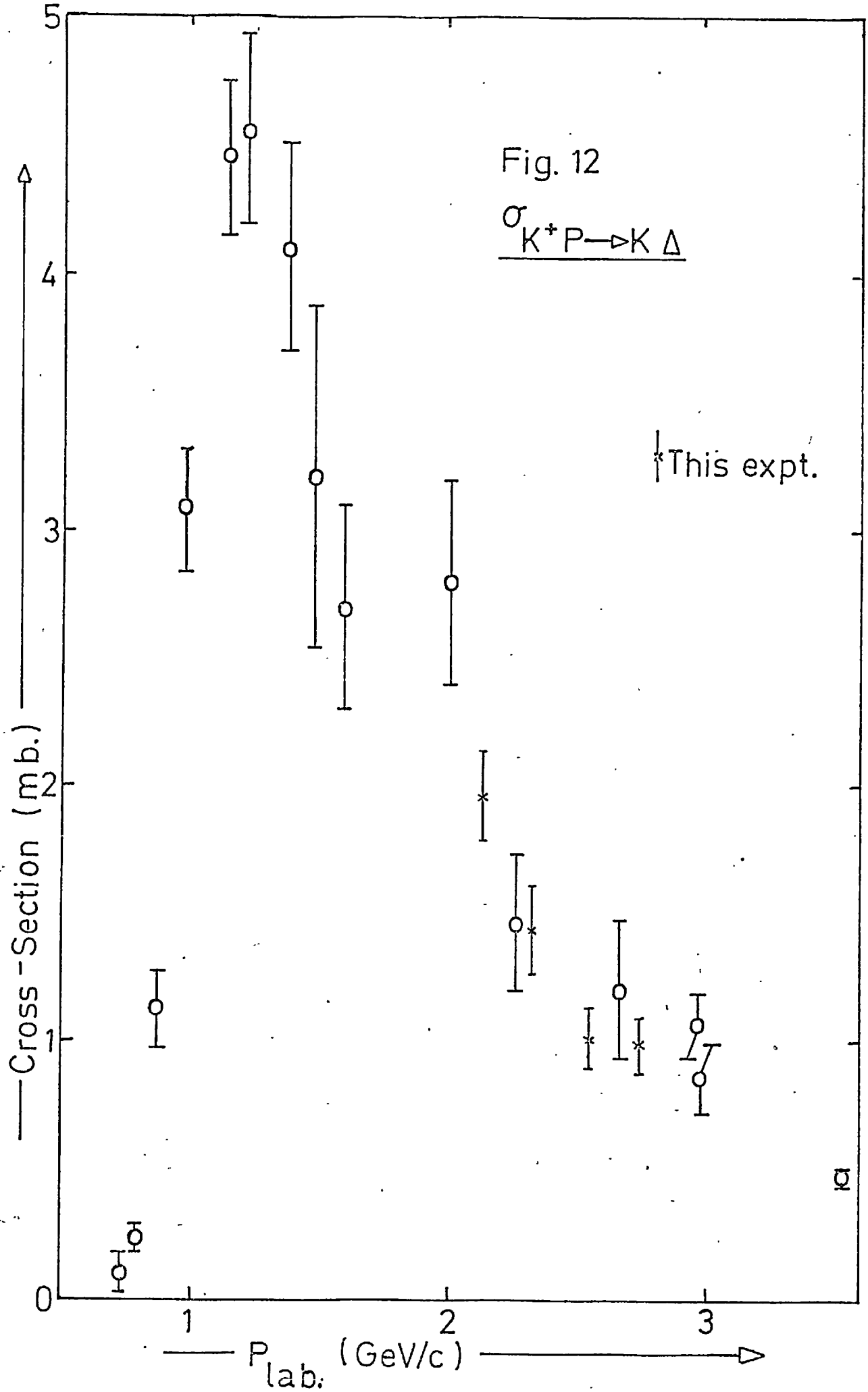
Fig. 12
$\sigma_{K^+P \to K\Delta}$
This expt.
Cross-Section (mb.)
$P_{lab.}$ (GeV/c)
0
1
2
3
4
5

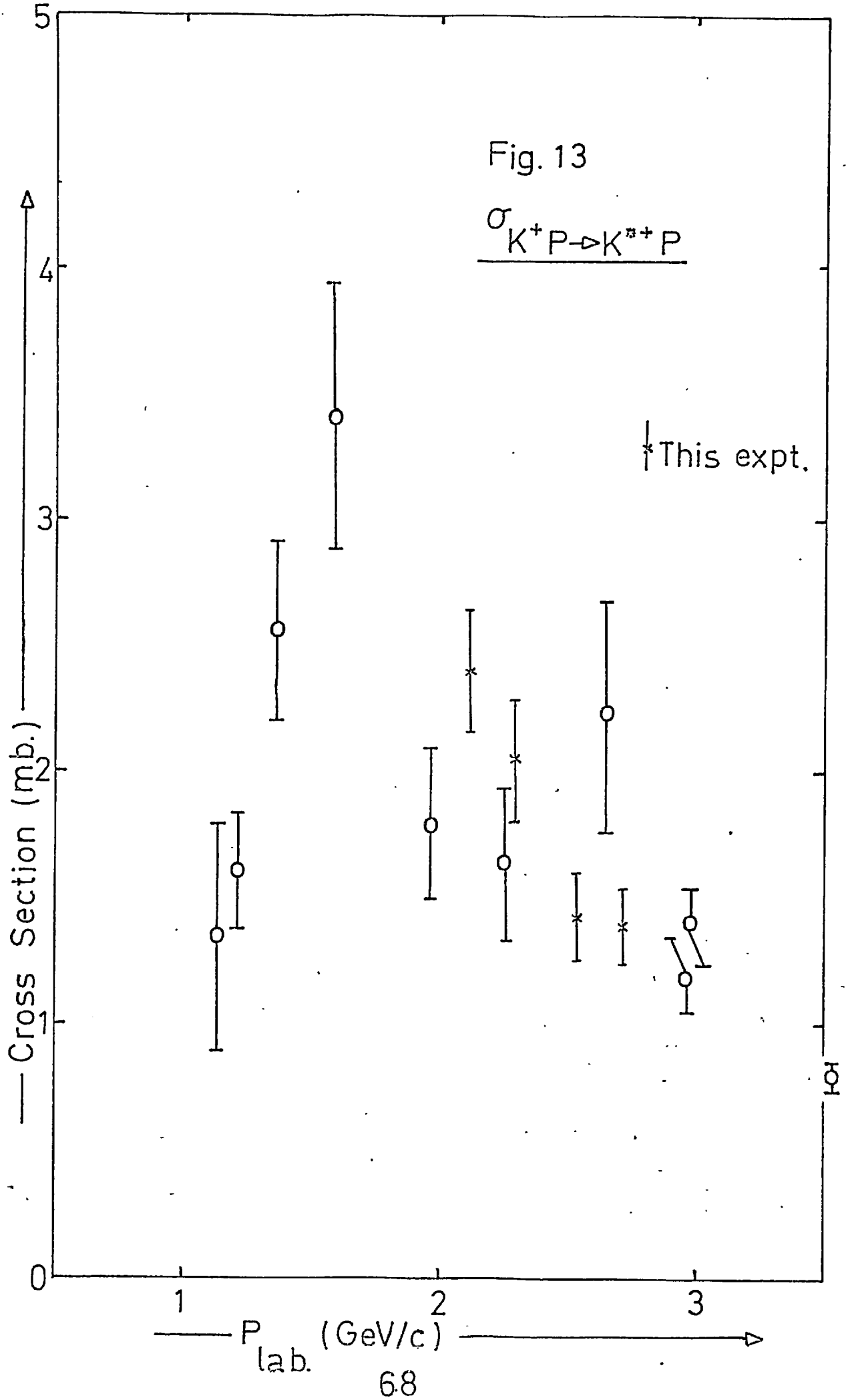
Fig. 13
$\sigma_{K^+P\to K^{*+}P}$
This expt.
Cross Section (mb.)
$P_{lab.}$ (GeV/c)
0
1
2
3
4
5
1
2
3

CHAPTER 5

PRODUCTION ANGULAR DISTRIBUTIONS

5.1 Methods of Analysis

To begin a systematic study of the production of the chief resonances the $K^*(892)$ and $\Delta(1236)$, the distribution of the centre of mass scattering angle θ^* is investigated. In the case of the K^* this is defined as the divergence from the meson line of flight, and for the Δ from the baryon line of flight in the centre of mass (See below Fig. (14)).

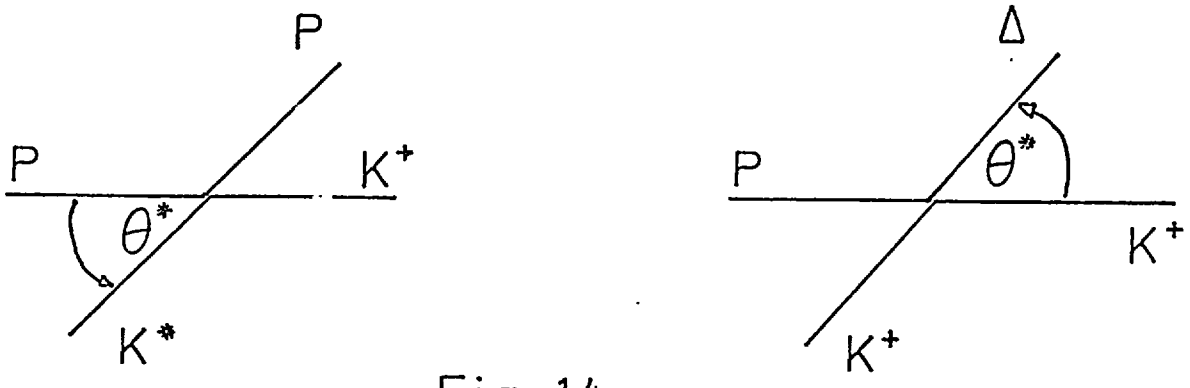

Fig. 14.

This convention has the advantage of showing the qualitative similarity of the two distributions. Both resonances are produced quite peripherally, the K^* "forward" in the centre of mass and the Δ "backwards".

The distribution of cos θ^* forms a differential cross-section. Assuming azimuthal symmetry about the incident direction,

$$\frac{d\sigma}{d\Omega} = \frac{\sigma}{2\pi N} \cdot \frac{dN}{d(\cos\theta^*)} \qquad \text{(5.1)}$$

Where σ is the resonance cross-section and N is the total number of events in the distribution, both constant. To investigate the detailed variation of $dN/d(\cos\theta^*)$ with

momentum it is expanded into the set of orthogonal Legendre polynomials:

$$\frac{dN}{d(\cos\theta^*)} = \sum_{m=0} A_m P_m(\cos\theta^*) \qquad \text{——————(5.2)}$$

Of course it is possible to express the differential cross-section in terms of a pure polynomial in $\cos\theta^*$, but the use of orthogonal functions imposes at least one very useful constraint. The n th term in the series theoretically will give the best fit to the accuracy of $(\cos\theta^*)^n$, the addition of more terms to the series will improve the accuracy of the overall fit but will not change the value of A_n. In practice, with some fitting methods, the value of A_n does change slightly. This is a reflection on poor statistics.

The orthogonality of Legendre polynomials also supplies a computationally very fast method to compute the A_m, this is the method of moments.[25]

Multiplying (5.2) by $P_n(\cos\theta^*)$ and integrating over the complete range of $\cos\theta^*$:

$$\int_{-1}^{1} \frac{dN}{d(\cos\theta^*)} \cdot P_n d(\cos\theta^*) = \int_{-1}^{1} \sum_m A_m P_m P_n \, d(\cos\theta^*) \quad -(5.3)$$

Now the ortho-normality relation is

$$\int_{-1}^{1} P_m P_n \, d(\cos\theta^*) = \frac{2}{2n+1} \cdot \delta_{mn} \qquad \text{——(5.4)}$$

Hence,

$$\int P_n \, dN = \frac{2}{2n+1} \cdot A_n \qquad -(5.5)$$

Subject to there being a large number of events and the sample being unbiased,

$$\int P_n \, dN = \sum_{i=1}^{N} P_n \qquad -(5.6)$$

The expression would have to be severely modified if there was a cos θ^* cut through scanning losses etc. This is unlikely to occur when considering the angular distribution of a resonance formed of two stable particles.

We now have,

$$A_n = \frac{2n+1}{2} \cdot \sum_{i=1}^{N} P_n(\cos \theta_i^*) \qquad -(5.7)$$

and in particular

$$A_o = \frac{1}{2} \cdot \sum_{i=1}^{N} P_o(\cos \theta_i^*) = \frac{N}{2} \qquad -(5.8)$$

or,

$$A_{n/A_o} = (2n+1) \cdot \overline{P_n(\cos \theta^*)} \qquad -(5.9)$$

The error on this is given by the error on the mean,

$$\delta\ (A_{n/A_o}) = \frac{2n+1}{\sqrt{N}} \left(\overline{P_n^2} - \overline{P_n}^2 \right)^{1/2} \qquad -(5.10)$$

Expressions (5.9) and (5.10) remain true for samples of weighted events, as used experimentally.

Having computed the A_n for n going from 0 to, say, K parameters, a fitted curve $f(\cos \theta^*)$, may be calculated.

$$f(\cos \theta^*) = \sum_{n=0}^{K} A_n P_n(\cos \theta^*) \qquad -(5.11)$$

To compare this with the data a chi-square is calculated, taking the approximation of Poisson errors on the experimental distribution δN for a given range $\delta \cos \theta^*$

$$\chi^2 = \sum_m \frac{(\delta N - f(\cos \theta^*)\ \delta \cos \theta^*)^2}{\delta N^2} \qquad -(5.12)$$

The summation is taken over m bins of variable width,

$\delta \cos \theta^*$, such that the number of data points δN in the interval is sufficiently great to justify Poisson statistics, i.e. $\delta N \geqslant 20$. In practice this entails bins of width $\delta \cos \theta^* = 0.02$ in the forward direction and $\delta \cos \theta^* = 0.4$ in the centre region where there are fewer events.

The number of degrees of freedom for this χ^2 is $(m - k - 1)$ as $A_o = N/2$ is an additional constraint. From this we may calculate the probability of getting this χ^2 or greater, the confidence level of the fit.

As a diversion, it is interesting to note one of the disadvantages of the χ^2 fitting method, in which the A_n are calculated by minimising the left hand side of (5.12). In one of the obligatory wide bins it is possible to get the same value of $\int f(\cos \theta^*)\, \delta \cos \theta^*$ from widely different solutions. For example, an extreme complete oscillation in the bin will give the same solution, and hence same χ^2, as a flat solution.

Nevertheless, the χ^2 method remains a good one for checking the confidence level of fits obtained by other means. It is especially useful in determining the number of parameters needed to fit the data well. Generally, the χ^2 decreases as the number of parameters increases to a certain point. Beyond this the addition of further polynomials does not appreciably improve the fit to the data so the χ^2 levels off. Simultaneously, the confidence level rises up to the optimum point and then decreases slowly as the χ^2 remains the same but the degrees of freedom go down as the number of parameters goes up.

The number of polynomials contributing is related

to the number of partial waves in the reaction. In general, because of the laws of combination of angular momentum, it is possible to say that the square of an amplitude of spin J contributes to A_n for all even n with $n \leqslant 2J$, and that the interference between two partial waves of angular momentum J_1, J_2 contributes to A_n for $|J_1 + J_2| \geqslant n \geqslant |J_1 - J_2|$.

Physically, there is a semi-classical argument to discover l_{max}, the maximum contributing partial wave, and hence, from knowledge of the spin of the incident state, obtain an order of magnitude for n_{max}.

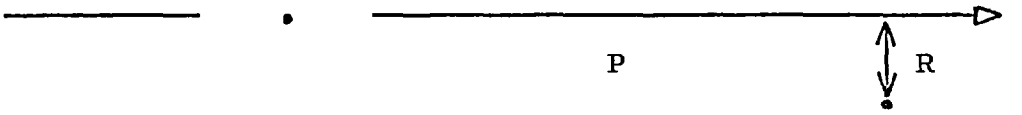

In the above diagram, a particle is approaching the target with an impact parameter R, representing the maximum radius of interaction. If the incident momentum is P then

$$PR \simeq \sqrt{l_{max}(l_{max} + 1)}\,\hbar$$

from which the maximum contributing partial wave may be found. It is common to insert the pion Compton wavelength for R, but as will be shown in Chapters 6 and 7 the reactions $K^+P \rightarrow K^*N$ and $K^+P \rightarrow K\Delta$ are dominated by vector meson exchange so it is more relevant to insert ρ or ω Compton wavelengths to obtain l_{max}. This technique gives a D- wave contribution (l = 2) beginning around P_{lab} = 1.5 GeV/c and affecting up to the A_4 coefficient and, considering spin, possibly A_5 too. At around 2.3 GeV/c l = 3 F-Waves might begin to become significant and these could affect A_6 and possibly A_7.

For speed and ease of computation the method of moments for calculating the (A_n/A_o) was found most convenient.

However, in order to check the basic assumptions of the method, a maximum likelihood program was written. This used MINUIT to maximise the function

$$\mathcal{L} = \prod_{\text{events, i}} \sum_{\text{parameters, k}} A_k P_k(\cos \theta_i^*)$$

with A_o set constant at $N/2$. This method imposes all parameters beyond A_k to be zero and hence the ratios change slightly when k is increased. In practice it was found that so long as sufficient parameters ($k \geq 4$) were being used the values were very constant and differed as little as $\frac{1}{3}$ standard deviation from those obtained from the moments program. Table (6) shows a comparison of answers obtained from the two methods. In general the maximum likelihood method gives smaller errors than the moments method.

5.2 Δ - Production

The experimental production angular distributions for the Δ^{++} produced in all the reactions of final state $PK^o\pi^+$ are displayed in Figs. (15a,b). The continuous lines on these plots represent a four parameter fit by the method of moments.

Throughout all momenta the Δ has been defined using mass cuts on the $(P\pi)$ distribution of,

$$1.18 \text{ GeV/c}^2 < M(P\pi) < 1.28 \text{ GeV/c}^2$$

This means that the resonance, as examined, sits on a background composed of both phase space and some reflection of the K^* in the $(K\pi)$ combination.

It may be seen that the reaction is already quite peripheral even at the lowest momentum, most of the events

Table 6.

COMPARISON OF METHOD OF MOMENTS TO MAXIMUM LIKELIHOOD PROGRAM

Analysis performed on 542 $K^{o}p\pi^{+}$ events from 2.7 GeV/c data.

	MOMENTS	MAXIMUM LIKELIHOOD			
		3 parameters	4 parameters	5 parameters	6 parameters
A_1/A_0	2.012 $\pm$0.054	2.107 $\pm$0.035	2.004 $\pm$0.044	2.007 $\pm$0.034	2.012 $\pm$0.056
A_2/A_0	2.184 $\pm$0.087	1.880 $\pm$0.051	2.160 $\pm$0.074	2.172 $\pm$0.040	2.184 $\pm$0.090
A_3/A_0	1.508 $\pm$0.129	1.675 $\pm$0.092	1.471 $\pm$0.088	1.492 $\pm$0.022	1.507 $\pm$0.137
A_4/A_0	0.520 $\pm$0.159		0.484 $\pm$0.088	0.521 $\pm$0.088	0.532 $\pm$0.159
A_5/A_0	-0.042 $\pm$0.180			0.047 $\pm$0.092	0.051 $\pm$0.146
A_6/A_0	-0.260 $\pm$0.197				0.011 $\pm$0.111

(No background correction, or allowance for Δ^{++} in the above)

Fig 15a.

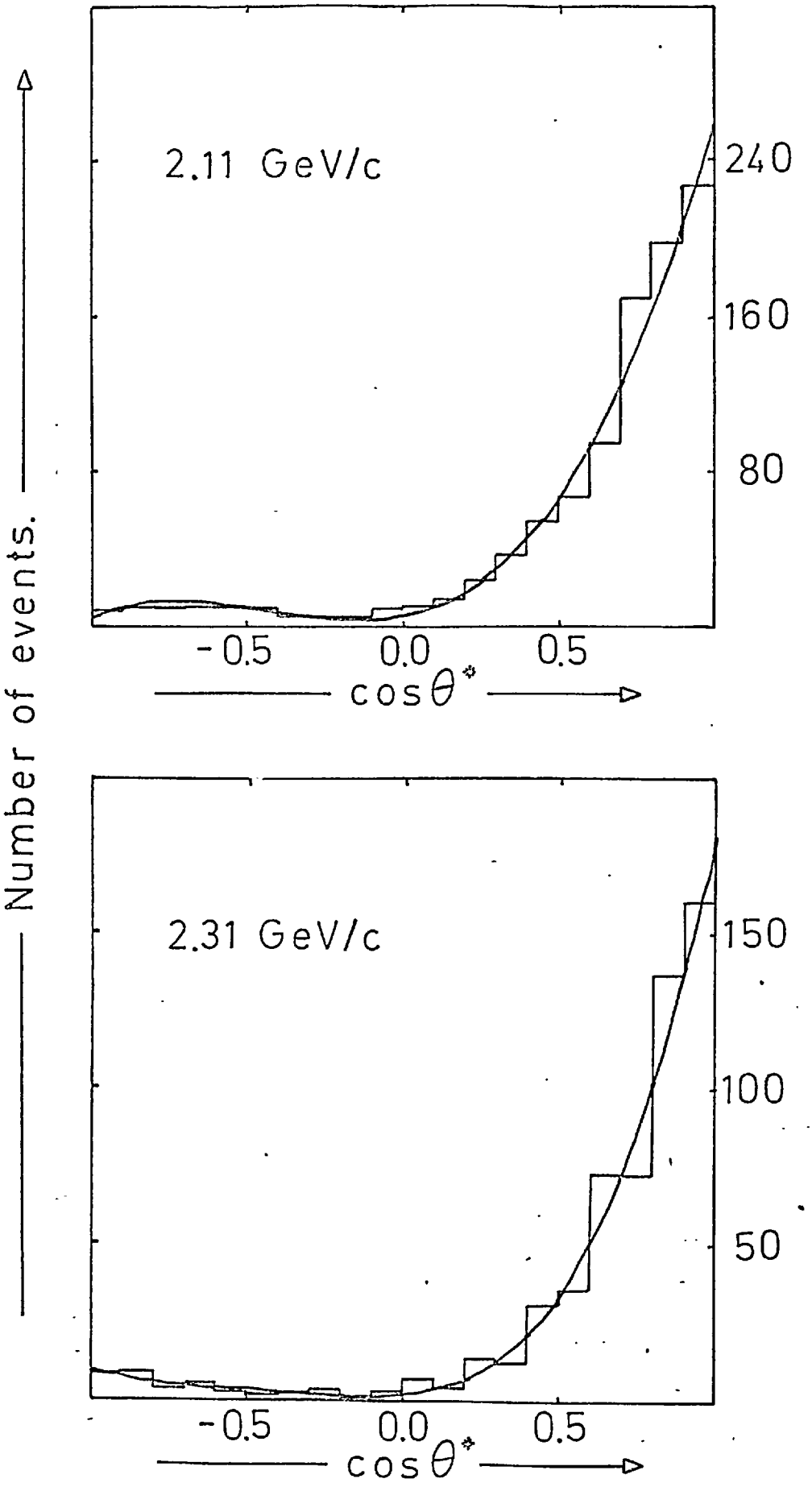

$\Delta^{++}(1236)$ Production angle distribution.

Fig 15 b.

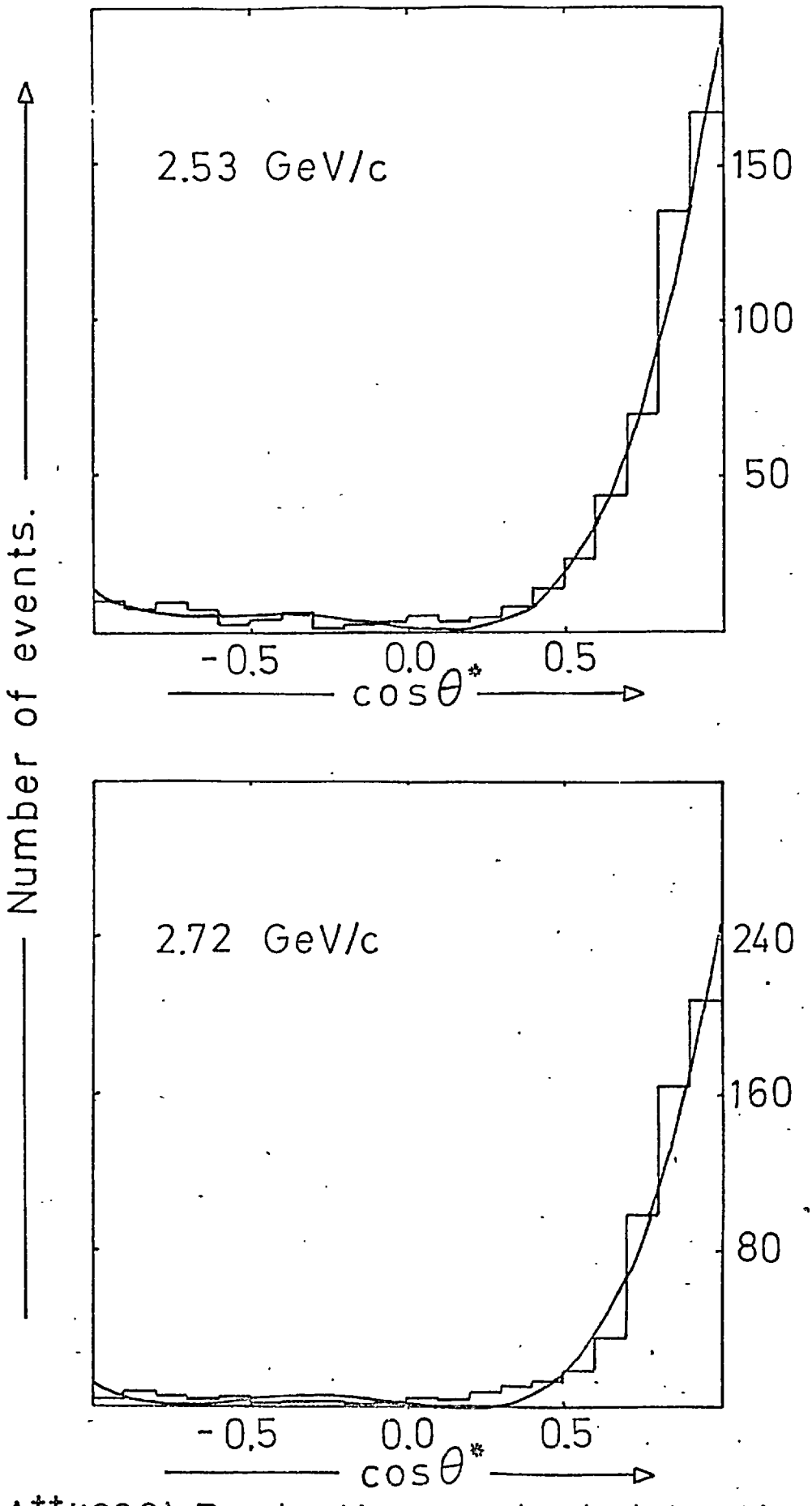

$\Delta^{++}(1236)$ Production angle distribution.

being grouped in the forward peak. There are, however, some events in the backward direction. Chew-Low plots do not indicate that these events are genuinely in the resonance band, it being more likely that they are phase space events included by the mass cuts.

As has already been noted the final state $pK^{o}\pi^{+}$ is the one favoured by Clebsch-Gordan coefficients for study of both major resonances. A check on the $pK^{+}\pi^{o}$ final state shows similar behaviour for the Δ^{+} but no clear Δ^{+} may be seen in the $nK^{+}\pi^{+}$ final state.

The (A_n/A_o) for the Δ^{++}, as calculated by the method of moments, are displayed as functions of momentum in Figs. (16,17). For the first four polynomial coefficients in Fig.(16), there are also five data points from reference (20), taken directly as published, and one data point at 1.97 GeV/c computed by the author, using an amended moments program, from published $\cos\theta^{*}$ histograms.(2)

(A_1/A_o) and (A_2/A_o) show a slow and regular rise with momentum as the distribution becomes more and more forward peaked. (A_3/A_o) and (A_4/A_o) are slightly negative but almost compatible with zero until around 2 GeV/c when there is once again a regular rise, corresponding to the late onset of D-wave contributions.

If the coefficients for the Δ^{+} (not shown) may be said to differ from those of the Δ^{++} in any systematic way it is that they are generally lower. This probably indicates that the resonance is sitting on rather more non-peripheral background.

Unlike the method at the end of (5.1) suggested,

Fig.16 Legendre polynomial coefficients. $K^+P \to K^0\Delta^{++}$

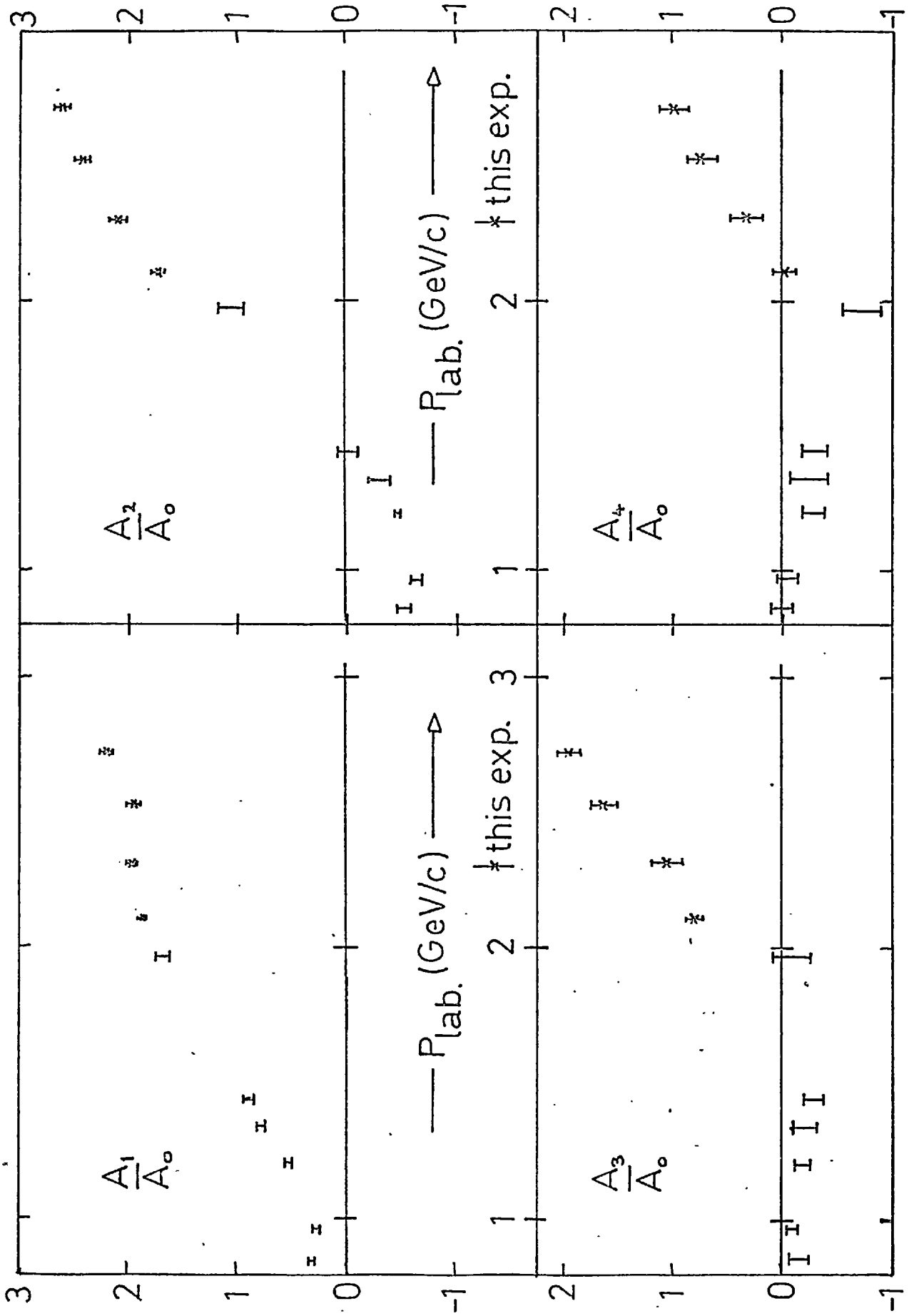

Fig. 17

Higher Legendre polynomial coefficients. $K^+P \rightarrow K^0\Delta^{++}$

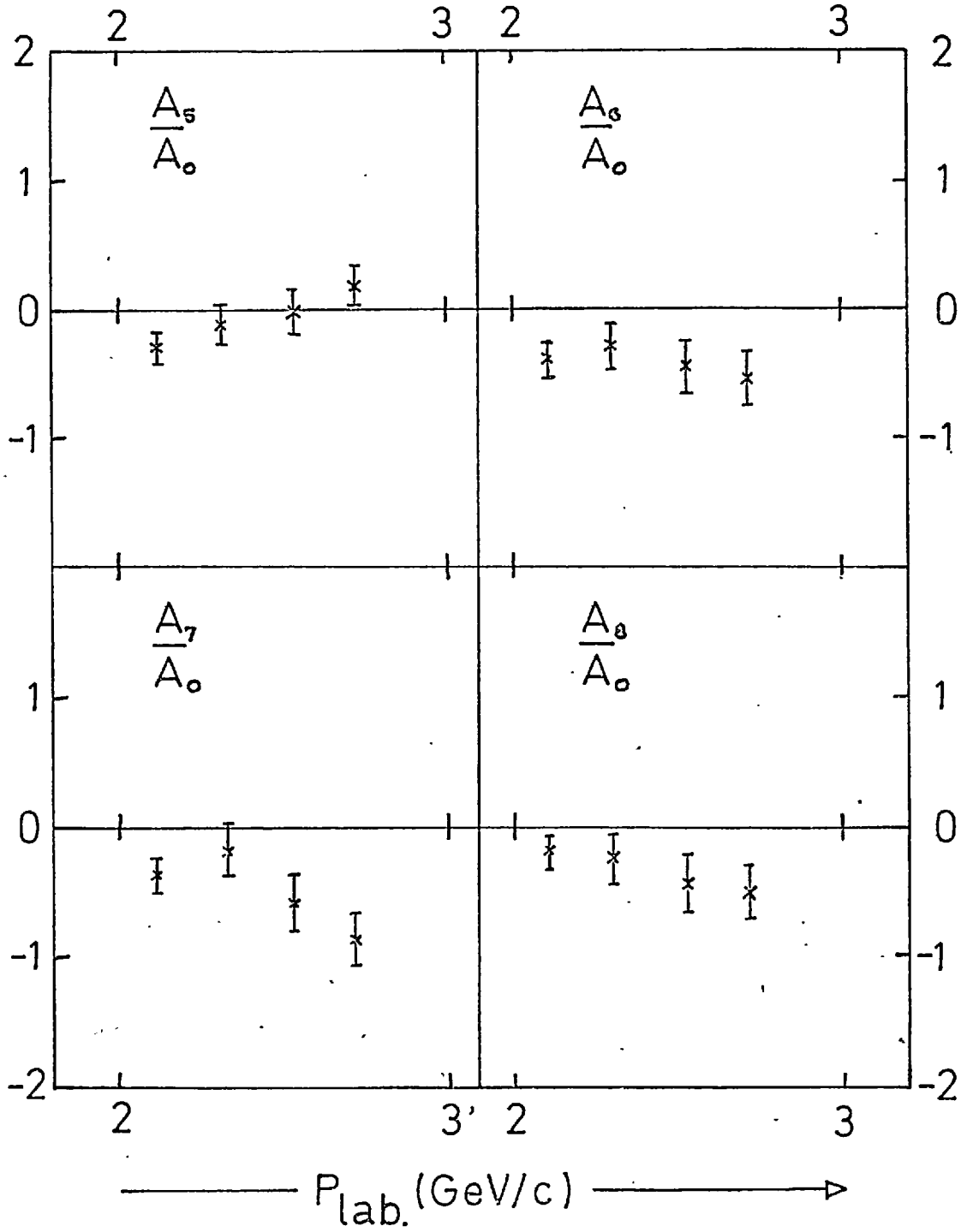

although A_4 becomes reasonably well established, the evidence of the higher coefficients being significantly different from zero is doubtful, especially as comparisons with the maximum likelihood method and methods of removing the effect of the K^* and phase space background were prone to vary these values somewhat. The plots of χ^2 and confidence level versus the number of parameters used (Fig. (18)) are slightly erratic but, if anything tend to confirm that (A_4/A_0) is both necessary and sufficient to cover the data.

In general, the momentum dependence of the coefficients is, like so many features of K^+P reactions, extremely smooth, indicating a lack of s-channel activity between the K and Δ .

It is instructive to consider the variation of (A_n/A_0) with effective mass of the $(P\pi)$ combination. Fig. (19) shows this plotted for five effective mass bands from a sample of $PK^0\pi^+$ events at 2.72 GeV/c. The general trend of all coefficients is to zero, as increasing $(P\pi)$ effective masses imply that the combination is produced in a low-energy state in the centre of mass system, and thus probably in an S-wave. If there were any exotic resonance which preferentially decayed into a certain $(P\pi)$ mass, the corresponding coefficient would show structure.

5.3 K^* Production

In investigating the K^* production, the mass cuts used were:

$$0.84 \text{ GeV/c}^2 < M(K\pi) < 0.94 \text{ GeV/c}^2$$

The resulting $\cos\theta^*$ distributions for the four momenta are shown in Fig. (20). These plots are for the K^{*+}

Fig.18. χ^2 and confidence level variation (Δ^{++}).

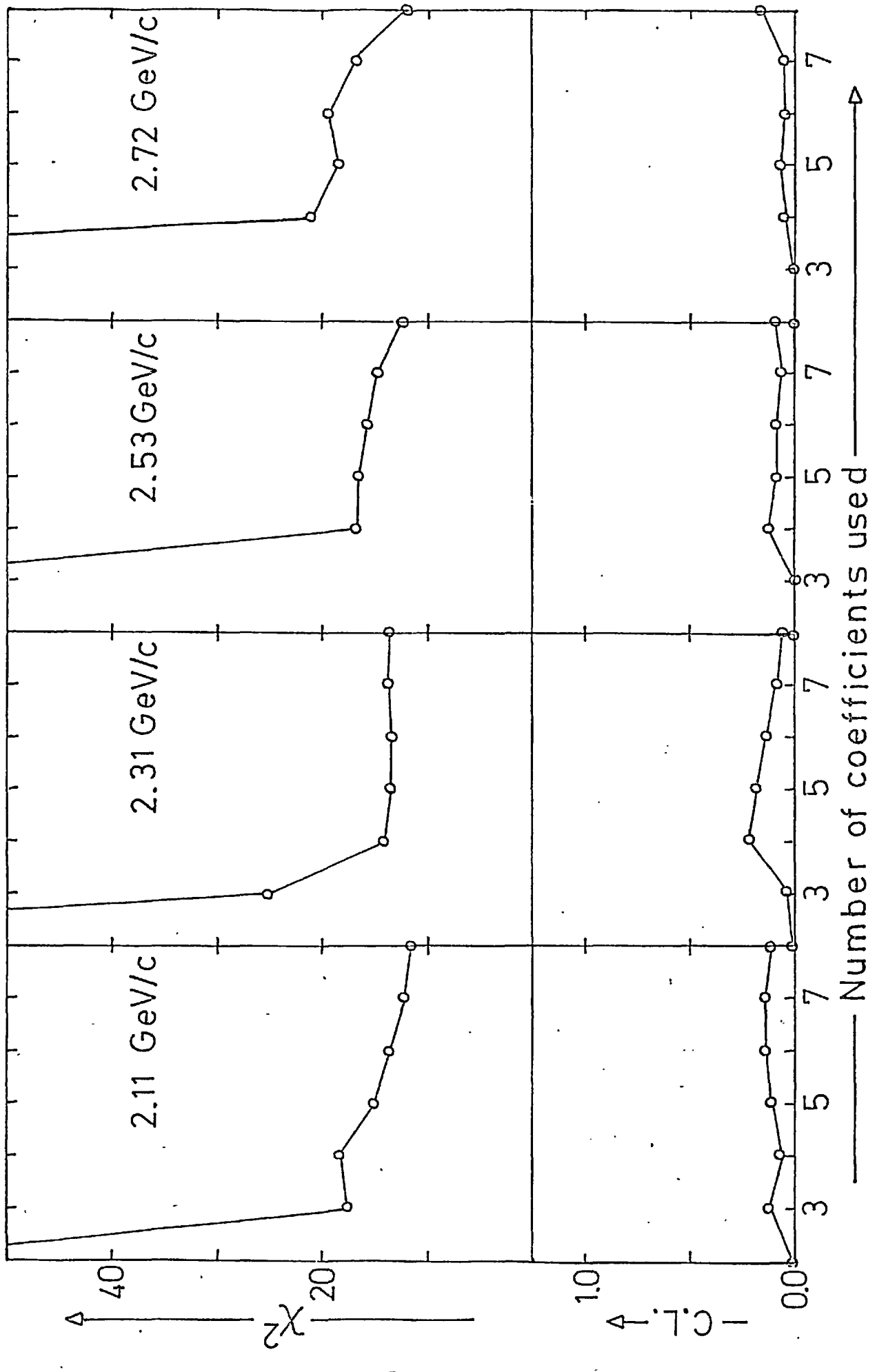

Fig.19. Variation of $\left(\frac{A_n}{A_o}\right)$ with $(P\pi)$ mass.

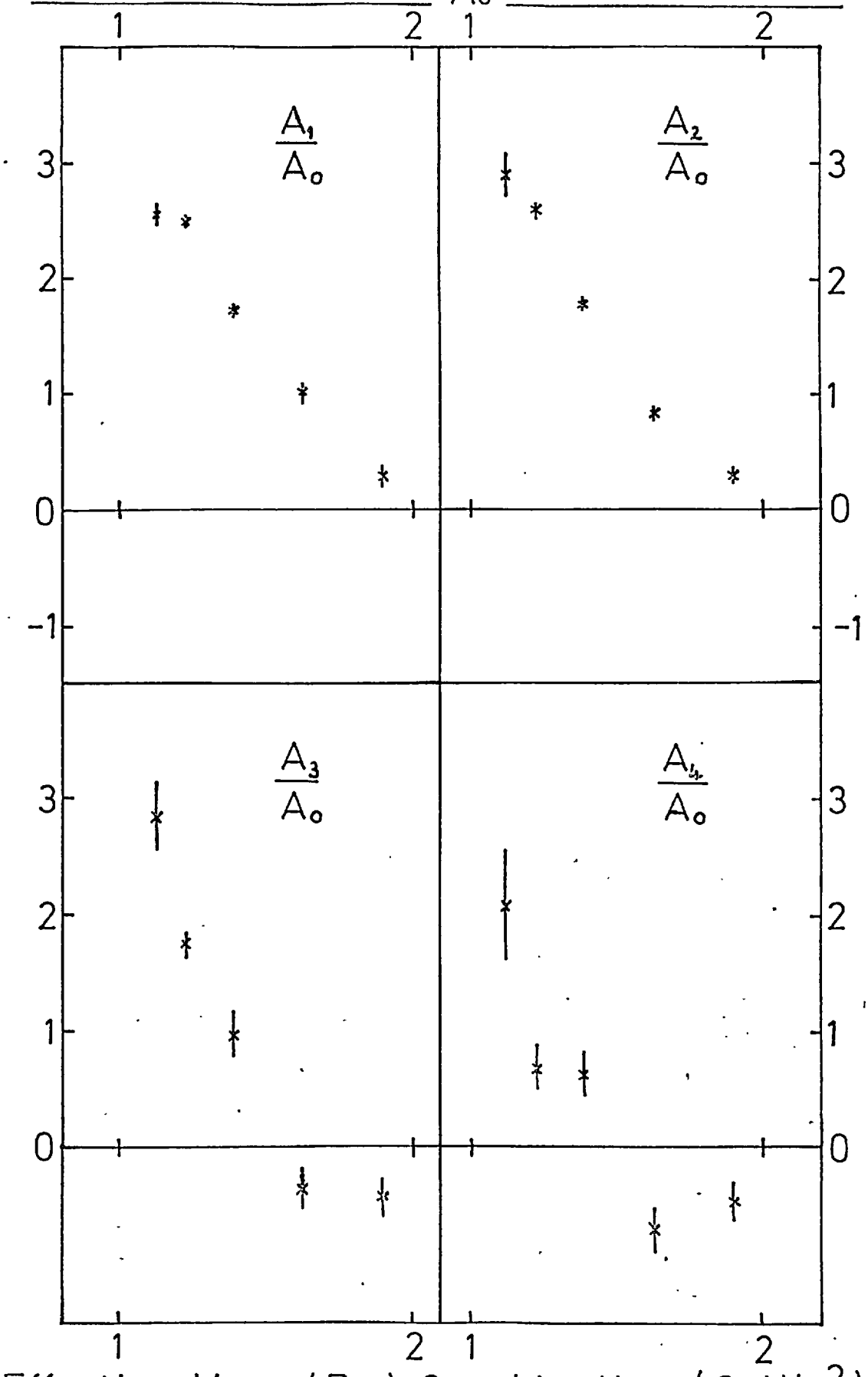

Effective Mass $(P\pi)$ Combination (GeV/c^2).

Fig 20a.

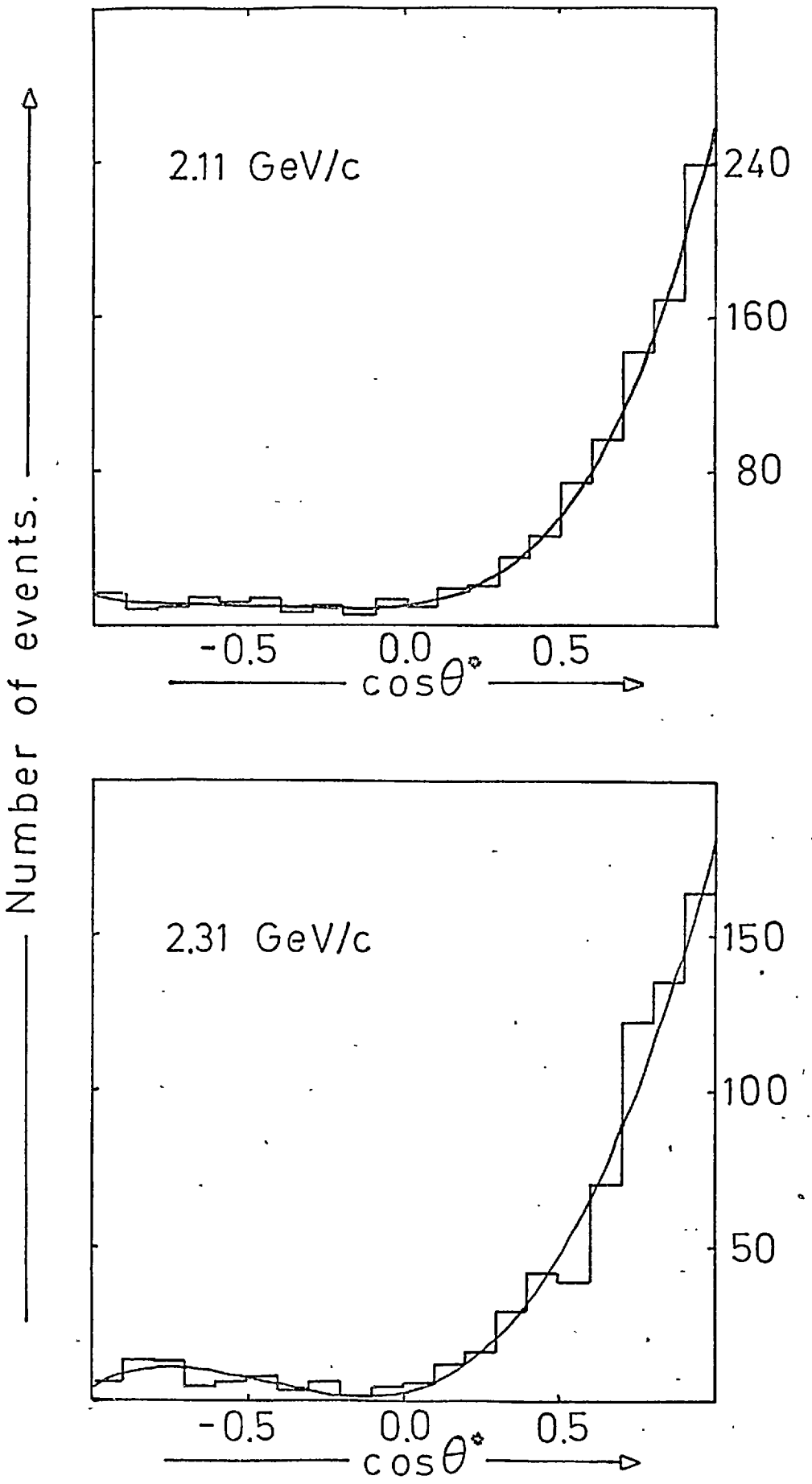

$K^{*+}(892)$ Production angle distribution.

Fig 20b.

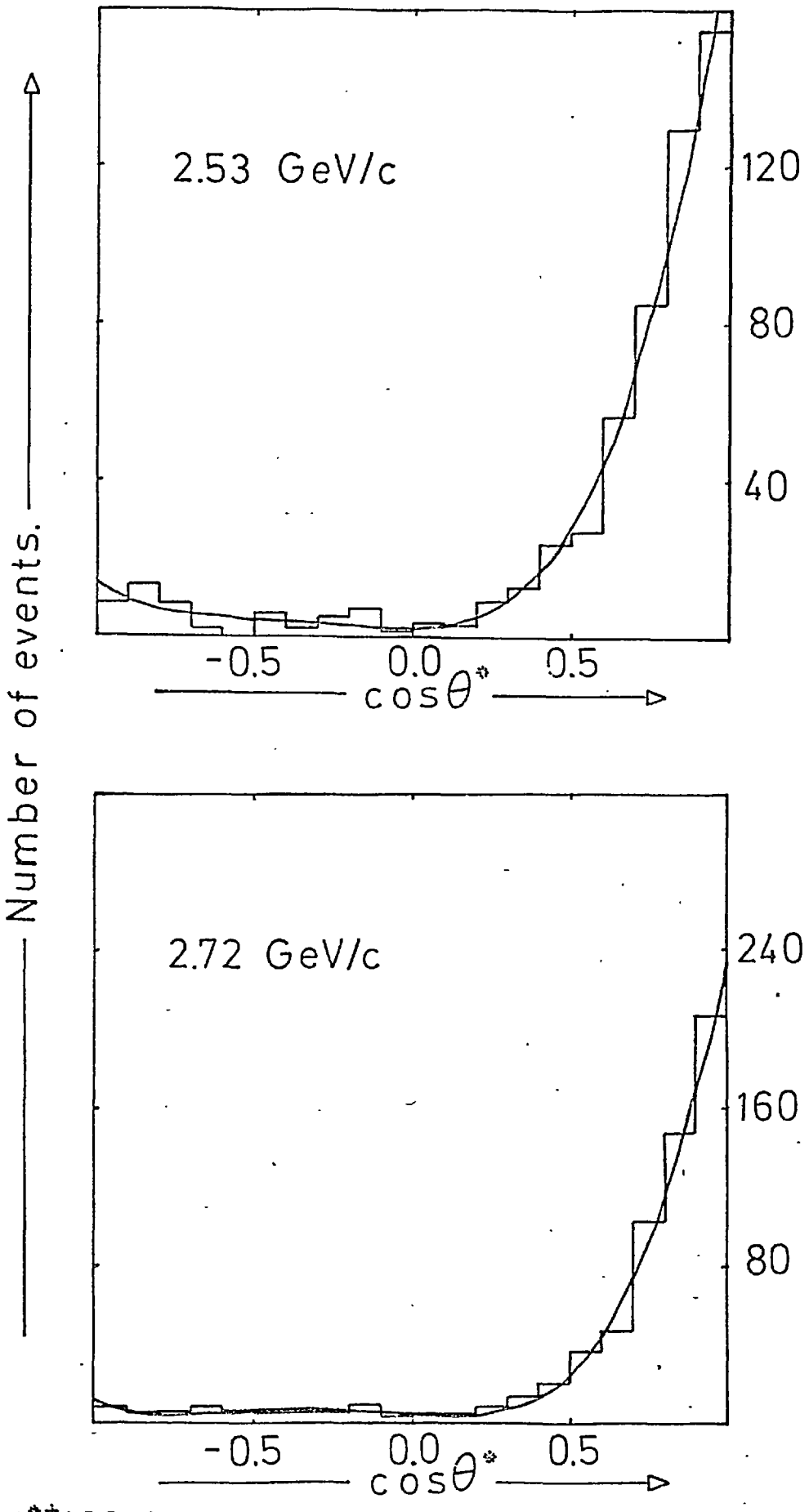

$K^{*+}(892)$ Production angle distribution.

taken from the $PK^{o}\pi^{+}$ final state using both seen and unseen K^{o}'s. The continuous lines represent method of moments four parameter fits and it can be seen that they represent the data very well.

As with experiments at lower momenta the distributions show even more peripherality than the corresponding Δ plots.

The resulting values of the (A_n/A_o) are plotted in Figs. (21,22), and for the first four polynomials are presented together with the five points from reference (20), taken directly as published, and other points analysed by the author, from $\cos\theta^{*}$ histograms (3,4,5,26). It must be pointed out that the coefficients at 1.7 GeV/c have been derived with raw and unpublished data (26) from an experiment originally designed to study weak interaction theories. Apart from this, the other resulting data points give a highly self-compatible and detailed description of $K^{*+}P$ production from threshold (at 1.08 GeV/c) to 3 GeV/c, covering the whole of the intermediate energy range.

Plots of χ^2 and confidence level against the numbers of parameters used are presented in Fig. (23). Again, as with the Δ, it seems reasonable to take four polynomials as being both necessary and sufficient to explain the data. (A_5/A_o) onwards also seem consistent with zero, within errors.

Referring to Fig. (21) the lower coefficients are all positive and, once more, increase smoothly with momentum, the rate of increase being greater just beyond threshold and then slowing down.

There is, however, one exception to this behaviour in the fourth coefficient (A_4/A_o). This begins to be different from zero just before 1.5 GeV/c corresponding to the onset of D-waves as expected. Up to 2 GeV/c there is the usual smooth

Fig.21 Legendre polynomial coefficients. $K^+P \to K^{*+}P$

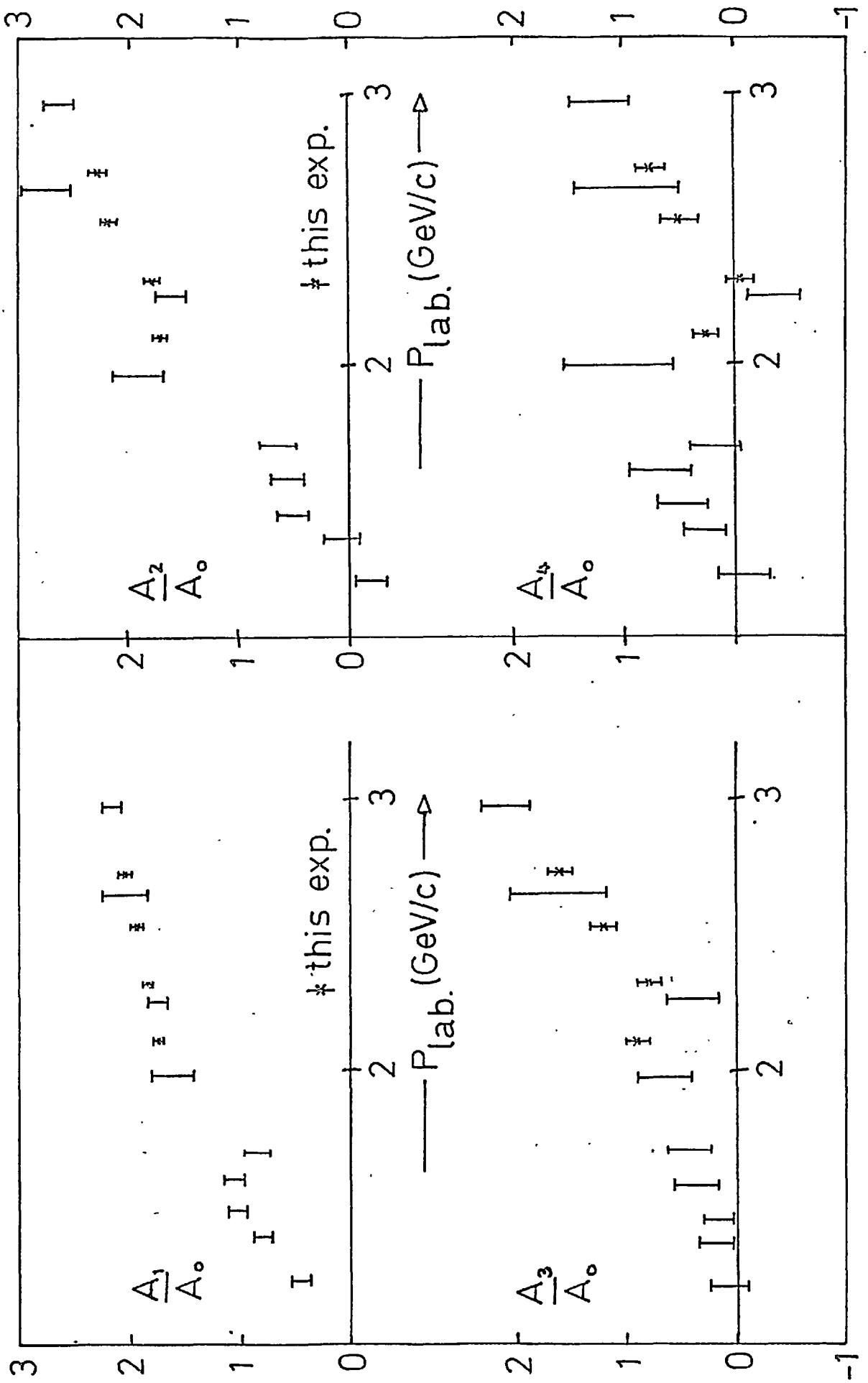

Fig. 22

Higher Legendre polynomial coefficients. $K^+P \rightarrow K^{*+}P$

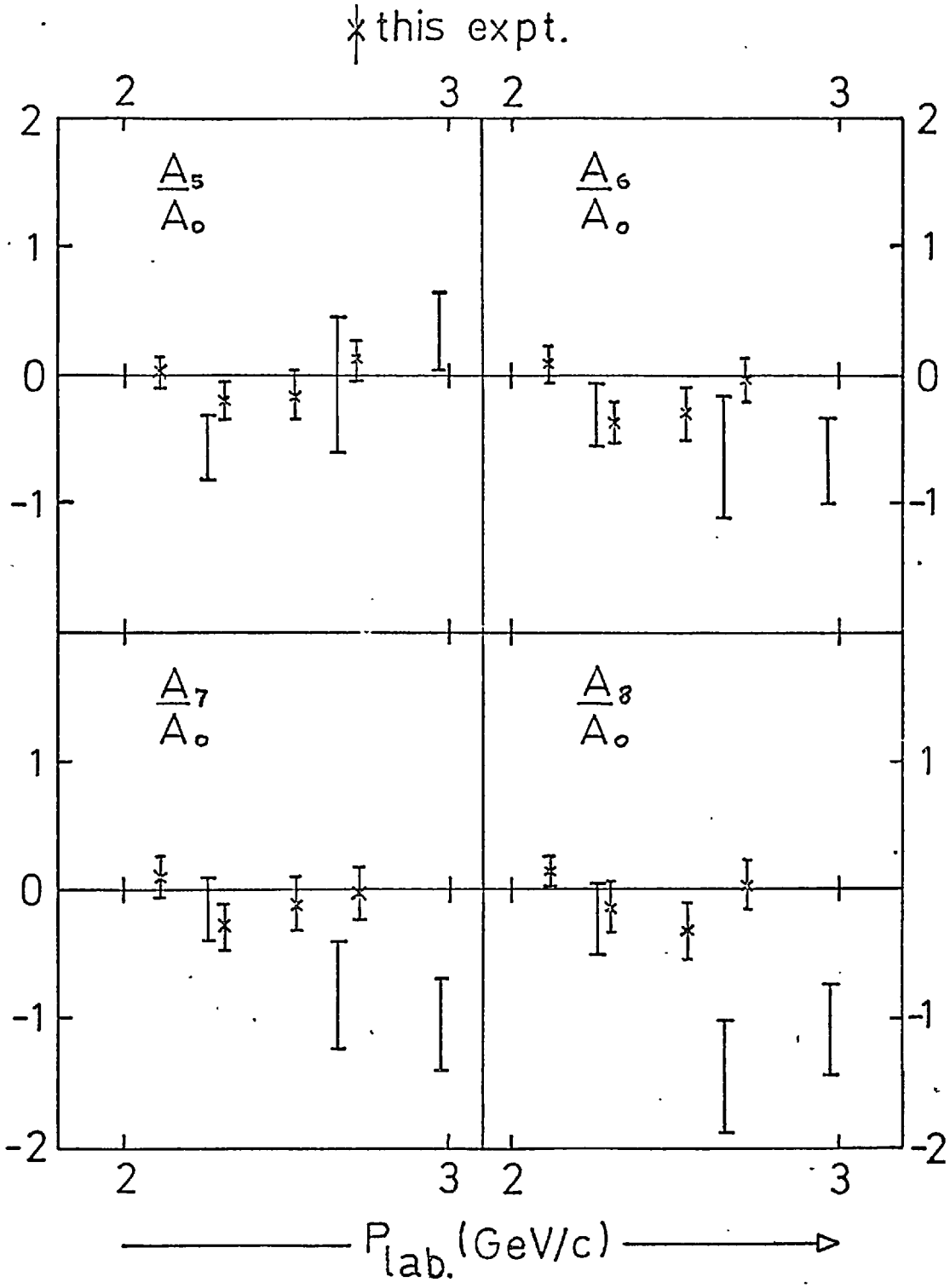

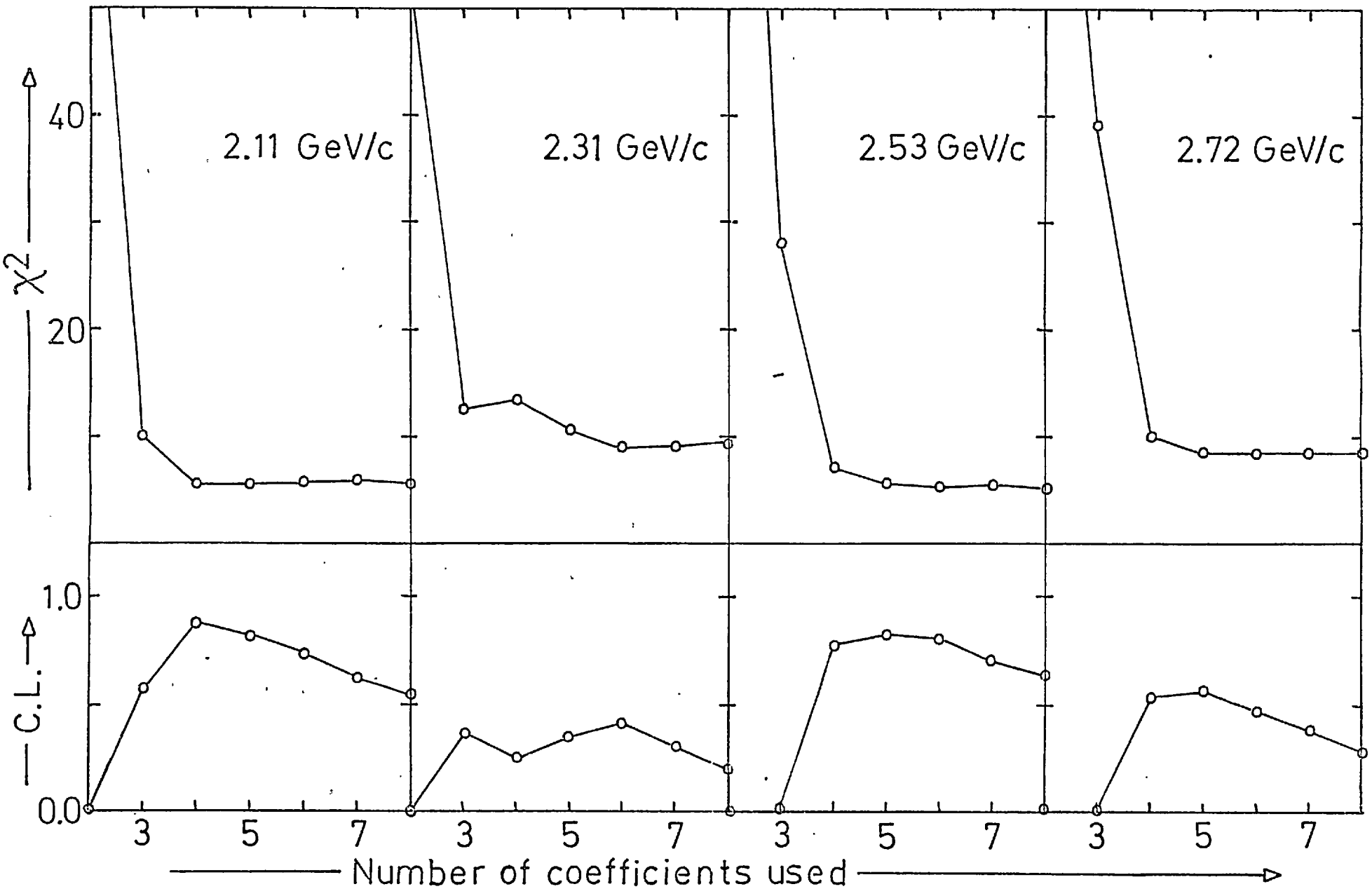

Fig.23 χ^2 and confidence level variation (K^*).

increase, but then our data and that of Bomse et al.[3] confirm that there is a steep drop in the space of some 200 MeV/c from $(A_4/A_0) \sim 1$ to ~ 0. After 2.3 GeV/c our data, confirmed by Newman et al.[4], shows that the value is rising again until finally the author's analysis of the 2.97 GeV/c data[5] gives $(A_4/A_0) \sim 1.2$.

This severe dip in a Legendre polynomial coefficient is extremely surprising as, without exception, all other phenomena in K^+P reactions have a very smooth momentum dependence. Structures in the coefficients representing $(\pi^{\pm} P)$ scattering have long since been indentified as effects due to the nucleon isobars and Δ resonances, and in $K^- P \longrightarrow \overline{K^o} N$ and $\Lambda\pi^o$ Wohl et al.[27] got confirmation of the $\frac{7}{2}$ spin Y^*'s (2030) and (2100) first noted in total cross-section measurements by counter groups. If the (A_4/A_0) structure were to be similarly interpreted, this would imply an s-channel effect between the K^* and the P. Presumably this would be evidence for the existence of a so-called exotic resonance, the Z^*, as noted in the introduction.

Before coming to such startling conclusions as this, however, it is judicious to examine the evidence for the proposed structure a little more closely. So far, the whole of the final state $PK^o\pi^+$ has been used. In Chapter 3 the possibility of contamination by both pion events and other channels was discussed. To remove any doubt that this could be causing the structure, the final state containing only multi-vertex fitted seen K^o's was used. Here, there are no ambiguities and, because of phase space limitations for producing a strange particle pair, a vanishingly small

chance of pion contamination. The $(^{A_4}/_{A_0})$ points for this channel are displayed in Fig. (24a). Although the lower statistics lead to larger error bars, it is clear that the structure is even more in evidence. The lower coefficients are still reasonably compatible with smooth behaviour, though it is possible to believe that $(^{A_3}/_{A_0})$ kinks slightly in the relevant area.

All data points described so far have been analysed on the final state $PK^0\pi^+$. What of the other isotopic decay mode of the K^{*+}, the final state (3.2) $PK^+\pi^0$? The inherent difficulties with this channel have already been noted and can perhaps be illustrated by an analysis performed with the Dalitz plot fitting program which shows that with the mass cuts used in the $PK^0\pi^+$ channel there is 91% resonance on a 9% background, whereas in the $PK^+\pi^0$ state there is only 79% resonance contaminated by a 21% background. As well as this, there are smaller statistics and a bigger chance of contamination from other sources. Nevertheless, it still ought to be possible to at least see some sign of the rather violent structure already noted. A brief glance at Fig. (24b) is, in fact, enough to show that this is not the case. Contrary to the other evidence, it now seems as though it is possible to believe that $(^{A_4}/_{A_0})$ levels off at a value just less than 1 around 2 GeV/c and then remains constant.

In an effort to resolve the problems of interference from the Δ a method due to Eberhard and Pripstein (28) was used. This will be further elaborated in the next chapter. On the $PK^0\pi^+$ channel this had little effect. Simultaneously in the $PK^+\pi^0$ channel a method of automatic correction for

Fig 24. Variation of K^{*+} (A_4/A_0).

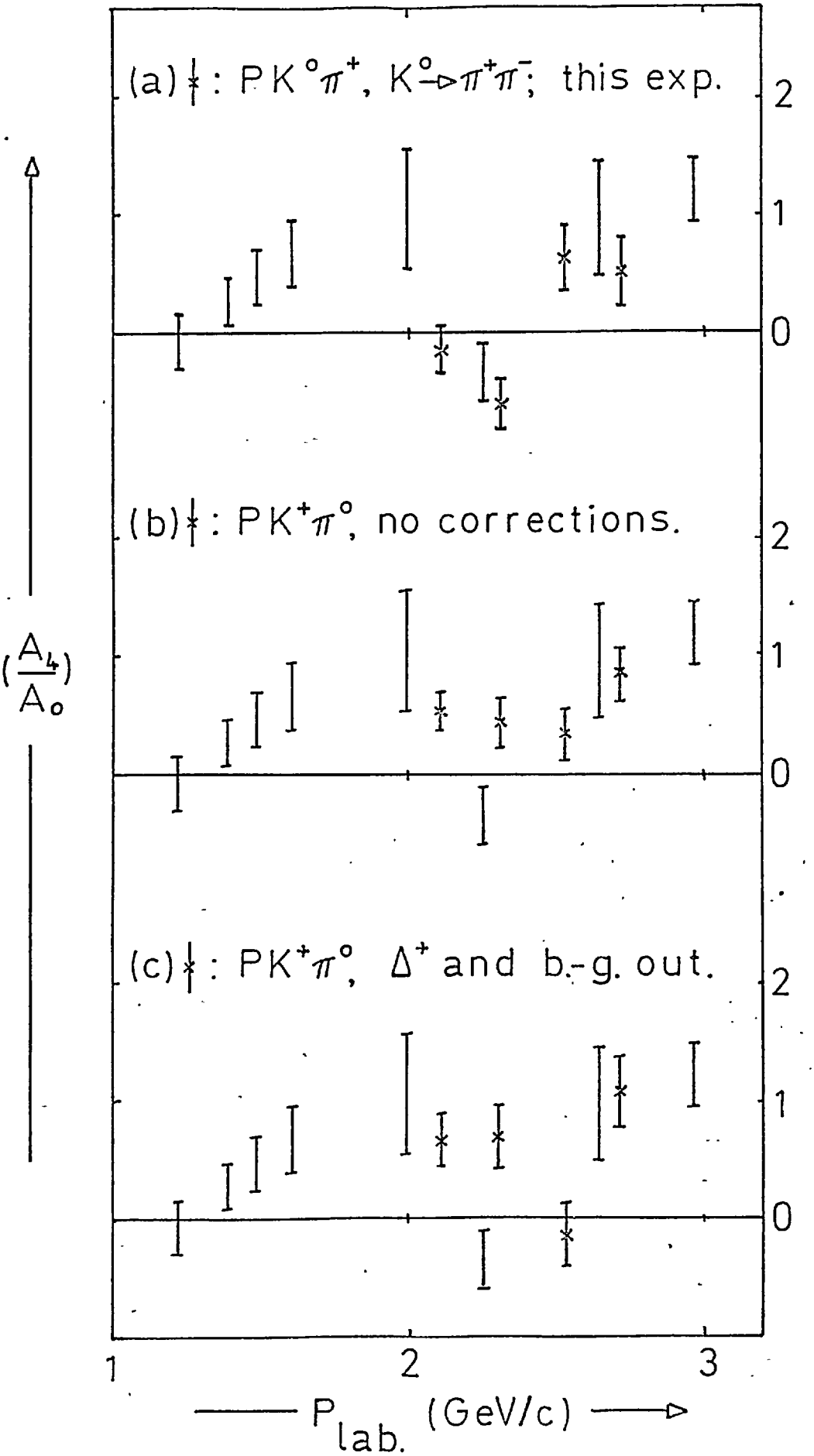

background was attempted. This can be understood by referring to the diagram below:

Fig. (25)

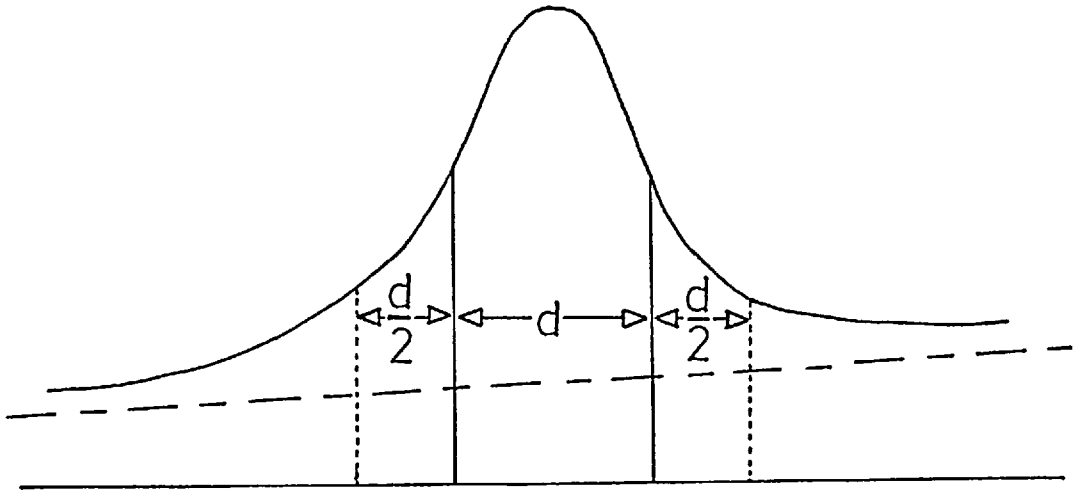

As well as accepting events in the resonance mass-cut region, of width d, events from the two wings of width $^{d}/_{2}$ are also taken but with negative weight. This has the effect of reducing the statistics of the resonance, but has the advantage of cancelling out any linearly behaving phase space background, a good approximation considering the narrow region. When these techniques are applied, the resulting form of the $PK^{+}\pi^{o}$ $(^{A_4}/_{A_o})$ coefficient is as on Fig. (24c). The 2.3 GeV/c point, where statistics is somewhat limited, is rather stubborn, but looking at the other points the behaviour is more consistent with the structure in the $PK^{o}\pi^{+}$ channel. In general, however, these techniques increase error bars very much and also cause some of the other coefficients to lose their smoothness. It is not clear how much the evidence of the $PK^{+}\pi^{o}$ channel is to be believed. Certainly, these techniques had very little effect on the $PK^{o}\pi^{+}$ channel as might be expected with so little background.

It is worth noting here that the lower energy experiments corrected for a considerable Δ overlap and even interference by taking only events with a forward going π in the K^* system, thus cutting out the Δ band. This was also performed on the 1.7 GeV/c data[26] but the values of the coefficients remain somewhat incompatible with surrounding points.

Assuming, then, that the structure does exist, is it possible to say what part of the data it is that requires the fourth coefficient? Fig. (26) displays the whole of the 2.11 GeV/c data and the tails of the data at the other three momenta fitted with only three parameters. Comparing this with Fig. (20) it can be seen that the forward peripheral peak is fitted almost equally as well as with four parameters but that the "ripple" induced in the backward direction is not borne out well in the data and even predicts negative numbers of events as the momentum increases. It seems then, that the need or lack of need for the fourth coefficient is based on the level of non-peripheral events. In the case of the K^* it is evident from Chew-Low plots that these events are definitely to be associated with the resonance and not with phase space background. This is further illustrated by Fig. (27) which displays effective mass histograms for $(K\pi)$ and $(P\pi)$ combinations in the case where the nucleon or kaon respectively goes "backwards" in the c.m.s. Although there is clear evidence for a K^* in the former there is virtually no Δ in the latter histograms.

Naturally this kind of behaviour could occur with the u-channel exchange of negative strangeness baryons (Y^*'s or Λ) but a small amplitude s-channel process competing with the major

Fig. 26. Three Parameter Fits for $K^{*+}(892)$.

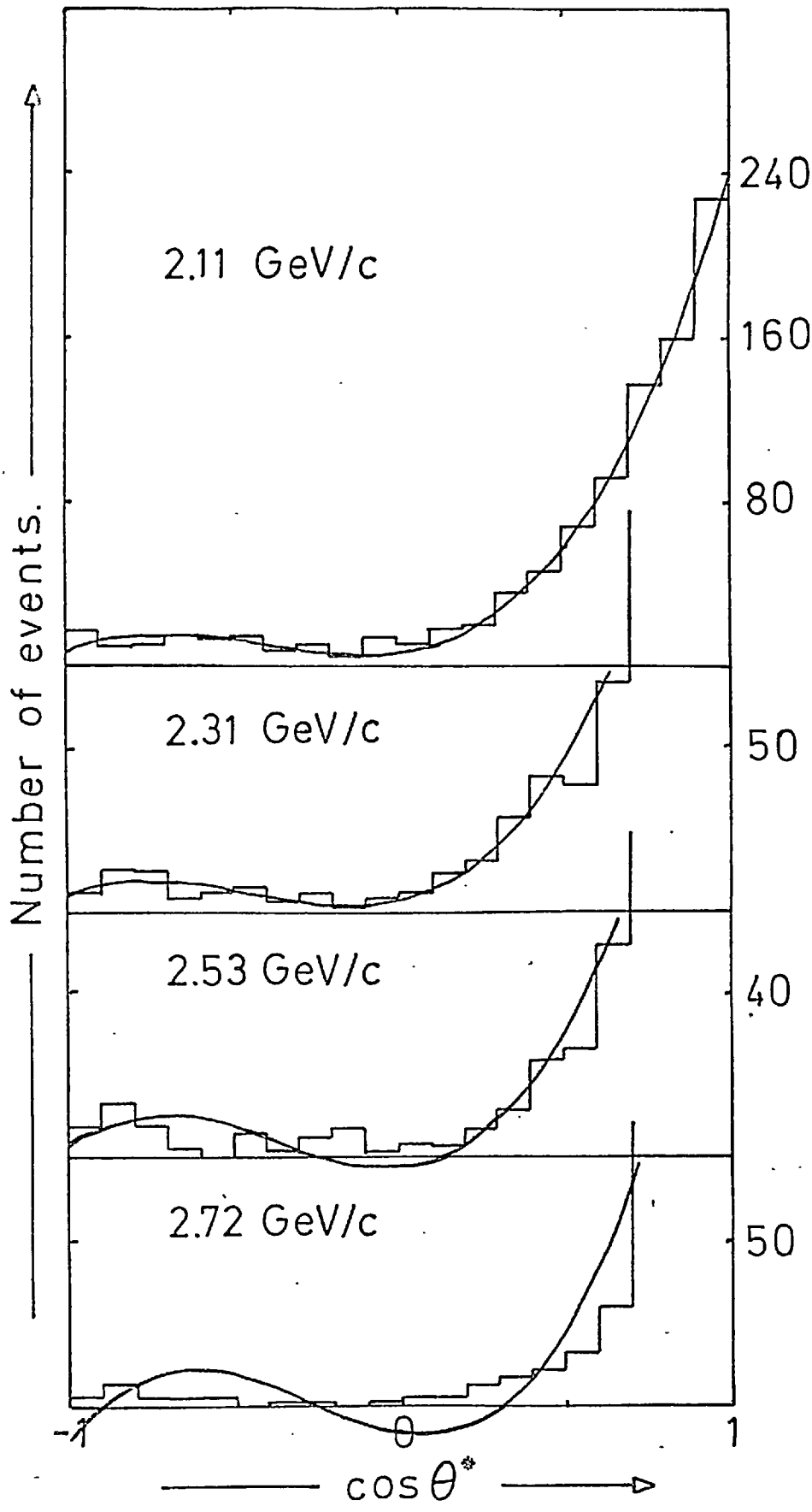

Fig 27. Mass plots for backward events.

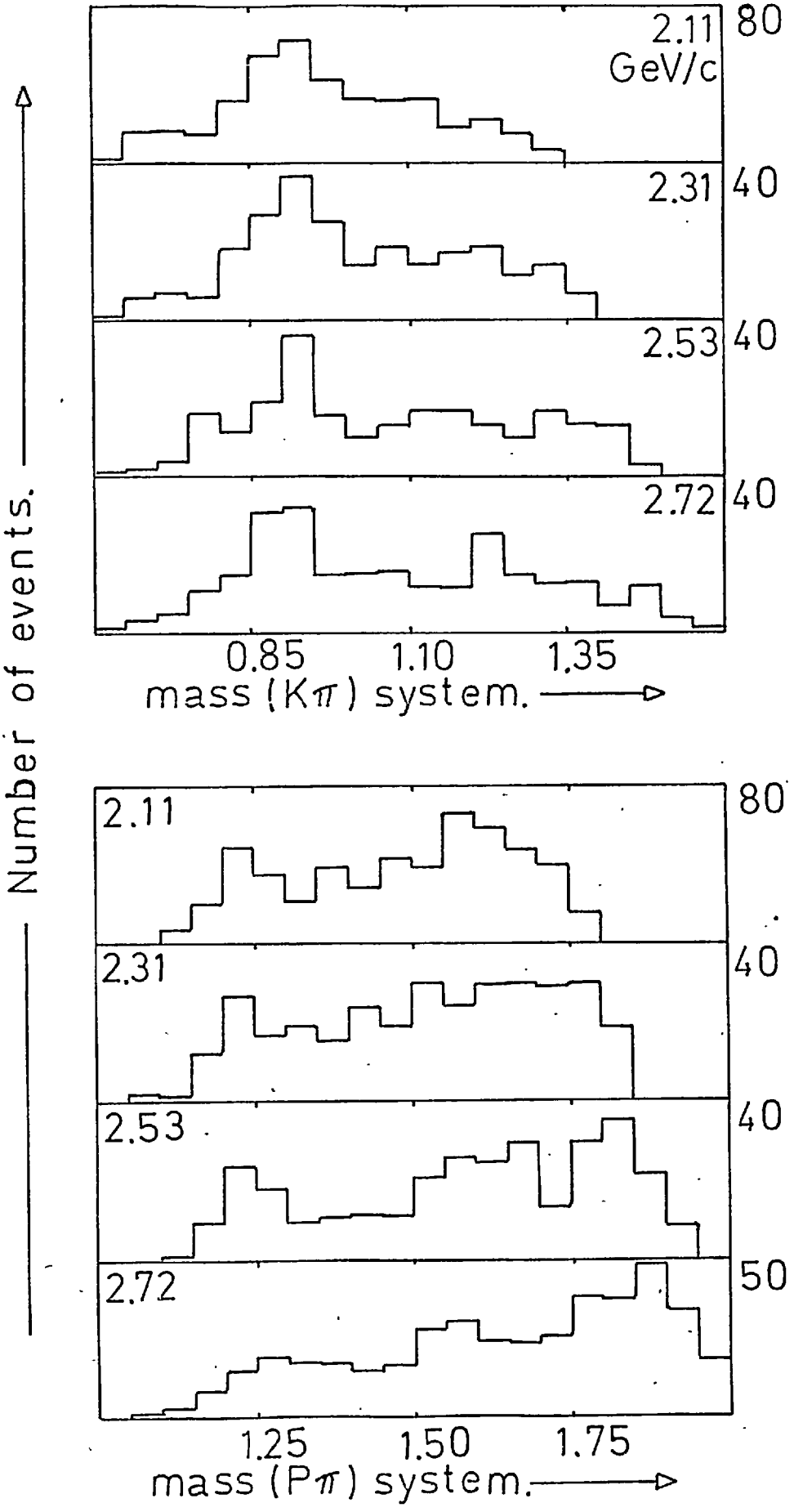

peripheral production could also have this result.

The result of a $(K\pi)$ mass variation experiment is shown in Fig. (28) at 2.31 GeV/c. The trend of all coefficients to lower values is similar to the case of the Δ. There is a slight dip of (A_4/A_0) at the K^* mass, however, and although not very significant it shows that the low value of this coefficient is probably a genuine effect connected with the K^*.

If, then, the structure in (A_4/A_0) is confirmed and can indeed be related to s-channel activity between the K^* and proton, it becomes increasingly tempting to associate it with the Z^*'s. As will be shown, a resonance can display itself as a bump or a dip in coefficient structure. Hence, it could be said that the effect was due to the 2nd Cool bump Z_1^* (2190) at $P_{lab.} = 1.89$ GeV/c producing an increased (A_4/A_0) or perhaps an over-estimated 3rd Cool bump Z_1^* (2505) at $P_{lab.} = 2.70$ GeV/c, producing a dip at a somewhat smaller $P_{lab.}$ Either way, the extent of the structure seems somewhat greater than the estimated half-width of $\Gamma \sim 120$ MeV/c^2.

To try to associate the observed structure with a definite resonant partial wave it is necessary to attempt at least a rudimentary partial wave analysis. The large number of contributing waves and difficulty of working with a quasi-two body state militates against an investigation in depth, but in fact the smooth behaviour of the other coefficients gives a considerable constraint on the system.

Fig 28. Variation of $(\frac{A_n}{A_o})$ with $(K\pi)$ mass.

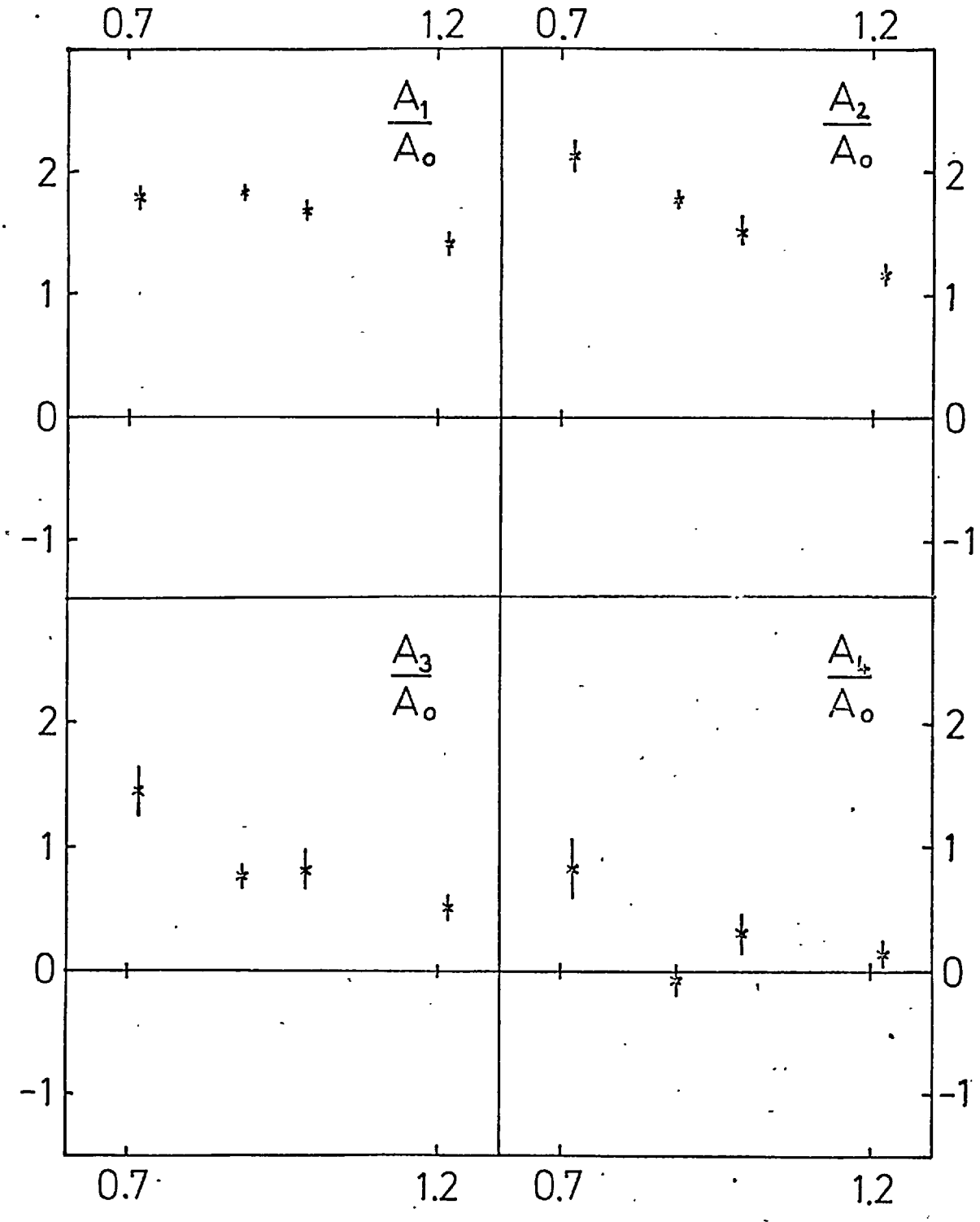

Effective Mass $(K\pi)$ Combination (GeV/c^2).

5.4 Partial Wave Analysis

To express the partial differential cross-section as a series in partial wave products and Legendre polynomials the approach of S.M. Deen[29], via helicity amplitudes, is used. If $f(\theta)$ is the scattering amplitude,

$$\frac{d\sigma}{d\Omega} = \left| f(\theta) \right|^2$$

$f(\theta)$ may be expressed in terms of the transition matrix $T(\cos\theta, E)$, E being the centre of mass energy, as

$$f(\theta) = \frac{1}{P\sqrt{(2S_a + 1)(2S_b + 1)}} \sum_{\text{all}\lambda} \langle \lambda_c \lambda_d | T(\cos\theta, E) | \lambda_a \lambda_b \rangle$$

where particles a, b with spins S_a, S_b and helicities λ_a, λ_b interact to form particles c, d of helicities λ_c, λ_d and $\underline{\hat{a}}.\underline{\hat{c}} = \cos\theta$. The term before the summation is merely a phase space normalisation, P being the momentum of particle a or b.

The plane wave S - matrix for this process taking a wave (P, θ^o, ϕ^o) to (P^1, θ, ϕ) may be expanded in terms of helicity amplitudes as:

$$\langle P^1 \theta\, \phi\, \lambda_c \lambda_d \left| S(E) \right| P\theta^o\phi^o\, \lambda_a \lambda_b \rangle$$

$$= \sum_{J.,M} \frac{2J + 1}{4\pi} D^{J*}_{M\lambda'}(\phi\ \theta\ 0) \langle \lambda_c \lambda_d \left| S^J(E) \right| \lambda'_a \lambda_b \rangle D^J_{M\lambda}(\phi^o\theta^o\, 0)$$

where $\lambda = \lambda_a - \lambda_b$, $\lambda' = \lambda_c - \lambda_d$

Using the property of the rotation D matrices that, for $\phi = \theta^o = \phi = 0$

$$D^J_{M\lambda}(\phi^o\ \theta^o\ 0) \cdot D^J_{M\lambda'}(\phi\theta 0) = d^J_{\lambda\lambda'}(\theta)$$

we have, as the expression is independent of ϕ ,

$$\langle p'\theta\,\phi\,\lambda_c\lambda_d|S(E)|p\;0\;0\,\lambda_a\lambda_b\rangle$$

$$= \sum_J (J+\tfrac{1}{2})\,\langle\lambda_c\,\lambda_d|S^J(E)|\lambda_a\lambda_b\rangle d^J_{\lambda\lambda'}(\theta)$$

Now the T - matrix is related to the S - matrix by

$$T^J(E) = S^J(E) - \delta_{ac}\,\delta_{bd}$$

Thus, for all except elastic scattering

$$f(\theta) =$$

$$\frac{1}{p\sqrt{(2S_a+1)(2S_b+1)}} \sum_J \sum (J+\tfrac{1}{2})\langle\lambda_c\lambda_d|T^J(E)|\lambda_a\lambda_b\rangle d^J_{\lambda\lambda'}(\theta).$$

Note that J is the total conserved angular momentum.

$$\underline{J} = \underline{L} + \underline{S} = \underline{L}' + \underline{S}'$$

To expand into more familiar orbital angular momentum states, use a Clebsch-Gordan transformation

$$\langle Jm|S|\,Jm\,\lambda_1\lambda_2\rangle = C^{l\;S\;J}_{0,\lambda,\lambda}\,C^{S_1S_2S}_{\lambda_1,-\lambda_2,\lambda_1-\lambda_2}\left(\frac{2l+1}{2J+1}\right)^{\frac{1}{2}}$$

where particles 1 and 2 have spins S_1 and S_2, helicities λ_1 and λ_2 and combine with total spin S and orbital angular momentum l to give J with z component m. The C represent Clebsch-Gordan coefficients for this process.

Thus, $f(\theta)$ may be expanded in terms of orbital angular momentum states

$$f(\theta) = \frac{1}{p\sqrt{(2S_a+1)(2S_b+1)}} \sum_{J,\lambda} \sqrt{(l'+\tfrac{1}{2})(l+\tfrac{1}{2})}$$

$$\times\; C^{l'S'J'}_{0\lambda'\lambda'}\,C^{S_cS_dS}_{\lambda_c,-\lambda_d,\lambda'}\,C^{l\;S\;J}_{0\lambda\lambda}\,C^{S_aS_bS}_{\lambda_a,-\lambda_b,\lambda}\langle l',S'|T^J(E)|l,S\rangle d^J_{\lambda\lambda'}(\theta)$$

To get $\frac{d\sigma}{d\Omega}$ the product of $f(\theta)$ with its own complex conjugate is taken. In doing this the property of multiplying two d functions to make a third is used:

$$d^{J_1}_{\lambda_1\lambda_1'} \; d^{J_2}_{\lambda_2\lambda_2'} = \sum_{l=|J_1-J_2|}^{l=|J_1+J_2|} C^{J_1J_2}{}_{l} C^{J_1J_2}{}_{l} \; (-1)^{\lambda_2-\lambda_2'} \; d^{l}_{\lambda_1-\lambda_2,\lambda_1'-\lambda_2'}(\theta)$$

Also using the relationship,

$$d^{l}_{om}(\theta) = (-1)^m \, d^{l}_{mo}(\theta) = \left(\frac{(l-m)!}{(l+m)!}\right)^{\frac{1}{2}} P^m_l \; (\cos\theta).$$

and hence

$$d^{l}_{oo}(\theta) = P_l(\cos\theta).$$

We find that under the assumption of no target polarisation the entire expression simplifies (!) to

$$\frac{d\sigma}{d\Omega} = \frac{1}{p^2(2S_a+1)(2S_b+1)} \sum \sqrt{(l_1'+\tfrac{1}{2})(l_1+\tfrac{1}{2})(l_2'+\tfrac{1}{2})(l_2+\tfrac{1}{2})}\,(-1)^{\lambda_2-\lambda_2'}$$

$$\times \prod_{i=1}^{10} C_i \langle l_1' S_1' | T^{J_1}(E) | l_1 S_1 \rangle \langle l_2' S_2' | T^{J}(E) | l_2 S_2 \rangle^{*} P_l(\cos\theta)$$

The C_i being 10 Clebsch-Gordan coefficients.

Taking out a wave-number ($\lambda\!\!\!^{-} = \frac{\hbar}{p}$) squared we can express

$$\frac{d\sigma}{d\Omega} = \lambda\!\!\!^{-2} \sum_{n=0} A_n \, P_n(\cos\theta)$$

And hence relate the contributions of each partial wave product to each polynomial coefficient in the form

$$A_n = \sum^{n}_{\substack{l_1 l_1' J_1 \\ l_2 l_2' J_2}} a \; \langle l_1' | T^{J_1} | l_1 \rangle \, . \, \langle l_2' | T^{J_2} | l_2 \rangle$$

Fortunately, Deen has written a program to evaluate the above rather frightening expression in the general case. An extract from the output of this program (30) for this case of

$$K^+P \longrightarrow K^*P$$

$$\text{or} \quad 0^-\tfrac{1}{2}^+ \longrightarrow 1^-\tfrac{1}{2}^+$$

is given below (Table (7)) where all terms to all coefficients are given which affect A_4 also.

TABLE 7.

A_4 - Contributing Partial Waves

WAVE PRODUCT	A_4 CONTRIBUTION	A_2 CONTRIBUTION	A_6 CONTRIBUTION	
$(DD5)^2$	0.368	4.653	-	1
DD3 DD5	4.788	4.005	-	2
PP1 FF7	4.734	-	-	3
PP3 FF5	5.143	4.457	-	4
PP3 FF7	-0.188	18.253	-	5
$(FF5)^2$	1.295	5.315	-	6
FF5 FF7	8.296	3.061	6.456	7
FP5 PF3	-8.398	-0.420	-	8
FP5 FF5	-6.299	-2.519	-	9
FP5 FF7	5.421	2.168	-	10
PF3 FF5	5.143	2.057	-	11
PF3 FF7	-4.426	-1.771	-	12
$(FF7)^2$	3.740	1.587	-1.010	13

Throughout, spectroscopic notation is used, i.e. if the incoming K^+ and P are in a relative S state ($l=0$) and the outgoing K^* and P are in a relative D state ($l=2$), the interaction occurring through a total angular momentum $J = \frac{1}{2}$ amplitude, then the partial wave is designated by SD1. There is an understood summation over spin states. The complex

conjugate notation * is omitted from the second member of the product, though it should be borne in mind that the product is one of two complex amplitudes. As it is ultimately ratios with A_0 which are compared, common factors are omitted and contributions to A_0 itself (from the square of each amplitude) are not given.

Because the sign of a particular partial wave product is unknown, only the magnitudes of contributions to (A_n/A_0) are relevant, whether the structure is dip or bump. Re-examining the plots it is clear that any structure in A_2 must be at least a factor four or five down on the A_4 contribution, and of the same sign. On these grounds examining entries 1 and 2 in the above table it is clear that DD5 and DD3 may be ruled out as causing the structure. Line 3 shows that the product PP1 FF7 could be responsible for the structure but line 5 shows that it is doubtful that FF7 is the resonant wave unless PP3 is made to vary in a very odd manner. Similar critical analysis of all lines in the table reveals that there are only three candidates which give what is at all reasonable effects with not too unreasonable assumptions. These are PP1, FP5 and PF3.

The contributions of these waves in product with all other waves are given in three further extracts from progam output in the tables below. Once more, contributions to A_0 are omitted.

TABLE 8.

Examination of Candidate Resonances
Contributions to other polynomials.

(a) PP1 Candidacy

	A_1	A_2	A_3	
$(PP1)^2$	A_o only			1
PP1 PP3		2.735		2
PP1 DD3	6.828			3
PP1 DD5			3.732	4
PP1 FF5		9.795		5
PP1 FP5		-4.648		6
PP1 SD1	2.000			7
PP1 PF3		3.795		8
SS1 PP1	2.000			9
DS3 PP1	2.828			10

(b) PF3 Candidacy

	A_1	A_2	A_3
DS3 PF3			-5.367
PP1 PF3		3.795	
PP3 PF3		-2.400	
SD1 PF3	3.795		
DD3 PF3	1.073		4.293
DD5 PF3	-0.861		-3.442
$(PF3)^2$		1.600	

(c) FP5 Candidacy

	A_1	A_2	A_3
DS3 FP5	6.573		
PP3 FP5		2.939	
$(FP5)^2$		2.400	
PP1 FP5		-4.648	
FP5 SD1			-4.648
FP5 DD3	-1.315		-5.258
FP5 DD5	1.054		4.216

It is considerably more difficult to draw firm conclusions from this evidence as there is no A_4 contribution to compare it with. Effectively these are the mass of background contributions to the lower polynomials. Nevertheless, it can be seen that if PP1 is indeed resonating Table (8a) requires many of its products with other low waves to be unexpectedly small so as not to give A_1, A_2 and A_3 structure. The assumptions of the FP5 and PF3 candidacies need neither be so numerous or so extreme and for this reason are rather more favoured. PF3 ought especially to be singled out as a recent phase shift analysis of Asbury et al. at Argonne [15] gave resonant solutions to a highly inelastic $P\frac{3}{2}$ wave at a rather lower energy; it could easily be possible for this to stimulate an outgoing F wave in the K^*P channel.

As a cautionary note it should be realised that the short analysis described above has been based on the possibility that observed structure is caused by rapid variation of one partial wave. This does not necessarily mean

that the amplitude is describing an anti-clockwise circle in the Argand diagram, and even if it were, there would still be some debate as to whether this therefore represents a resonant state of that partial wave.

CHAPTER 6

Δ^{++} (1236) PRODUCTION CHARACTERISTICS

6.1 Differential Cross-Section

As was seen in the last chapter the principal characteristic of the production of both major resonances was its peripheral nature. Even such simple models as the "black disc" predict an exponential dependence of $d\sigma/dt$ on momentum transfer squared, at least for small values, so it is convenient to go over to a parametrisation defined by

$$\frac{d\sigma}{dt} = Ae^{Bt} \qquad - (6.1)$$

A,B are constants, t is the Mandelstam variable defined as the square of the difference between the four momenta of the incoming proton and exiting Δ .

$$\text{i.e.} \qquad t = (\underset{\sim}{p}_p - \underset{\sim}{p}_\Delta)^2 \qquad - (6.2)$$

Physical values of t are negative. Although in the case of elastic scattering t may assume t = 0 for $\theta^* = 0$, in the case of unequal masses there is a certain, mass dependent, maximum for t. For 1.236 GeV/c^2, the central value of the Δ, this is $t_m = -0.008\,(\text{GeV})^2$ at the incident momentum of 2.11 GeV/c, the worst case.

Because of the non-zero value of t_m, and also because of flattening effects produced by different exchange characteristics, the highest bin of a $\frac{d\sigma}{dt}$ (t) plot is often depressed. For this reason, in fitting the formula (6.1) this bin is omitted. Taking logarithms of both sides of (6.1)

$$\log \frac{d\sigma}{dt} = \log A + Bt \qquad - (6.3)$$

Thus, a logarithmic plot of $d\sigma/dt$ should produce

a straight line of gradient B, intercept log A. Such plots are shown for the four momenta in Fig. (29), for the reaction $K^+P \longrightarrow K^o \Delta^{++}$ cross-sections normalised to a smooth curve through Fig. (12). The results of these fits are summarised in the table below where they are also compared to the data from the CERN-Brussels collaboration.[31]

TABLE 9.

P (GeV/c) LAB	2.11	2.31	2.53	2.72	3.0	3.5	5.0
Slope (mb/GeV^2)	2.4 ±.1	2.5±.1	3.0±.3	2.8±.1	3.2±.6	3.5±.5	4.1±.7
Intercept (mb)	3.2	2.8	2.7	2.2	2.8	2.1	1.2

As can be seen, the general tendency is towards a shrinking, sharper, peak with higher energy, just the prediction of the one Regge pole exchange model. This model may be simplified to the formulation:

$$\frac{d\sigma}{dt} = F(t) \left(\frac{s}{s_o}\right)^{2\alpha(t)-2} \qquad - (6.4)$$

where F(t) is a conglomerate slowly varying function including the residual and signature factor of the dominating trajectory. Putting $s_o = 1$, making the approximation of laboratory momentum, $P_K = \lambda s$ (constant), and taking logarithms

$$\log \frac{d\sigma}{dt} = \log F(t) + (2\alpha(t) - 2) \log P_K \qquad - (6.5)$$

$\alpha(t)$ here is the real part of the actual t- dependent Regge trajectory. It is clear from (6.5) that plots of $\log d\sigma/dt$ versus $\log P_K$ for fixed t should produce straight lines of gradient $(2\alpha(t) - 2)$.

Fig 29

Differential cross sections for Δ^{++}.

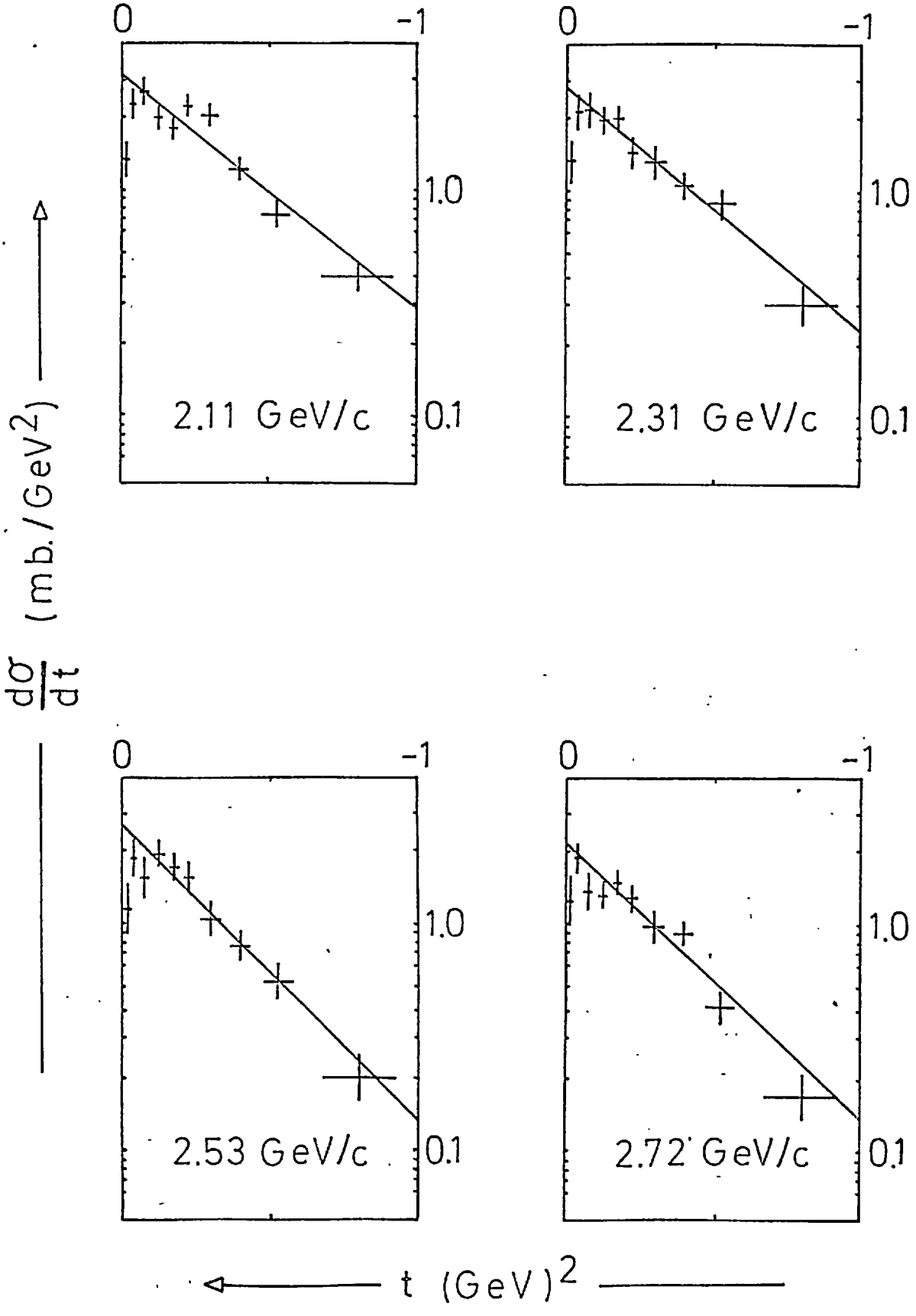

Using this formalism the work of reference (31) was extended to this lower momentum region and five independent values of $\alpha(t)$ were calculated for the process governing the reaction $K^+P \rightarrow K^o \Delta^{++}$. These are displayed on the Chew-Frautschi diagram of Fig. (30) with the corresponding confidence levels for the fits.

A linear trajectory was fitted to these data points with a confidence level of 11% giving the following parametrisation:

$$\alpha(t) = (0.67 \pm 0.18) + (1.12 \pm 0.18)\, t \qquad - (6.6)$$

This straight line misses the position of the ρ pole in the unphysical region somewhat but compares favourably with results evaluated in the better defined π^-P charge exchange reaction [34] for a ρ trajectory of

$$\alpha(t) = 0.57 + 0.96t \qquad - (6.7)$$

6.2 Density Matrix Elements

To complete a study of resonance production by a peripheral process it is necessary to discover what meson(s) are exchanged in the reaction at different energies and different momentum transfers.

In the process represented by the diagram in Fig. (32a), the Δ^{++} decays via $\Delta^{++} \rightarrow P\pi^+$ after the production process by peripheral exchange:

$$K^+P \rightarrow K^o \Delta^{++} \qquad - (6.8)$$

In general, the Δ, will be in a quantum mechanical mixture of pure spin states, depending, via the lower vertex on the spin and parity, J^P, of the exchanged particle. In general for a resonance of spin J, the mixture may be described

Fig 30.

Chew - Frautschi plot, $K^+P \rightarrow K^0\Delta^{++}$

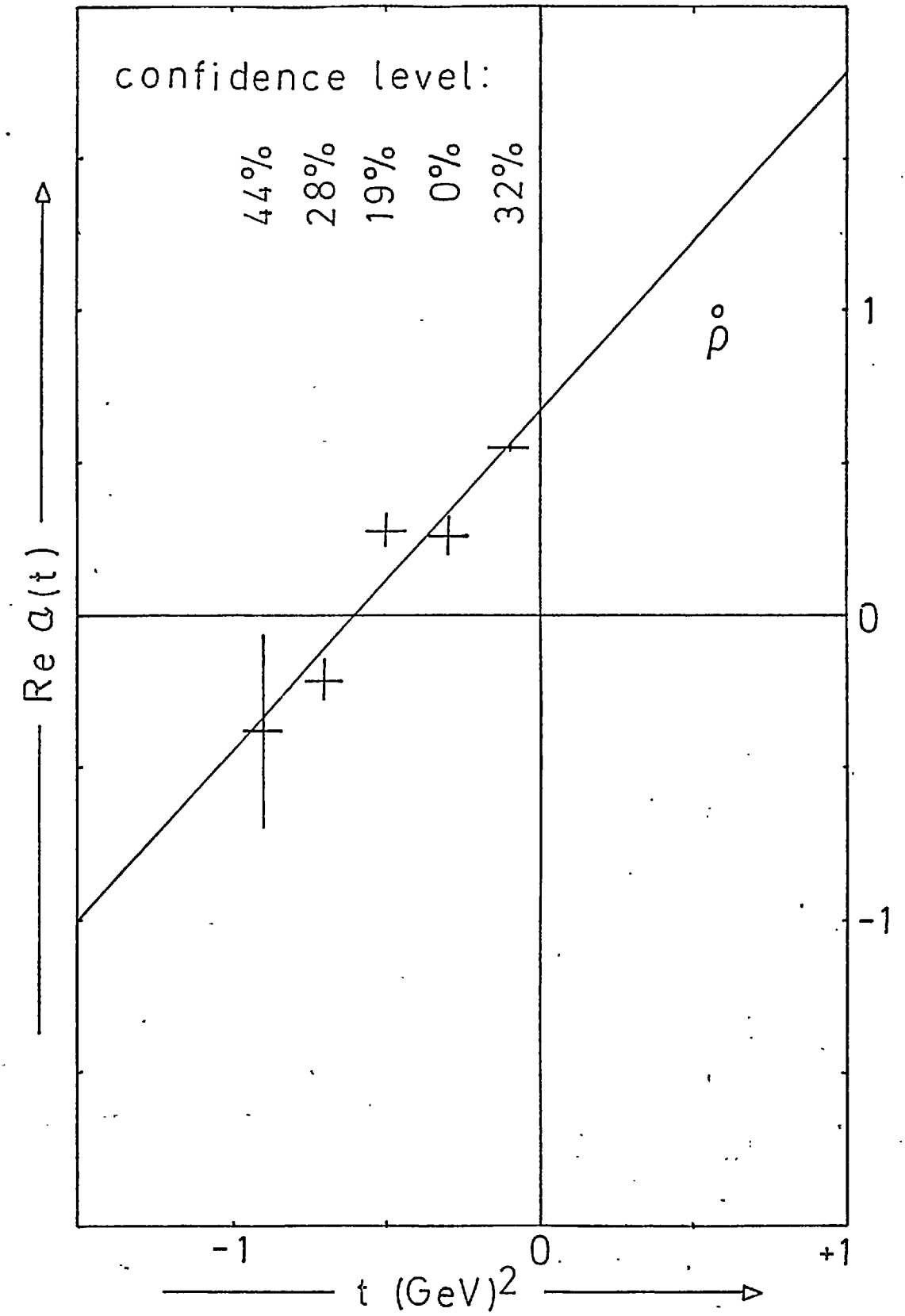

by a (2J+1) dimensional matrix ρ_{ij}, referred to as the density matrix. Each pure state is

$$|\psi_s\rangle = \sum_m a_{sm} |j,m\rangle \qquad - (6.9)$$

$|j,m\rangle$ being an eigenstate of $\hat{J}_z$.

If $|\psi_s\rangle$ is occupied with a probability P_s, then,

$$\rho_{ij} = \sum_s P_s a^*_{si} a_{sj} \qquad - (6.10)$$

Using the probability-density concept of quantum states, the decay angular distribution of a general mixed state is

$$W(\theta,\phi) = \sum_{m,m'} (Y_J^{m*} \cdot Y_J^{m'}) \rho_{m,m'} \qquad - (6.11)$$

Note the following restrictions on the values of ρ_{ij}

(a) $\rho_{ij} = \rho^*_{ji}$, hermitian, from definition (6.10)

(b) $Tr(\rho) = 1$, $\sum \rho_{jj} = 1$, by unitarity

(c) $\rho_{ij} = (-1)^{i-j} \cdot \rho_{-i-j}$, by parity conservation.

By choosing a suitable co-ordinate system in the rest frame of the resonance the associated Legendre functions may be expanded to get the decay distribution of the π from the Δ in terms of the density matrix elements. The most commonly used co-ordinate system, the Jackson system[21], is defined diagramatically in Fig. (32b). The z-axis is the direction of the incident particle, in this case the proton, which, as this is the rest frame of the resonance, is directly opposed to the direction of the exchanged particle e. The y-axis

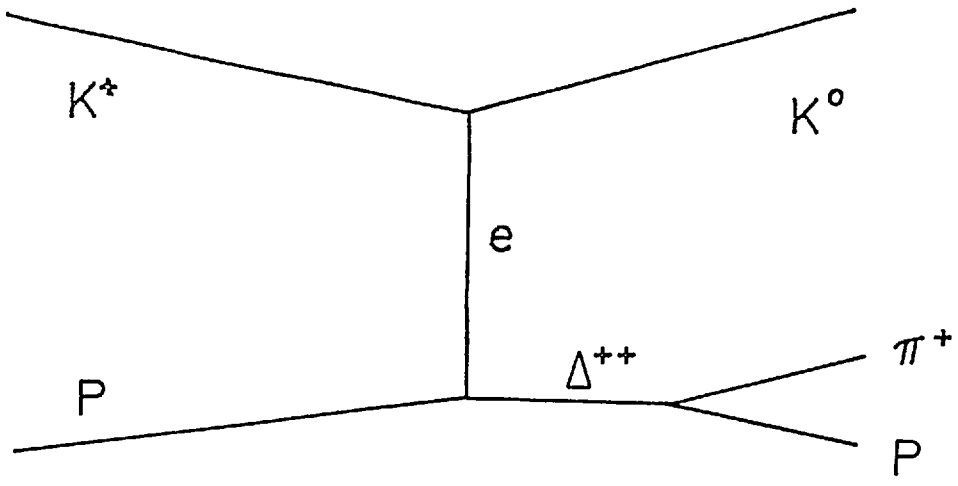

Fig. 32a. One Meson Exchange Diagram.

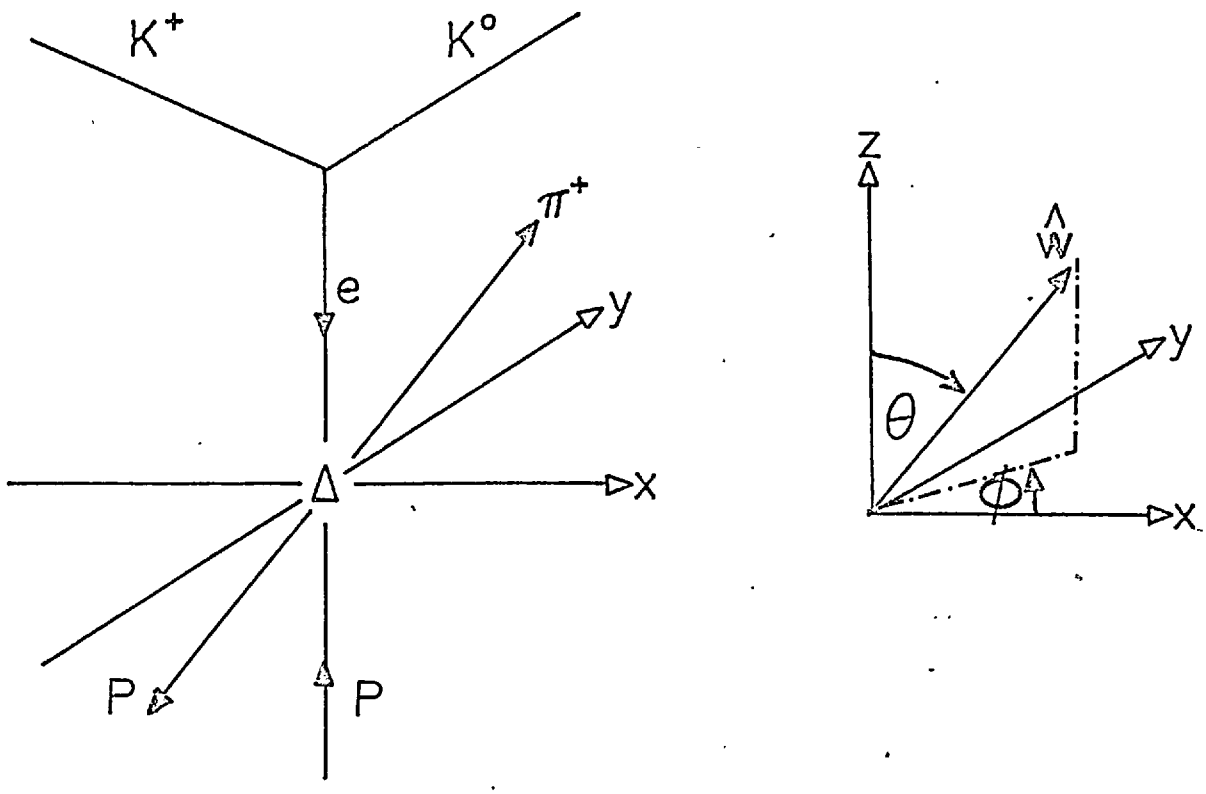

Fig.32b. The Jackson Coordinate System.

is the normal to the plane of production in the c.m.s. defined by:

$$\hat{y} = (\text{beam direction}) \wedge (\text{resonance direction})$$

The x-axis then follows by adopting a right-handed co-ordinate system.

The polar angle, θ, sometimes referred to as the Jackson angle, is then the angle between the z-axis and the decay line of flight, $\hat{W}$. The azimuthal angle ϕ, equal to the Trieman-Yang angle, is the angle the projection of $\hat{W}$ on the xy plane makes with the forward x-axis. The constraint of parity conservation ensures that production intensity at angle ϕ is the same as at $(\phi + \pi)$ so the distribution of this angle is commonly displayed folded in the range $0 \leqslant \phi < \pi$. An expansion of (6.11) for a $J = \frac{3}{2}$ Δ, decaying to a $J = \frac{1}{2}$ proton and $J = 0$ pion then gives the normalized decay distribution:[32]

$$W_{\Delta}(\cos\theta, \phi) = \frac{3}{4\pi}\,\frac{1}{6}\Big[(1+4\rho_{3,3}) + \tfrac{1}{2}(1-4\rho_{3,3})\cos^2\theta - \tfrac{2}{\sqrt{3}}\,\mathrm{Re}\,\rho_{3,-1}\sin^2\theta\cos 2\phi - \tfrac{2}{\sqrt{3}}\,\mathrm{Re}\,\rho_{3,1}\sin 2\theta\cos\phi\Big] \qquad (6.12)$$

where the indices of the density matrix are $2m$, $2m'$.

Thus, without polarization information the only density matrix elements which are observables are $\rho_{3,3}$ (equal to $\rho_{-3,-3}$ and giving ρ_{-1-1}, ρ_{11}) and the real parts of $\rho_{3,-1}$, $\rho_{3,1}$. Being hermitian the diagonal elements are wholly real. $\rho_{3,-1}$, $\rho_{3,1}$ are related to $\rho_{-3,+1}$ and $\rho_{-3,-1}$ via the parity rule.

A method of computing the ρ_{ij} is suggested by the method of moments as used in chapter 5. Multiplying both

sides of (6.12) by $\cos^2\theta$ and integrating over all of θ and ϕ :

$$\langle\cos^2\theta\rangle = \int_0^2 d\phi \int_\pi^0 d\theta \quad \cos^2\theta \cdot W(\cos\theta,\phi) = \frac{1}{15}(7-8\rho_{3,3})$$

or,
$$\rho_{3,3} = \frac{7-15\langle\cos^2\theta\rangle}{8} \qquad -(6.13)$$

Similarly,

$$\text{Re}\ \rho_{3,-1} = -\frac{5\sqrt{3}}{8}\langle\sin^2\theta\cos2\phi\rangle \qquad -(6.14)$$

$$\text{Re}\ \rho_{3,1} = -\frac{5\sqrt{3}}{8}\langle\sin2\theta\cos\phi\rangle \qquad -(6.15)$$

The errors on these quantities are derived from the error on the mean by dividing the standard deviation by the square root of the number of events, N, so that e.g.

$$\Delta\rho_{3,3} = \frac{15}{8\sqrt{N}}\langle(\delta\cos^2\theta)^2\rangle \text{ etc.} \qquad -(6.16)$$

One serious criticism of the method, so far discussed, is that it takes no account of the cross-over region with the other major resonance, the K^* (892). The extent of the problem may be seen by referring to the Dalitz plots of chapter 4, diagramatically represented in Fig. (33). A straight computation over the events falling in the Δ mass band includes also many extra events in which the K and the π form a K^* and the P π mass is only accidentally that of the Δ .

A method of overcoming this problem is suggested by P. Eberhard and M. Pripstein.[28] The events which fall in both the K^* and Δ bands, region A in Fig. (33), are excluded altogether. Simultaneously, events which lie in that region of the Dalitz plot, B, which represents a parity reversal of region A, with the proton and pion interchanged in the rest system of the Δ , are used to repopulate A with pure Δ events

Fig. 33 Eberhard - Pripstein parity reversal.

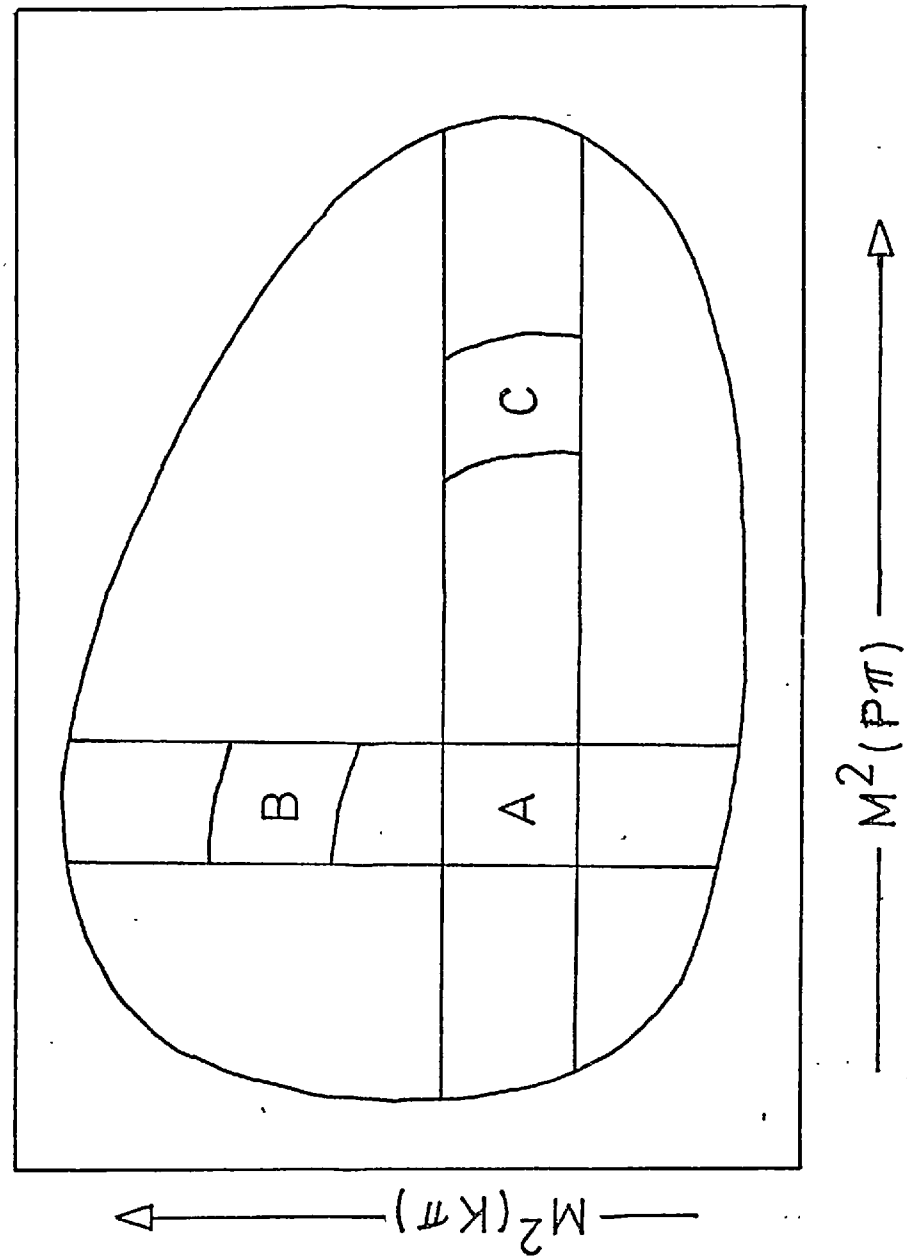

by performing this parity reversal. The effect on expressions (6.13) to (6.15) is merely to take these events with twice their weight.

It should be noted that the symmetry is only valid if the $P\pi$ system is produced in a state of definite parity. Interference between states of opposite parities introduces terms not satisfying the $P\pi$ interchange symmetry.

Naturally, when the K^* is being studied the blank area of region A is repopulated by an equivalent area, C in Fig. (33). By adding together the events of regions B + C and comparing to the number in region A, it is possible to test for interference between the K^* and Δ production amplitudes. Of course the sum (B + C) does include two lots of phase space events and A only includes one, but as there are few of these and they are distributed uniformly over the whole Dalitz plot, this is not a great problem.

The results of such a test on samples of data from the two channels where simultaneous resonance production can occur is given below in Table (10).

TABLE 10.

Evidence for No Resonance Interference

CHANNEL	REGION	2.11	2.31	2.53	2.72
$PK^o\pi^+$	A	262	155	106	98
	B + C	264	127	98	116
$PK^+\pi^o$	A	110	63	34	39
	B + C	103	68	40	50

As can be seen, the events in A tend to be a straight sum of (B + C). Within experimental error it is neither significantly greater, the case with positive interference, nor significantly less, as with negative interference. There could still be structure within region A which integrates out to give this result, but as this is by no means obvious from the various plots the conclusion of the experiment is that in this momentum region there is negligible interference in simultaneous K^* and Δ production.

6.3 One Meson Exchange Model (O.M.E.)

It is interesting to speculate that the peripheral nature of the differential cross-section discussed in (6.1) is due to the exchange of a single meson.

Referring to the diagram of Fig. (32a), it is clear that by conservation of isotopic spin at both upper and lower vertices I = 1 in the t channel. The 0^- K^+ dissociating into a 0^- K^0 and an exchange particle with arbitrary angular momentum between them requires an exchange of normal spin-parity, i.e. $J^P = 0^+, \ 1^-, \ 2^+, \ \ldots$

For spin-zero exchange, conservation of the z-component of angular momentum at the lower vertex implies $m = \pm \frac{1}{2}$. The states $|m = \pm \frac{3}{2}\rangle$ thus do not occur in the mixture of states of the resonance. Hence, we may predict

$$\rho_{\pm 3,m} = \rho_{m,\pm 3} = 0, \text{ in particular } \rho_{3,3} = 0.$$

This is, in fact, very far from being the case so scalar exchange may be ignored.

L. Stodolsky and J.J. Sakurai[35] have formulated a model for Δ production via the I = 1, $J = 1^-$ ρ meson by

treating the $N\rho\Delta$ vertex in analogy to the $N\gamma\Delta$ vertex in terms of electromagnetic multipole transitions. This latter vertex occurs in pion photoproduction:

$$\gamma N \longrightarrow \Delta \longrightarrow N\pi$$

which is dominated by the M1 magnetic dipole transition. In this reaction the produced Δ has only the spin orientations $m = \pm \frac{1}{2}$, normal to the production plane. Following through the implications of this it is possible to derive in the Jackson co-ordinate system, the Stodolsky-Sakurai predictions on the density matrix elements for ρ exchange in an M1 transition. They are:

$$\rho_{3,3} = \frac{3}{8} = 0.375$$

$$\text{Re}\,\rho_{3,-1} = \frac{\sqrt{3}}{8} = 0.216$$

$$\text{Re}\,\rho_{3,1} = 0$$

6.4 Experimental Results

The actual distribution of the decay angles of the π^+, θ, and ϕ, are shown for the four momenta in Fig. (34). On these plots the continuous lines represent the best fits obtained via the described method of moments. The dotted line is the above prediction of the Stodolsky-Sakurai model as normalised to the correct total number of events. In the past, the ρ - exchange model has failed to predict cross-sections over a wide range of momenta whatever (constant) values of the coupling constants are taken. This is not too surprising as, without s-dependent absorption, the model violates unitarity.

The computed values of the density matrix elements are given in Table (11) and are displayed graphically in

Fig 34a.

Decay angle distributions for $\Delta^{++}(1236)$.

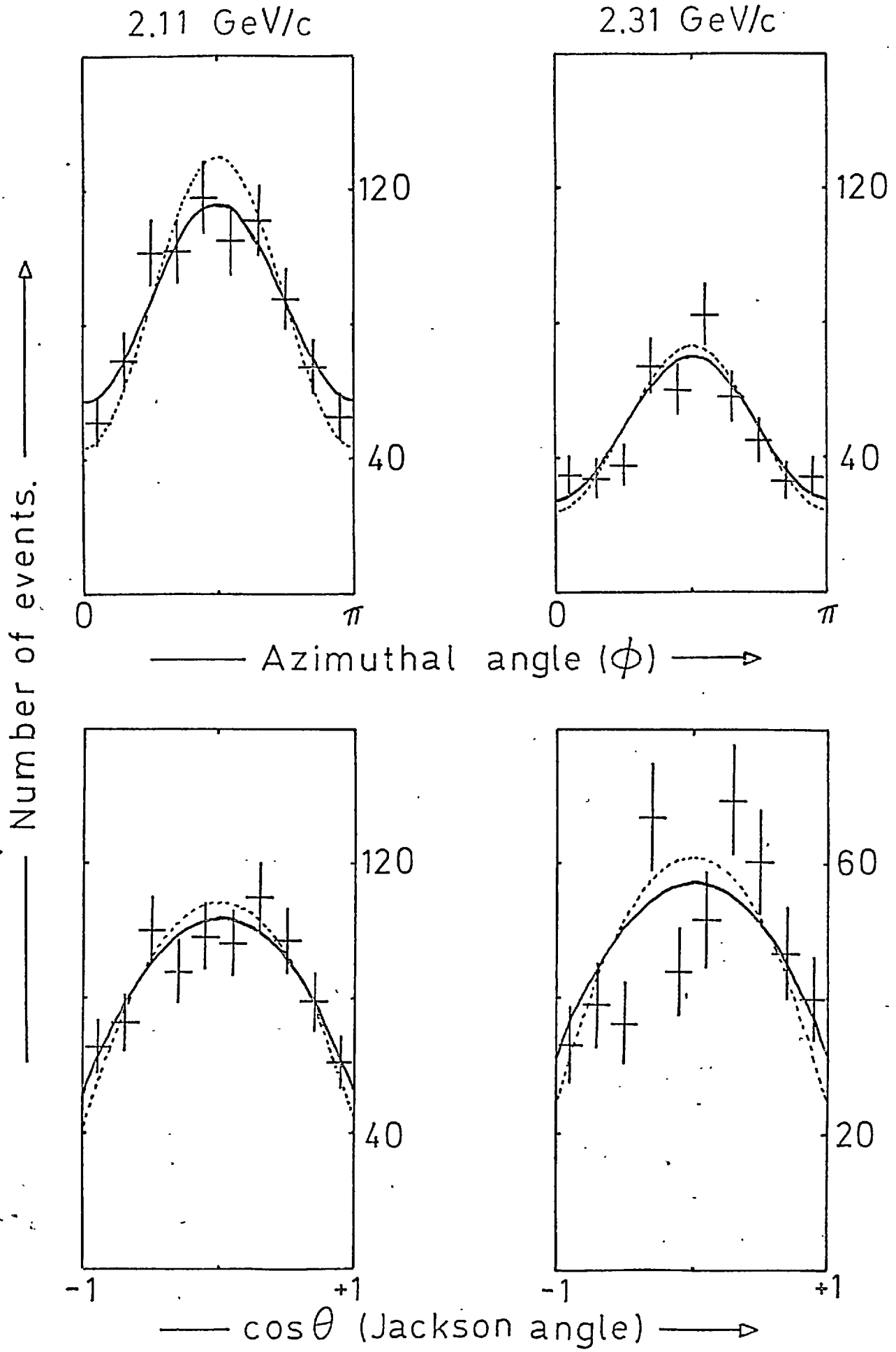

Fig 34b.

Decay angle distributions for $\Delta^{++}(1236)$.

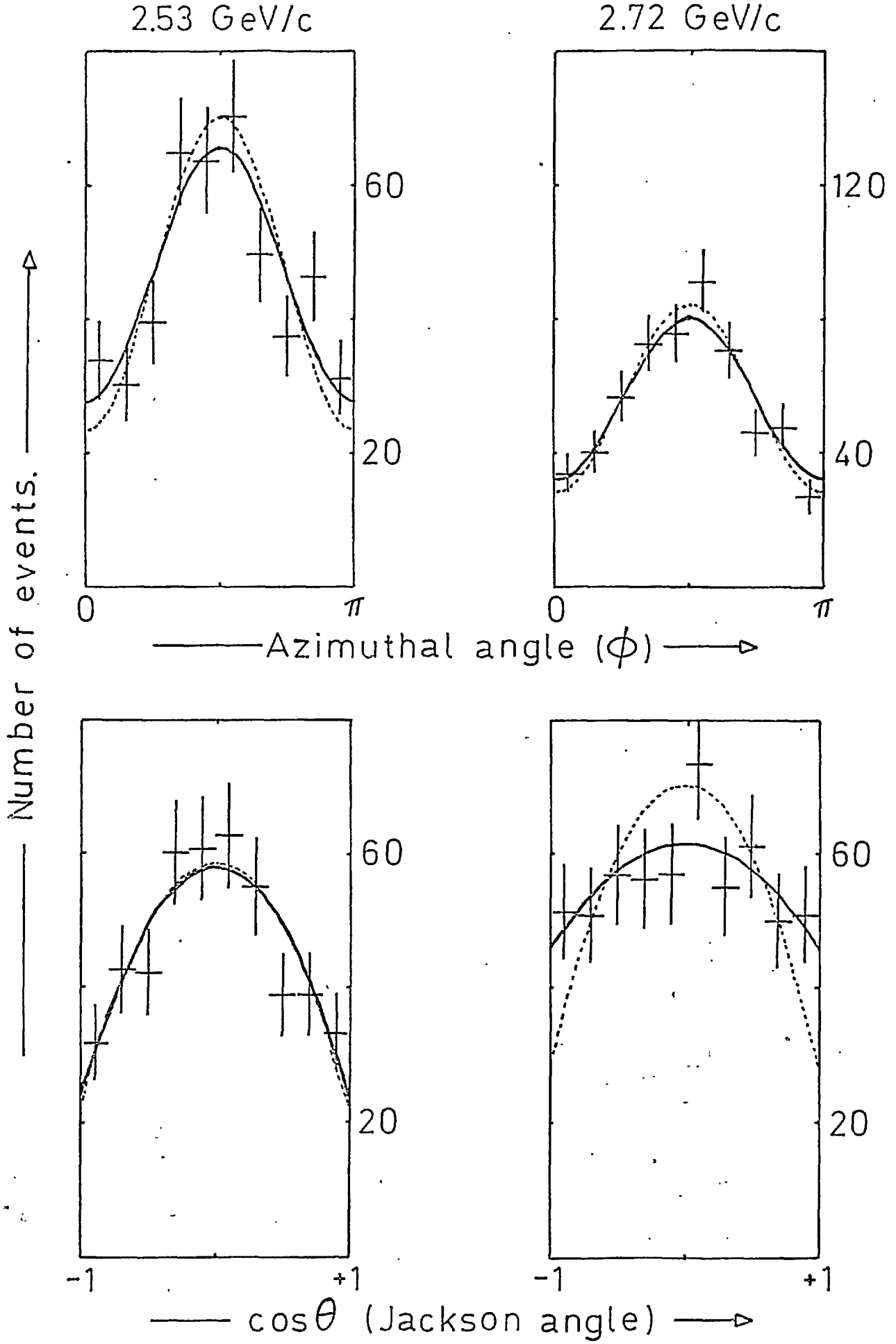

TABLE 11.

Δ^{++} (1236) Density Matrix Elements

The upper entry is that obtained using the technique of event conjugation, the lower is derived from raw data only

ρ_{ij}	t region $(GeV)^2$	2.11 GeV/c	2.31 GeV/c	2.53 GeV/c	2.72 GeV/c
ρ_{33}	(-1.0,-0.3)	.346±.032 .360±.026	.357±.042 .373±.033	.436±.044 .411±.038	.323±.040 .310±.036
	(-0.3,-0.1)	.347±.033 .372±.027	.321±.043 .333±.034	.296±.046 .296±.039	.336±.041 .314±.036
	(-0.1,-0.01)	.313±.049 .325±.040	.287±.065 .310±.054	.330±.063 .325±.055	.235±.057 .226±.052
	All t	.347±.020 .361±.016	.337±.026 .345±.021	.371±.026 .357±.023	.296±.025 .282±.022
Re $\rho_{3,-1}$	(-1.0,-0.3)	.199±.034 .239±.029	.172±.048 .238±.039	.202±.054 .217±.047	.216±.044 .252±.039
	(-0.3,-0.1)	.086±.035 .172±.030	.180±.047 .226±.039	.166±.047 .192±.040	.105±.043 .096±.038
	(-0.1,-0.01)	.198±.052 .185±.045	.216±.069 .193±.059	.233±.068 .170±.061	.214±.055 .136±.051
	All t	.147±.021 .190±.018	.189±.029 .224±.024	.176±.029 .186±.026	.186±.025 .177±.023
Re $\rho_{3,1}$	(-1.0,-0.1)	-.073±.029 -.097±.025	-.083±.040 -.014±.031	-.131±.038 -.127±.034	.013±.038 .008±.035
	(-0.3,-0.1)	-.055±.032 -.071±.026	-.028±.041 -.108±.035	-.054±.041 -.071±.036	-.028±.039 -.061±.037
	(-0.1,-0.01)	-.053±.046 -.099±.040	.045±.059 -.065±.048	-.097±.052 -.144±.050	.004±.045 -.039±.049
	All t	-.055±.018 -.081±.015	-.044±.024 -.064±.020	-.089±.023 -.103±.021	-.010±.022 -.026±.021

Fig. (35), together with other published data, as a function of beam momentum from threshold to 3 GeV/c. It can be seen that the prediction of the Stodolsky-Sakurai model is closely followed, there being no evidence of any s-channel activity. In common with most of the other experiments, however, the obtained values of the ρ_{ij} are consistently slightly below the predictions of the model. In the diagrams of Fig. (34), this has the effect of the fitted curve displaying rather less structure than the model and could be due to the inclusion of rather more isotropic phase space by the mass cuts.

To complete a full description of the Δ production characteristics, it is necessary to give the variation of the density matrix elements with the momentum transfer. These are shown for the four momenta in Fig. (36). Within errors there is no sign of any structure, the values being reconcilable with the non-absorptive Stodolsky-Sakurai predictions.

Fig 35.

Density matrix elements of $\Delta^{++}(1236)$ as a function of momentum.

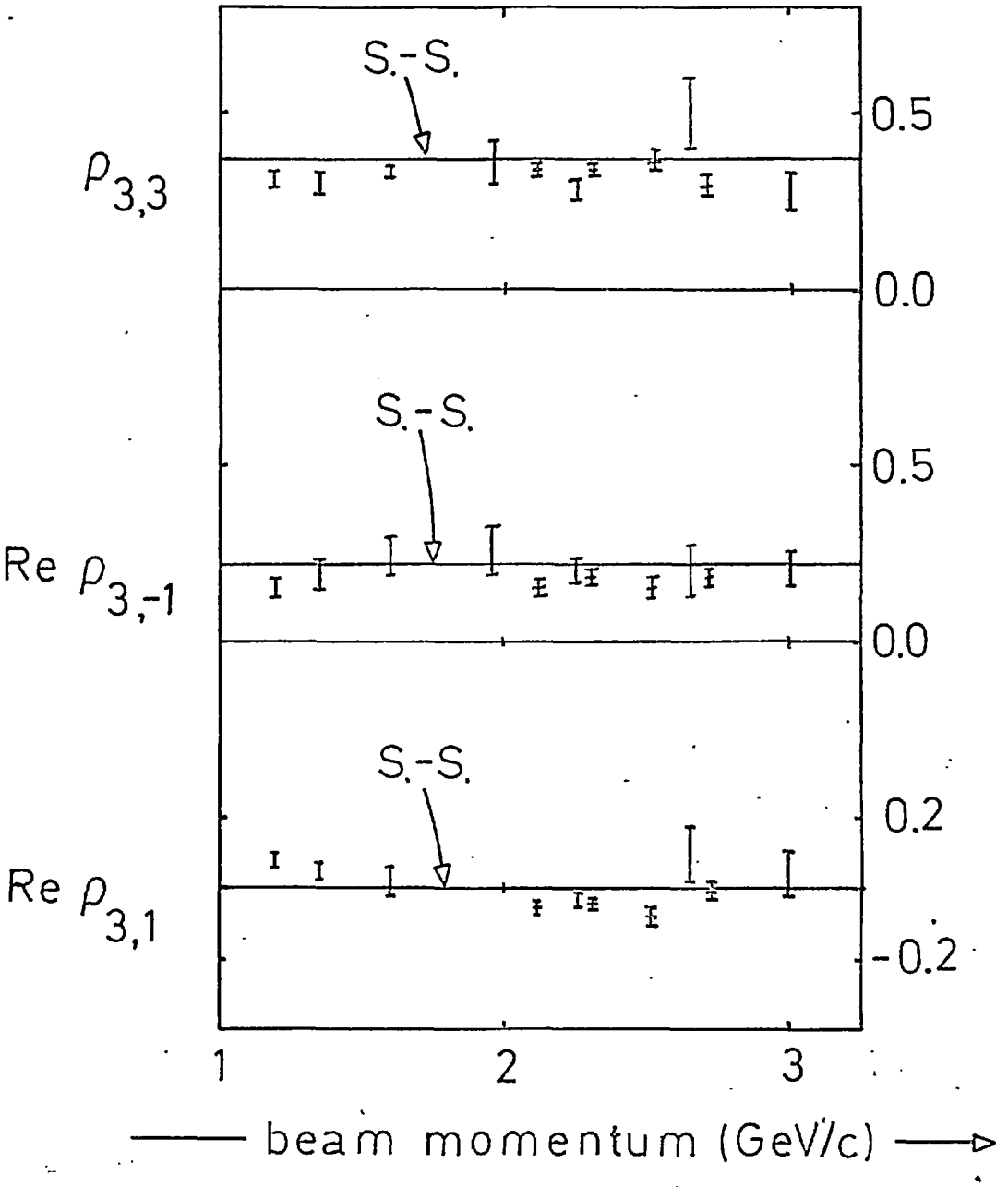

$\dagger$: this experiment.

Fig36a Density matrix elements of $\Delta^{++}(1236)$ as a function of momentum transfer.

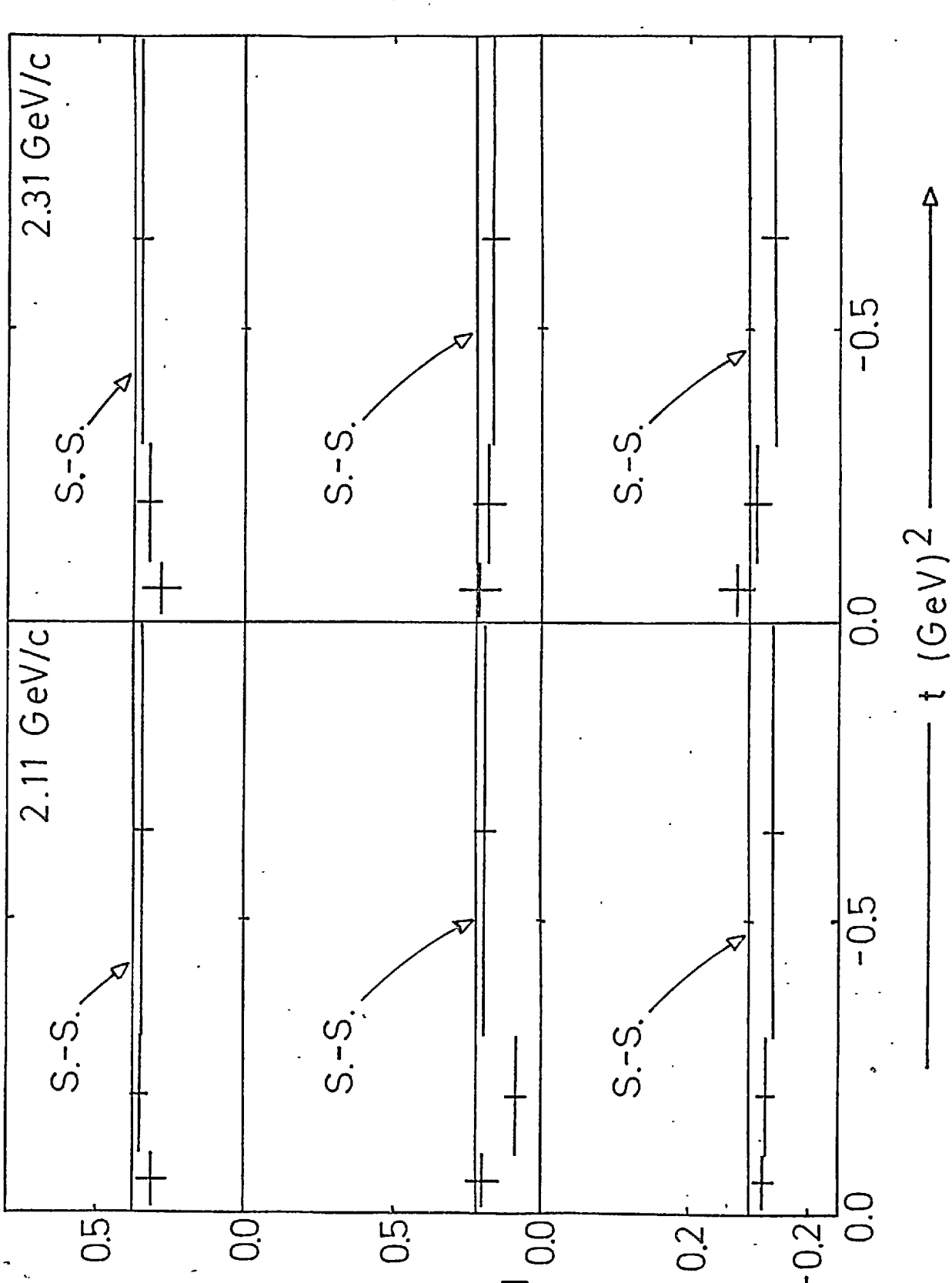

Fig36b. Density matrix elements of $\Delta^{++}(1236)$ as a function of momentum transfer.

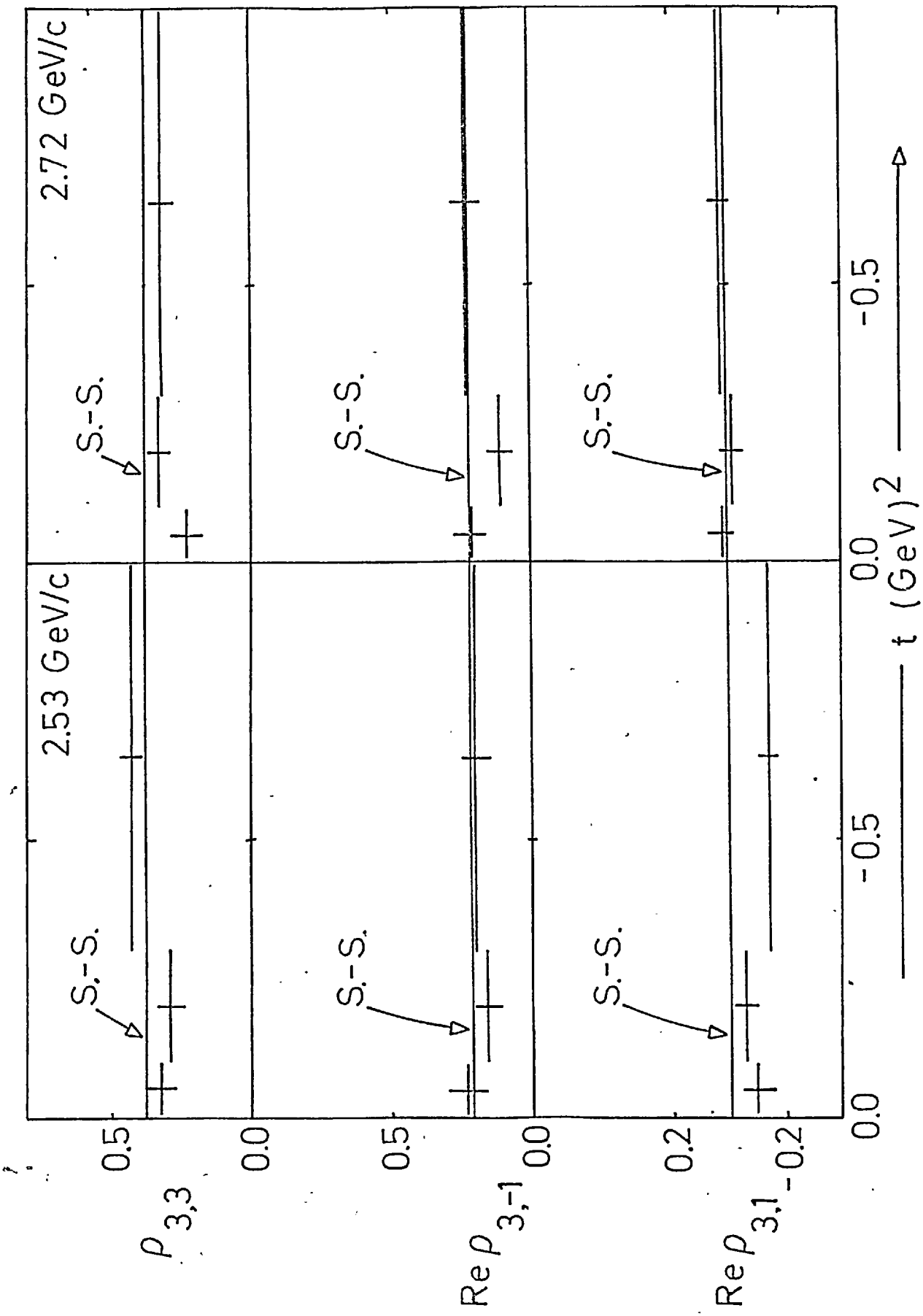

CHAPTER 7

K^{*+} (892) PRODUCTION CHARACTERISTICS

7.1 Differential Cross-Section

In attempting a straight line fit to log $(\frac{d\sigma}{dt})$ for the K^*, the problem of the non-zero t_m is much more acute owing to the higher mass of this resonance above the K mass. Here, t_m extends from -0.012 GeV^2 at the highest momentum, to -0.022 GeV^2 at 2.11 GeV/c. However, both of these figures are well contained in the first plotting bin of $t = -0.0125 \pm 0.0125$ GeV^2 so the previous technique of obtaining the differential cross-section slopes by omitting this bin is still valid. The actual plots obtained for $d\sigma/dt$ are shown in Fig. (37a,b) for the four incident momenta. As with the Δ the distributions show a flattening and a slight dip as t approaches zero. In addition there appears to be a slight dip at $t \sim -0.15(GeV)^2$ which, although hardly significant statistically, is present at all momenta. The data points of Fig. (37) are superimposed over the predictions of a Regge model to be discussed in section (7.3).

The values for the slopes and intercepts from straight line fits omitting the first point are given in Table 12 with the results from the CERN-Brussels collaboration and the author's fits to other published data.(33)

The behaviour is by no means as regular as with the Δ, but it is not clear to what extent the slope variation between 2 and 3 GeV/c may be associated with the K^* properties discussed in chapter 5. On the whole, however, there is still a shrinking forward peak.

Fig 37a. Differential cross sections for K^{*+}.

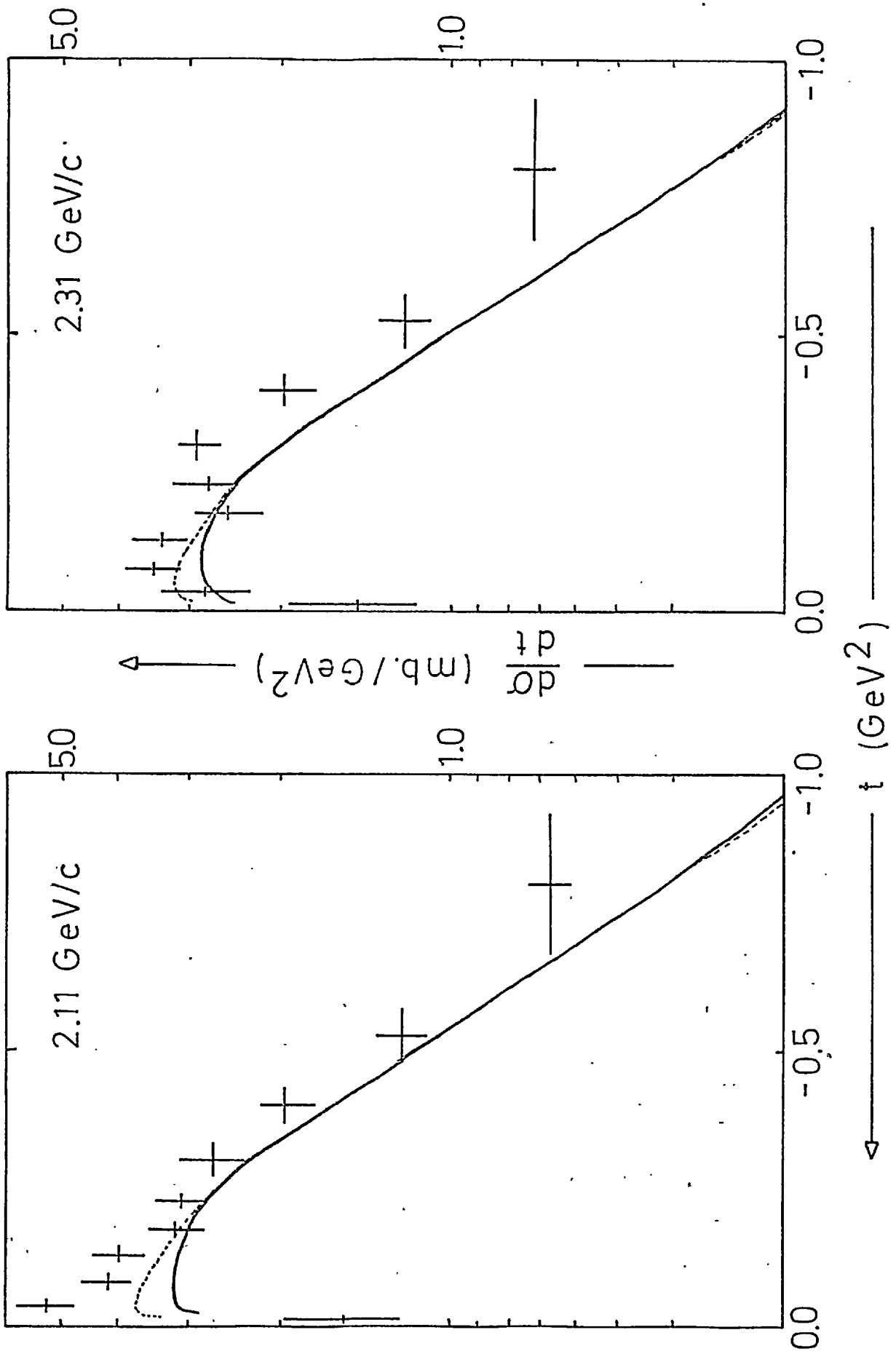

Fig 37b. Differential cross sections for K^{*+}

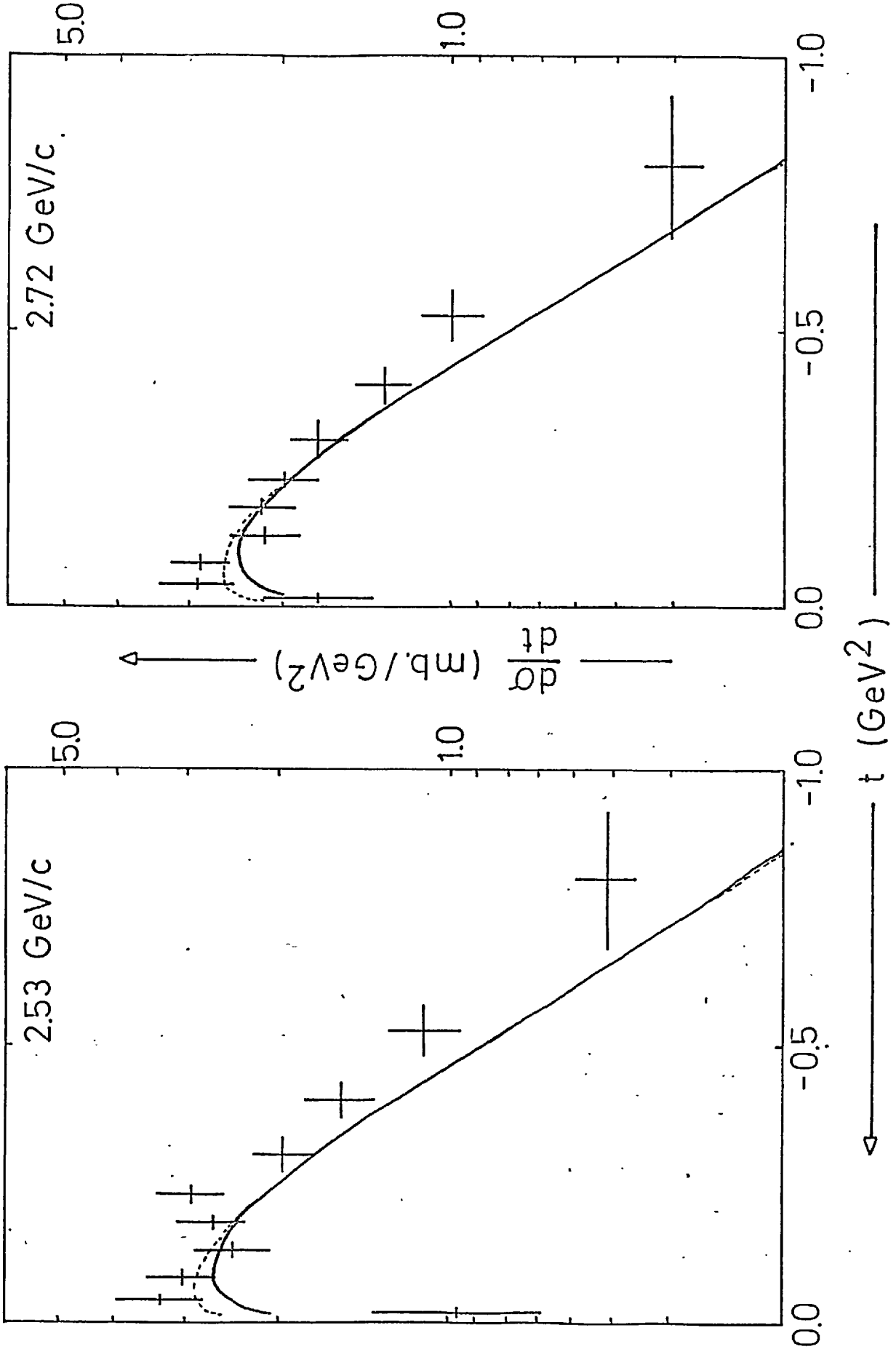

TABLE 12.

Slopes and Intercepts of $\frac{d\sigma(K^*)}{dt}$ plots

P_{LAB}(GeV/c)	1.21	1.36	1.96			
Slope (mb/GeV^2)	1.8±0.3	1.8±0.3	3.2±0.4			
Intercept (mb)	5.7	13.2	6.3			
P_{LAB}(GeV/c)	2.11	2.31	2.53	2.65	2.72	
Slope (mb/Gev^2)	2.7±0.1	2.0±0.1	2.4±0.2	2.9±0.8	2.5±0.1	
Intercept (mb)	5.5	4.8	3.9	4.5	3.3	
P_{LAB}(GeV/c)	3.0	3.5	4.6	5.0		
Slope (mb/GeV^2)	3.6±0.4	3.2±0.3	3.5±1.0	4.2±1.1		
Intercept (mb)	2.9	2.0	3.5	1.5		

The slopes obtained are all in the neighbourhood of ~3 mb/(GeV)^2 as opposed to the much steeper slope ~9 mb/(GeV)^2 obtained in K^{*o} production in deuterium around the same energy.[7] As will be discussed in section (7.2) it is thought that pion exchange dominates in this latter reaction, but with K^{*+} production it is clear that the dominant exchange is from a much heavier particle.

Although it is doubtful whether the data justifies it, the single pole dominance Regge model was applied in the same manner as section (6.1) and the values of $\alpha(t)$ shown in

Fig. (38) obtained. A straight line was fitted with confidence level 44% giving the trajectory parametrisation:

$$\alpha(t) = (0.24 \pm 0.33) + (1.08 \pm 0.34)\ t \qquad -(7.1)$$

This has much the same gradient as the trajectory governing peripheral Δ^{++} production (6.6) but a much lower intercept. It is interesting to note that it passes between the positions of the ρ(or ω) and π poles.

7.2 Density Matrix Elements

As the K^* (892) has a well established $J^P = 1^-$ the density matrix has dimension 2J+1 = 3. The observables are chosen to be $\rho_{0,0}$ (which gives $\rho_{1,1}$ in turn equal to $\rho_{-1,-1}$ via the trace and parity rules), $\rho_{1,-1} = \rho_{-1,1}$ (and real by the same rules) and $\mathrm{Re}\rho_{1,0} = \mathrm{Re}\rho_{0,1}$. $\mathrm{Im}\rho_{1,0}$ needs polarization data to be determined.

The decay angular distribution of a 1^- vector meson decaying into two pseudo-scalar mesons is, in terms of these elements:[32]

$$W(\cos\theta,\phi) = \frac{3}{4\pi} \cdot \left[\frac{1}{2}(1-\rho_{0,0}) + \frac{1}{2}(3\rho_{0,0}-1)\cos^2\theta - \rho_{-1,1}\sin^2\theta\cos 2\phi - \sqrt{2}\,\mathrm{Re}\rho_{1,0}\sin 2\theta\cos\phi \right] \qquad -(7.2)$$

Using the method of moments this expression gives:

$$\rho_{0,0} = \frac{5\langle\cos^2\theta\rangle - 1}{2}\ ;\ \Delta\rho_{0,0} = \frac{5}{2\sqrt{N}}\langle(\delta\cos^2\theta)^2\rangle$$

$$\rho_{1,-1} = -\frac{5}{4}\langle\sin^2\theta\cos 2\phi\rangle\ ;\ \Delta\rho_{1,-1} = \frac{5}{4\sqrt{N}}\langle(\delta\sin^2\theta\cos 2\phi)^2\rangle$$

$$\mathrm{Re}\,\rho_{1,0} = -\frac{5}{4\sqrt{2}}\langle\sin 2\theta\cos\phi\rangle\ ;\ \Delta\mathrm{Re}\,\rho_{1,0} = \frac{5}{4\sqrt{2N}}\langle(\delta\sin 2\theta\cos\phi)^2\rangle \qquad -(7.3)$$

Fig 38.

Chew - Frautschi plot, $K^+P \rightarrow K^{*+}P$

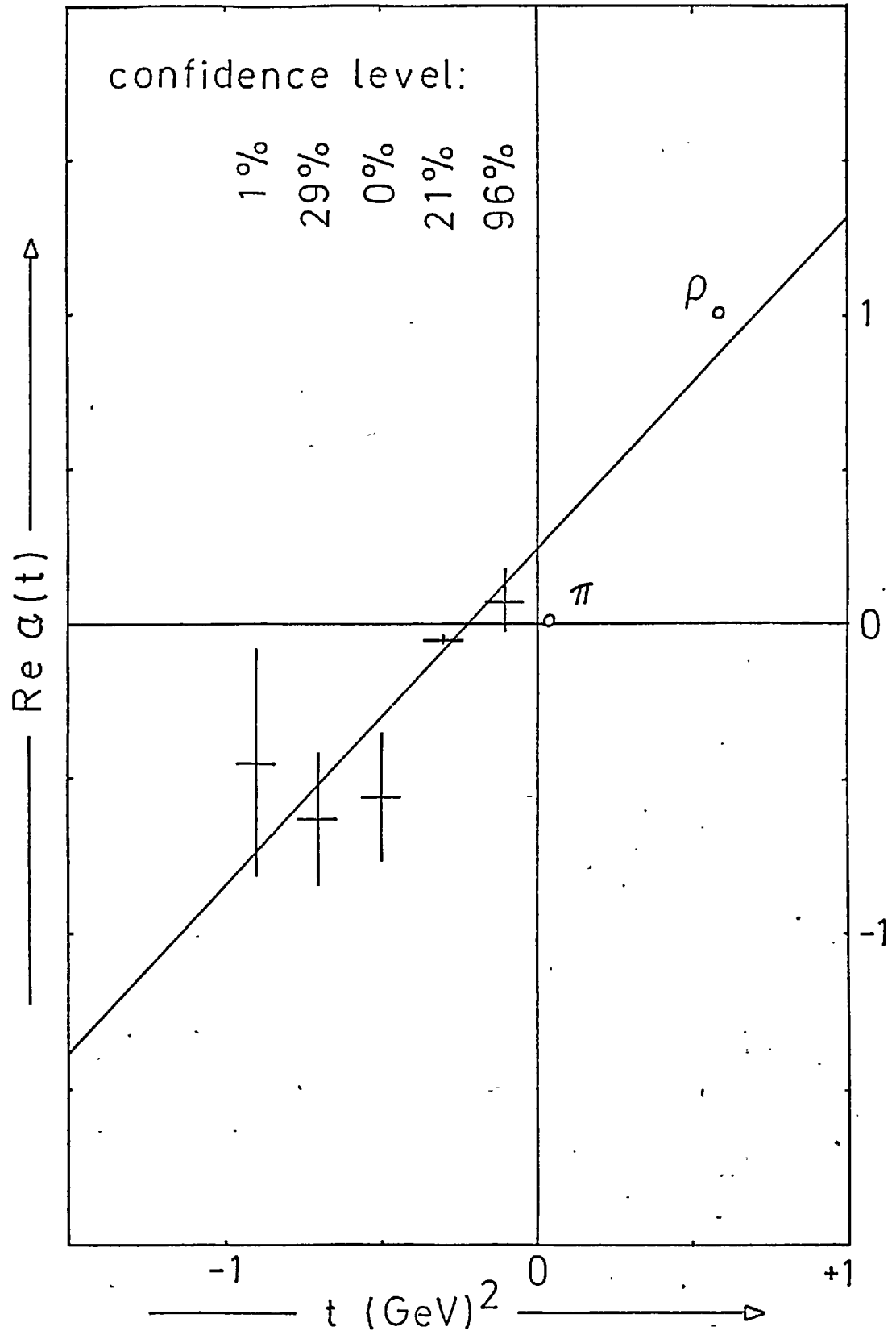

In the context of the O.M.E. model, it is clear that if the exchanged particle has no spin it must be in an angular momentum state of $l = 1$ with the incoming K^+ and hence must have negative parity, i.e. a pseudoscalar meson.

Quantizing along the direction of motion of the K^+, conservation of the z - component of angular momentum means that the states $m = \pm 1$ can never be occupied and hence,

$$\rho_{\pm 1,m} = \rho_{m,\pm 1} = 0$$

And from the trace condition

$$\rho_{0,0} = 1$$

As there is zero strangeness in the t channel the pseudoscalar meson would be a π or η.

In the case of natural parity exchange (i.e. in the series $J_e^P = 1^-$, 2^+, 3^- etc.) a combination of conservation of angular momentum, l, and conservation of parity gives $l = J_e$. Conservation of the z - component of angular momentum means that $(J_e)_z = m = 0, \pm 1$. However, the state $|J_e,0\rangle$ and $|1,0\rangle$ cannot be combined to $|J_K^* = 1, 0\rangle$ because of a vanishing Clebsch-Gordon coefficient. It follows that the state $|m = 0\rangle$ cannot appear in the mixture $|\psi\rangle$ and hence,

$$\rho_{0,m} = \rho_{m,0} = 0, \text{ and in particular, } \rho_{0,0} = 0$$

$$\rho_{1,-1} \text{ remains arbitrary and real} \qquad -(7.5)$$

If both pseudoscalar and vector exchange are taking place the degree of occupation of the $|m = 0\rangle$ state becomes a measure of the cross-section from each process, i.e. $\rho_{0,0}$ becomes the fraction of 0^- exchange. For this to be valid the 0^- and 1^- contributions must add incoherently, there must

be no interference between the Y_1^0 and $Y_1^{1,-1}$ states. A measure of this condition is that Re $\rho_{1,0} = 0$. Absorption effects destroy this condition and produce a Re $\rho_{1,0}$ which is small and negative. Reference (5) contains results of an absorptive model of Gottfried, Jackson and Svensson containing mixed 0^- and 1^- exchange. When averaged over production angles this predicts

$$\rho_{0,0} = 0.13$$

$$\rho_{1,-1} = 0.31$$

$$\text{Re } \rho_{1,0} = -0.07 \qquad -(7.6)$$

The results obtained from this experiment are given in Table (13) and shown together with the above prediction and results from experiments at nearby momenta in Fig. (39). There is no very significant evidence for s-channel structure, but it is interesting to speculate that the one standard deviation dip seen in $\rho_{0,0}$ is associated with the K^* structure already mentioned in this thesis. In the simple minded approach it could be said that there is about 20% pion exchange and 80% vector meson exchange from threshold upwards.

The actual decay angle distributions are shown in Fig. (40a,b) for the four momenta. Here, the solid line represents the best fit and the dotted line the normalised prediction of pure pseudoscalar exchange. It is clear that the distribution of the Trieman-Yang angle is not isotropic and the cosine of the Jackson angle displays an inverted parabola, i.e. it is the vector meson exchange which dominates. The variation in $\rho_{0,0}$ mentioned above can be seen in the data as a sharpening of this parabola between 2.11 and 2.31 GeV/c.

TABLE 13.

K^{*+} (892) Density Matrix Elements

The upper entry is that obtained using the technique of event conjugation, the lower is derived from raw data only

ρ_{ij}	t region $(GeV)^2$	2.11 GeV/c	2.31 GeV/c	2.53 GeV/c	2.72 GeV/c
$\rho_{0,0}$	(-1.0,-0.3)	.160±.040 .089±.032	.084±.038 .054±.033	.118±.047 .084±.042	.067±.039 .055±.035
	(-0.3,-0.1)	.256±.050 .227±.040	.110±.051 .148±.045	.273±.059 .251±.050	.171±.049 .164±.045
	(-0.1,-0.01)	.448±.068 .474±.059	.371±.083 .387±.045	.424±.084 .420±.074	.388±.075 .347±.067
	All t	.265±.027 .226±.022	.138±.027 .141±.024	.215±.031 .201±.028	.179±.027 .176±.025
$\rho_{1,-1}$	(-1.0,-0.3)	.232±.037 .175±.030	.298±.040 .230±.035	.306±.047 .231±.044	.283±.043 .209±.040
	(-0.3,-0.1)	.176±.044 .134±.033	.251±.052 .224±.042	.218±.050 .162±.045	.257±.048 .219±.045
	(-0.1,-0.01)	.193±.046 .213±.039	.178±.070 .148±.060	.021±.070 .004±.061	.067±.060 .009±.056
	All t	.174±.023 .143±.019	.228±.028 .193±.024	.193±.029 .141±.026	.203±.026 .156±.024
Re $\rho_{1,0}$	(-1.0,-0.3)	-.027±.024 -.064±.021	-.027±.023 -.040±.021	-.028±.026 -.046±.025	-.023±.025 -.054±.024
	(-0.3,-0.1)	-.057±.027 -.099±.022	-.026±.029 -.098±.025	-.073±.033 -.111±.031	-.037±.030 -.051±.029
	(-0.1,-0.01)	-.079±.032 -.096±.028	-.094±.046 -.132±.041	-.189±.056 -.182±.045	-.098±.042 -.121±.038
	All t	-.041±.015 -.070±.013	-.044±.016 -.072±.015	-.068±.019 -.080±.017	-.033±.016 -.053±.015

Fig 39.

Density matrix elements of $K^{*+}(892)$ as a function of momentum.

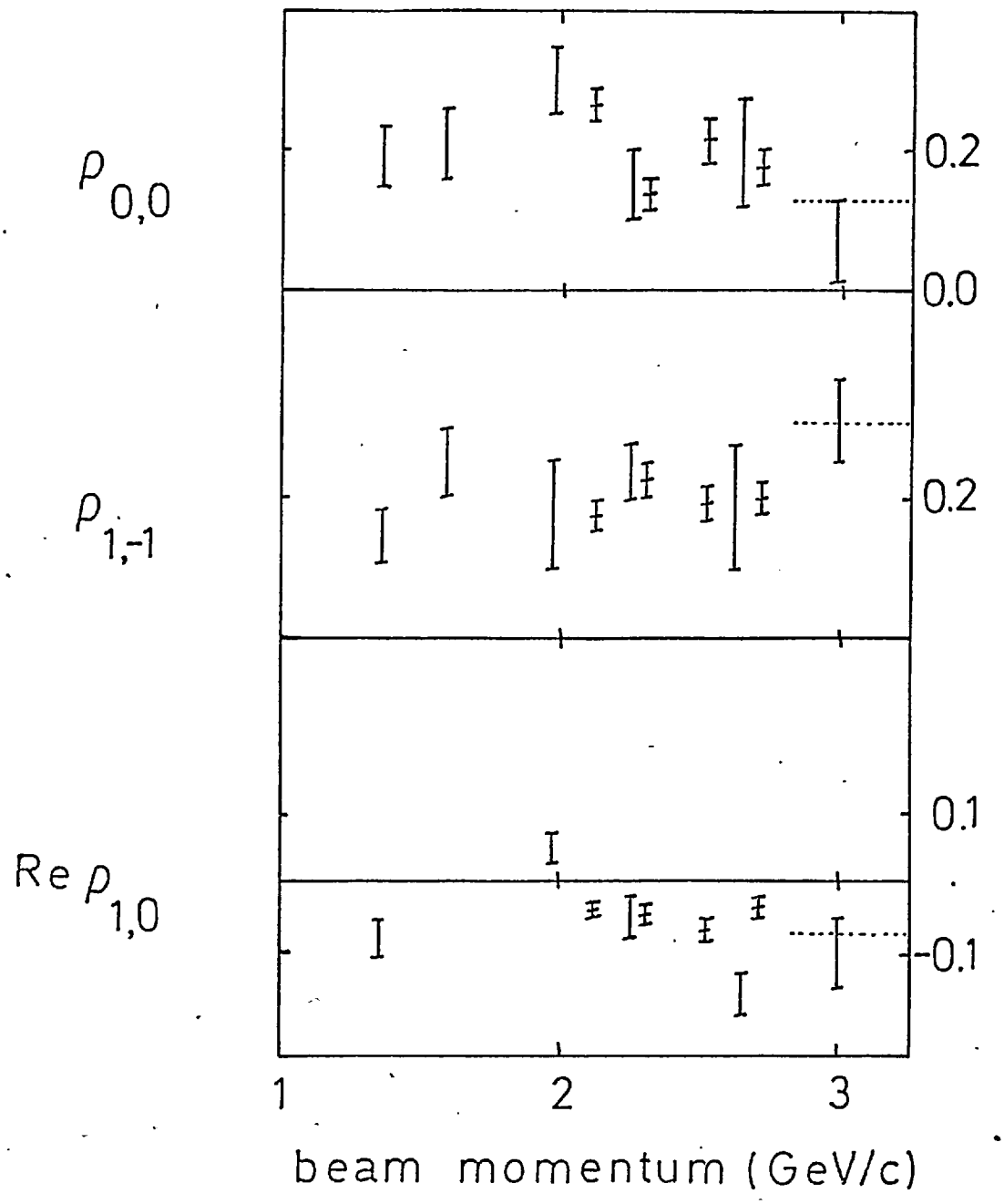

$\dagger$: this experiment.

····· : absorption model.

Fig 40a.

Decay angle distributions for $K^{*+}(892)$.

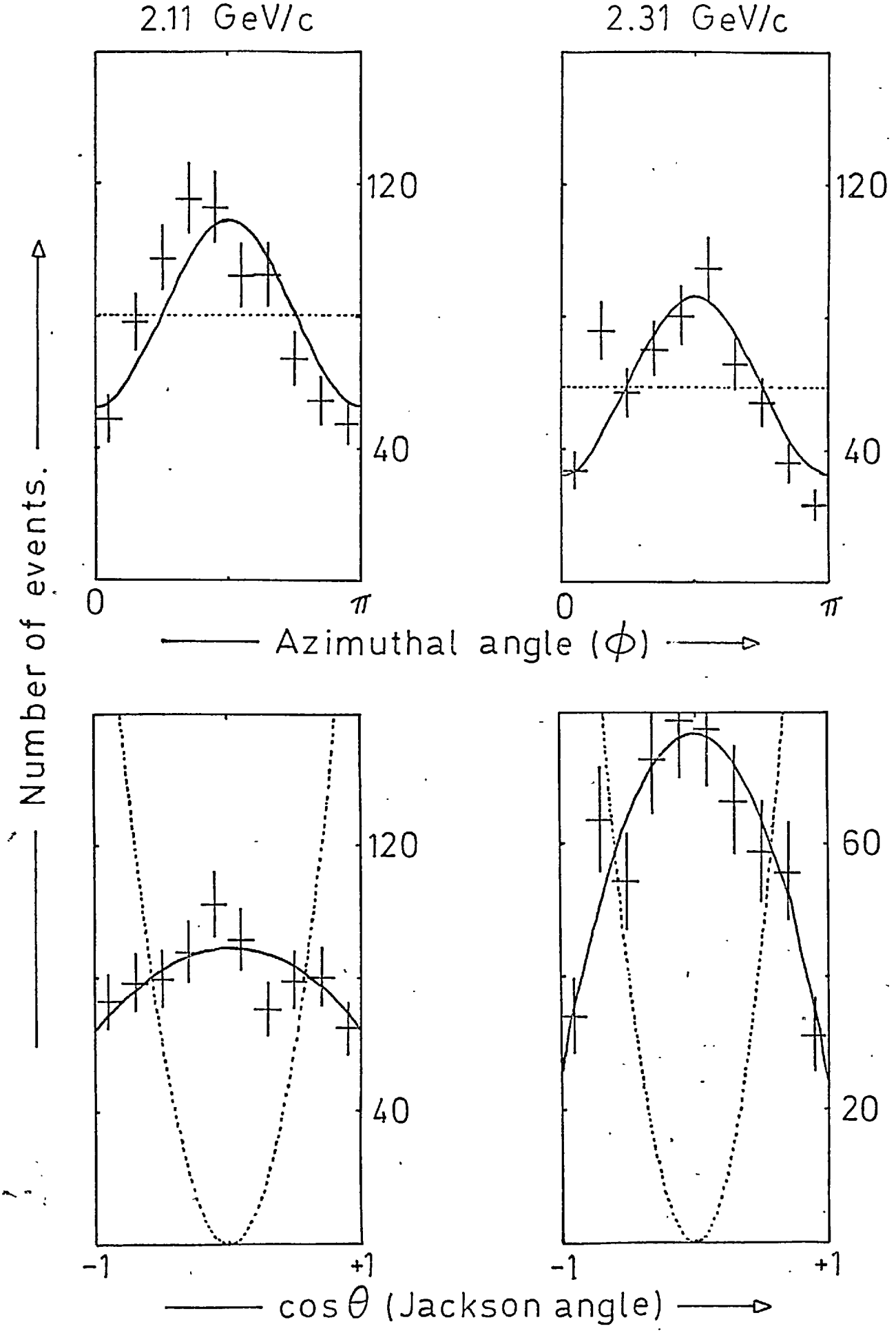

Fig 40b.

Decay angle distributions for $K^{++}(892)$.

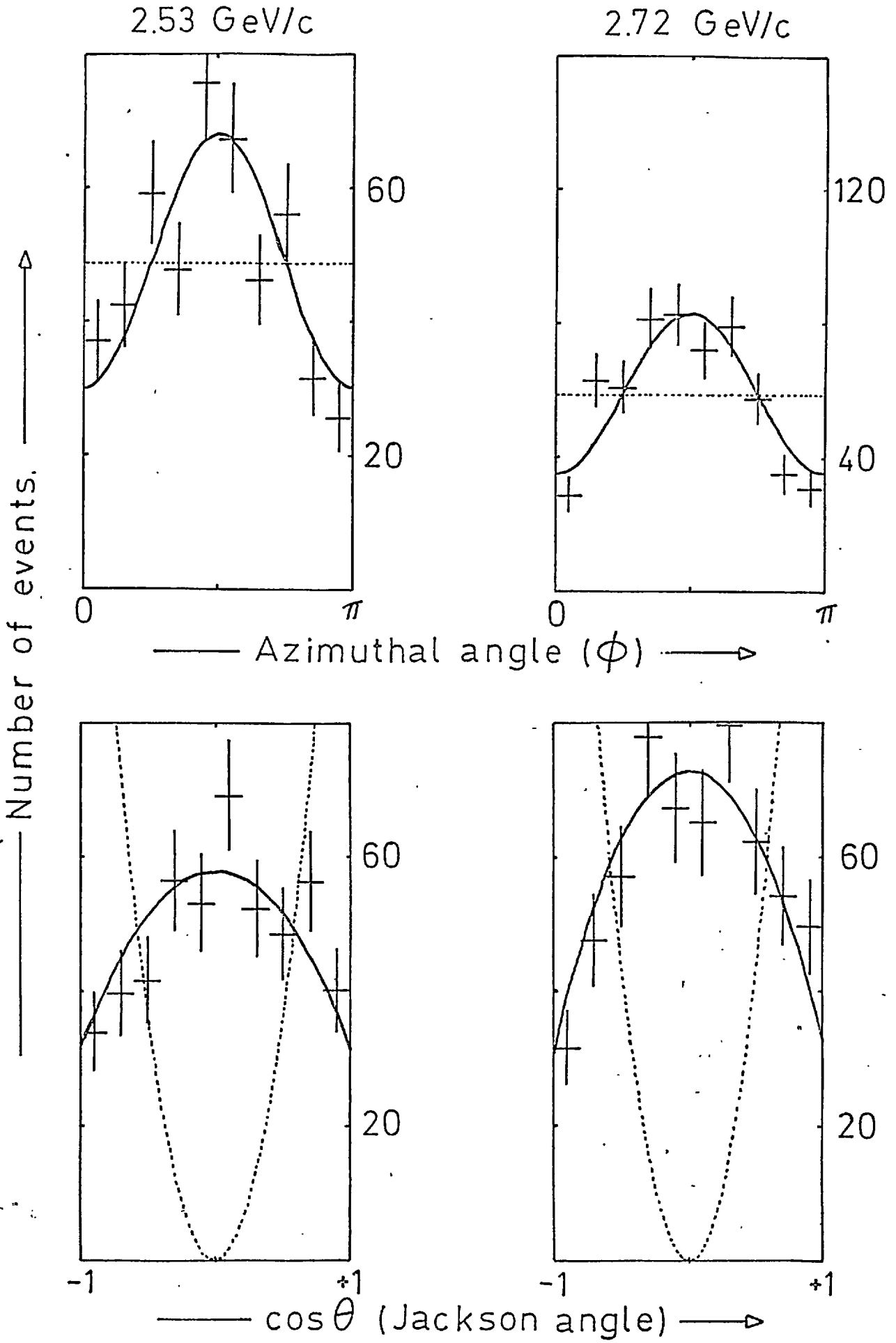

All of the plots shown incorporate the Eberhard-Pripstein event conjugation method as described in chapter 6.

The most likely vector mesons to be exchanged are the ρ^0 or the ω^0 (charge is zero in the t channel). However, in the charge exchange channel $K^+N \longrightarrow K^{*o}P$, the decay angular distributions are characteristic of only pion exchange.[7] As both the π and the ρ would be equally capable of transferring one unit of charge, it seems reasonable to suppose that the vector meson which contributes to K^* production is the isotopic singlet ω .

7.3 Dass and Froggatt Model

Although the simple one meson exchange model, modified by absorptive corrections, has had considerable success in the K^* production process, it suffers from the high energy cross-section dependence, $\sigma \sim s^{2J-2}$, for high spin J exchange. The Regge pole theory has provided what is, at least, a good method of parametrising many reactions and the energy dependence of most two body reaction cross-sections seem to follow its predictions.

Accordingly there has been some attempt at building Regge pole models for quasi two body processes. Unfortunately, the complications brought about by unequal masses and spin add a great deal to the complexity (and hence credibility) of the model.

Unequal masses introduce kinematic singularities in the amplitude which can only be eliminated by invoking a whole series of daughter trajectories of alternating parity to the parent and with intercepts at t = 0 at unit intervals below the parent intercept. Although their low intercepts mean that

the energy dependence effect of such trajectories could never be seen, it is interesting to note that the Veneziano model predicts just such daughters.

In treating the case of spin, a number of independent helicity amplitudes are constructed. In the general process $1 + 2 \rightarrow 3 + 4$ where the particles have helicities $\lambda_1, \lambda_2, \lambda_3$ and λ_4 it is possible to define a net helicity flip, n,

$$n = \left| (\lambda_3 - \lambda_4) - (\lambda_1 - \lambda_2) \right| \qquad -(7.7)$$

In the forward direction, by conservation of angular momentum, any helicity amplitude must vanish as $(\sin \frac{\theta}{2})^n$. This condition imposes a definite set of constraint equations on the crossed channel amplitudes. These constraints can be satisfied in two ways. Either the residues alone satisfy the equations by vanishing at the required point (EVASION), or there must exist, at least at this point, a CONSPIRING trajectory of exactly the same intercept but opposite parity to cancel the amplitudes out.

In the model proposed by G.V. Dass and C.D. Froggatt (17) alternative solutions including either evasive or conspiring pion contributions are presented, together with some A_2 exchange. In the differential cross-sections of Fig. (37) and t variation of density matrix elements of Fig. (41) the predictions from the latest fits are shown with a full line for the evasive solution and, where it is appreciably different, with a dotted line for the conspiracy solution.

It has already been noted that the data is dominated by an isoscalar natural parity pole. For this purpose, however, the ω-trajectory must be rejected. Having odd signature,

Fig 41a. Density matrix elements of $K^{*+}(892)$ as a function of momentum transfer.

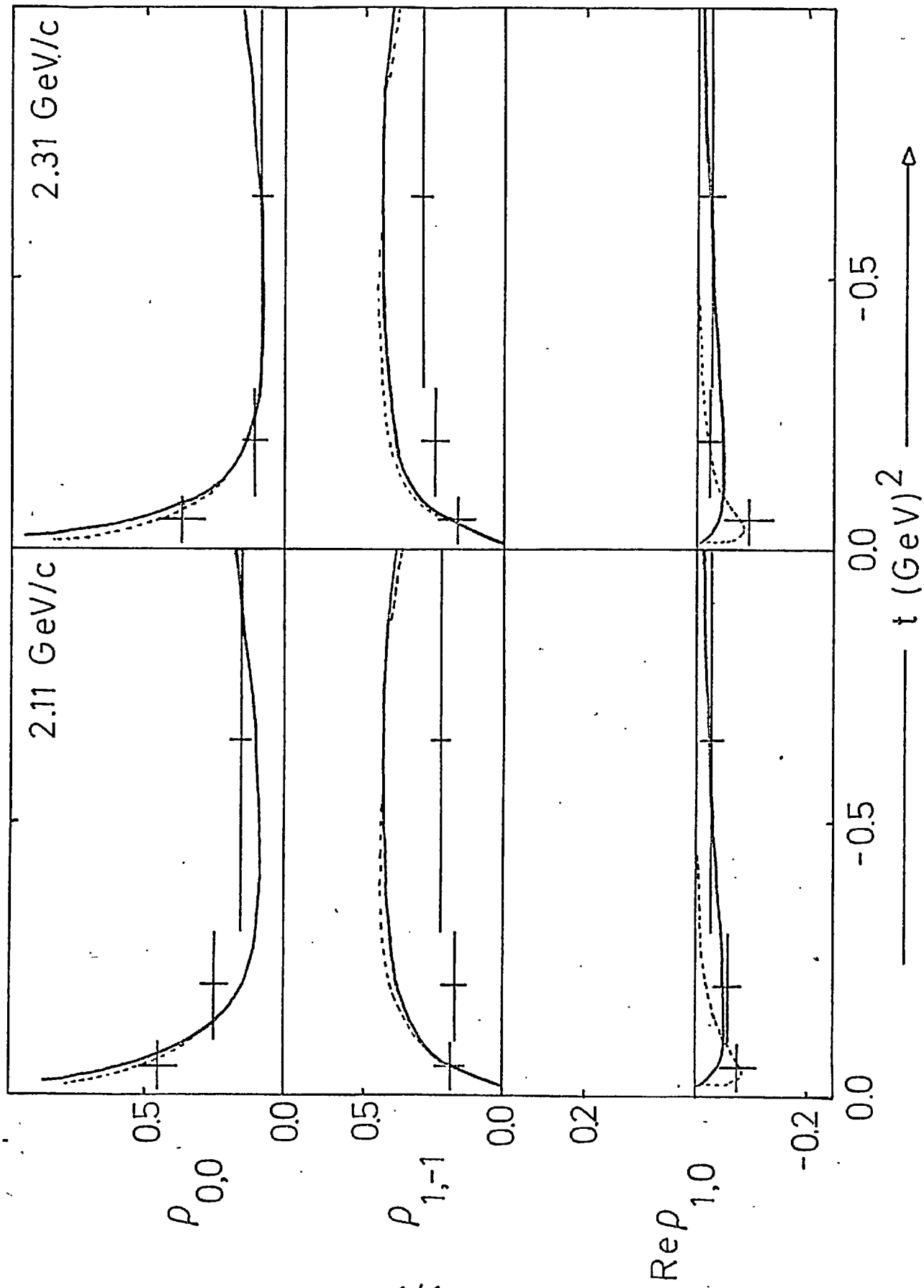

Fig 41b. Density matrix elements of $K^{*+}(892)$ as a function of momentum transfer.

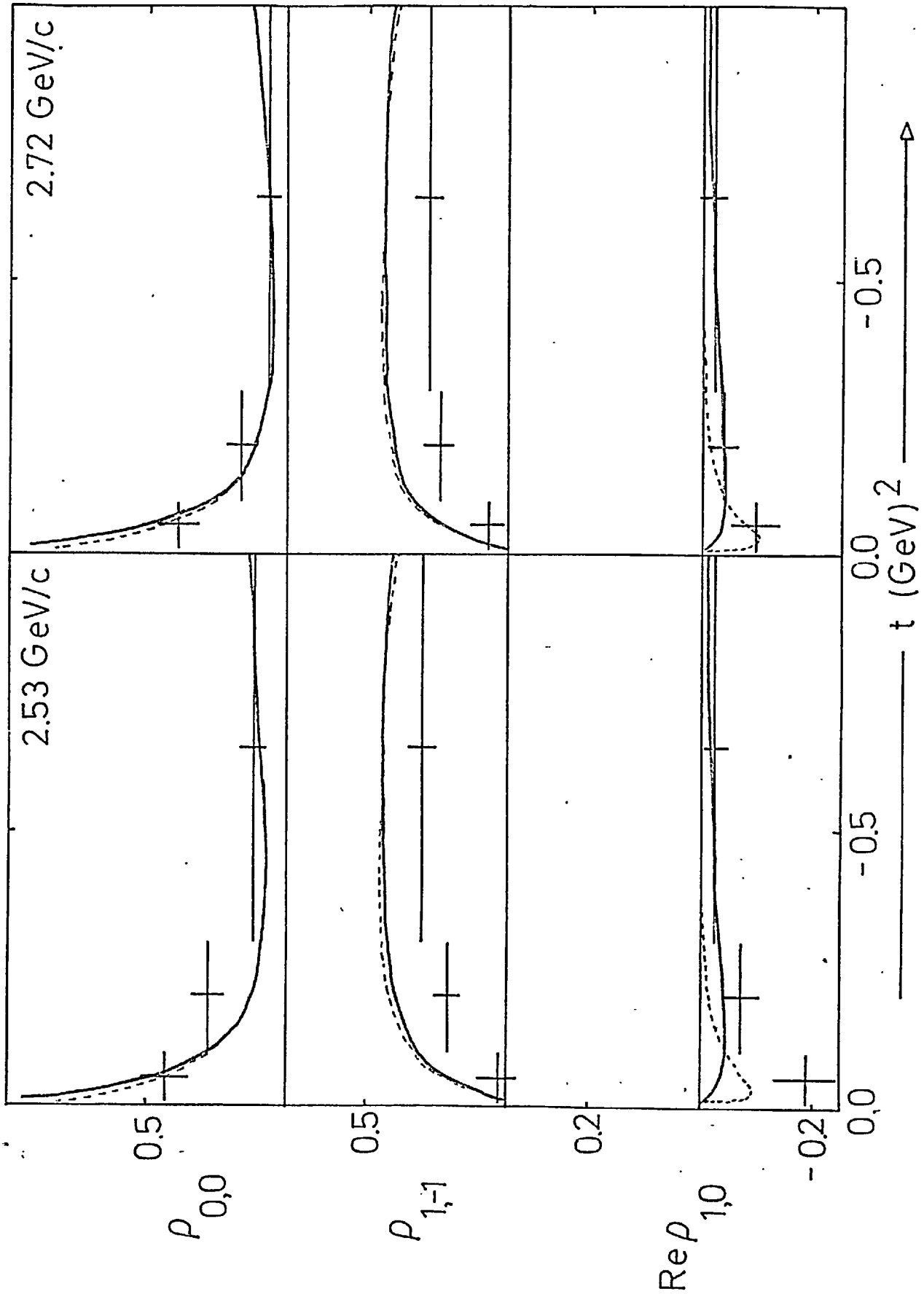

the point $\alpha(t)=0$ is a wrong signature point. The "nonsense" coupling at the pseudoscalar-vector meson vertex ($K^+ - K^{*+}$) then implies through the constraints of vertex factorisation that there would be a vanishing contribution from the amplitude at $\alpha = 0$. The experimental data displays no dips at all out to $-1(\text{GeV})^2$, so instead an even signature trajectory named P'' is adopted. The energy dependence of the reaction is too great to associate this with the P' trajectory, although later work by the same authors at higher energies suggests compatibility with significant contributions from P' and a comparatively flat ω trajectory with no cross-over zero.

The amplitudes used in the model are those of Dr. G.C. Fox who considers the asymptotic form:

$$f^t_{\lambda_2\lambda_4,\lambda_1\lambda_3} = \frac{1 + \tau e^{-i\pi\alpha(t)}}{\sin \pi\alpha(t)} \cdot e^{\frac{-i\pi}{2}(\lambda_{13}-\lambda_{24})} \cdot \gamma_{\lambda_3\lambda_1}\gamma_{\lambda_4\lambda_2}\left(\frac{s}{s_0}\right)^{\alpha(t)} \quad -(7.8$$

for exchange of a Regge pole $\alpha(t)$ with signature τ. The γ's are factorised vertex functions, containing the residue and hence functions of t.

In terms of these amplitudes the differential cross-section is then:

$$\frac{d\sigma}{dt} = \frac{\sum_\lambda \left| f^t_{\lambda_2\lambda_4,\lambda_1\lambda_3} \right|^2}{4\pi p_{12}^2 (2s_1 + 1)(2s_2 + 1)} \quad -(7.9)$$

where p_{12} is the centre of mass momentum and s_i is the spin of of particle i. The density matrix elements become, in the usual Jackson system:

$$\rho_{m,m'} = (-1)^{m-m'} \cdot \frac{\sum^{\lambda_1\lambda_2\lambda_4} f^t_{\lambda_2\lambda_4,\lambda_1 m} f^{*t}_{\lambda_2\lambda_4,\lambda_1 m'}}{\sum_\lambda \left| f^t_{\lambda_2\lambda_4,\lambda_1\lambda_3} \right|^2} \quad -(7.10$$

and it is these expressions which are evaluated in the diagrams

of cross-sections and density matrix elements presented. Throughout, the lines display simple predictions of the model at the relevant beam momenta, the original parameters for the residues etc. being fixed on a large data set extending up to 13 GeV/c.

In general, the actual differential cross-sections are rather higher and flatter than indicated and the value of $\rho_{1,-1}$ is consistently over-predicted but considering the low energies the Regge pole model has fair validity. In particular, it is worth noting that the variation of $\rho_{0,0}$ shows that although vector exchange dominates, at small t values the model indicates and the data confirms that there is a considerable non spin flip amplitude present.

This is one of the main points which makes use of the more recent Veneziano model difficult. At the present state of application it is possible to insert only one t channel trajectory between any pair of external lines. Between the incoming and exiting protons the dominant vector meson must be inserted and this then governs entirely K^* production in the limit of single Regge exchange. In turn, this then means that predicted t distributions turn, and begin to fall, as early as $t = -0.3(\text{GeV})^2$ and $\rho_{0,0}$ values are lower than found. Also, first attempts which have been made with this model using trajectory parameters from published fits give rather poor effective mass predictions, including a noticeable recurrence of the K^* (892) namely the K^* (1420).

REFERENCES

(1) I. Butterworth. Proposal No. 56 R.H.E.L.

(2) S. Goldhaber, W. Chinowsky, G. Goldhaber and T. O'Halloran. Single Pion Production by 1.96 BeV/c K^+ mesons. Phys. Rev., 142, 913, (1966). As it is of most immediate concern to this thesis references are usually directed to the principal three body analysis of an experiment. Other papers can be referenced via the reference given.

(3) F. Bomse, S. Borenstein, J. Cole, D. Gillespie, G. Luste, E. Moses, A. Pevsner and R. Zdanis. The reaction $K^+P \longrightarrow K^o\pi^+P$ at 2.26 BeV/c. Phys. Rev., 158, 1281, (1967).

(4) R. Newman, W. Chinowsky, J. Schultz, W.B. Johnson and R.R. Larsen. Inelastic K^+ proton interactions at 2.65 BeV/c. Phys. Rev., 158 , 1310, (1967).

(5) M. Ferro-Luzzi, R. George, Y. Goldschmidt-Clermont, V.P. Henri, B. Jongejans, D.W.G. Leith, G.R. Lynch, F. Muller and J.M. Perreau. The Reaction $K^+P \longrightarrow K^oP\pi^+$ at 3 GeV/c. Nuovo Cimento, 36, 1101, (1965).

(6) G. Bassompierre, Y. Goldschmidt-Clermont, A. Grant, V.P. Henri, R. Jennings, B. Jongejans, D. Linglin, F. Muller, J.-M. Perreau, R. Sekulin, W. De Baere, I. Debaisieux, P. Dufour, F. Grard, J. Heughebaert, L. Pape, P. Peeters, F. Verbeure and R. Windmolders. Search for baryonic resonances with S=+1 in K^+P production experiments. Phys. Letters 27B, 7, (1968). This is a later paper from this collaboration

containing a review of the experimental evidence for the Z^* with many references.

(7) S. Goldhaber, J.L. Brown, I. Butterworth, G. Goldhaber, A.A. Hirata, J.A. Kadyk and G.H. Trilling. Comparison of K^* production in the reactions $K^+n \rightarrow K^+\pi^-P$ and $K^+P \rightarrow K^0\pi^+P$ at 2.3 BeV/c. Phys. Rev. Letters, 15, 737, (1965).

(8) Later work, not available at this time came from the CERN-Brussels-Munich collaboration see e.g. K. Buchner, G. Dehm, G. Goebel, H. Hupe, T. Joldersma, I.S. Mittra, W. Wittek, J.M. Crispeels, J. Debaisieux, M. Delabaye, P. Dufour, F. Grard, J. Heughebaert, J. Naisse, G. Thill, A. Grant, V.P. Henri, B. Jongejans, U. Kundt, F. Muller, R.L. Sekulin and G. Wolf. Coherent K^* production in K^+d reactions at 3 GeV/c, Nuc. Phys. B9, 286, (1969).

(9) R.L. Cool, G. Giacomelli, T.F. Kycia, B.A. Leontic, K.K. Li, A. Lundby and J. Leiger. New Structure in the K^+P and K^+d total cross-sections between 0.9 and 2.4 GeV/c. Phys. Rev. Letters, 17, 102, (1966).

(10) R.J. Abrams, R.L. Cool, G. Giacomelli, T.F. Kycia, B.A. Leontic, K.K. Li and D.N. Michael. New Structures in the K^+P and K^+d total cross-sections between 1.55 and 3.30 GeV/c. Phys. Rev. Letters, 19, 259, (1967)

(11) J. Meyer, Baryonic Resonances with $S \neq o$. Heidelberg (1967) Conference Report. This is a review of evidence then available and has since been superseded.

(12) R.W. Bland, M.G. Bowler, J.L. Brown, G. Goldhaber, S. Goldhaber, V.H. Seeger and G.H. Trilling. Inelastic

processes near the T=1 K^+P peak at 1250 MeV/c. Phys. Rev. Letters, 18, 1077, (1967).

(13) A.T. Lea, B.R. Martin, and G.C. Oades. K^+P phase shift analysis. Phys. Letters, 23, 380, (1968).

(14) S. Andersson, C. Daum, F.C. Erne, J.P. Lagnaux, J.C. Sens and F. Udd. Elastic scattering of positive kaons and polarized protons at 1.22 and 2.48 GeV/c. Phys. Letters, 28B, 611, (1969).

(15) J.G. Asbury, J.D. Dowell, S. Kato, D. Lundquist, T.B. Navy, A. Yokosawa, B. Barnett, P.F.M. Koehler and P. Steinberg. Measurement of Polarization in K^+P elastic scattering at 1.37, 1.45, 1.71 and 1.89 GeV/c and phase shift analysis. Phys. Rev. Letters, 23, 194, (1969).

(16) G. Dass, C. Michael and R. Phillips. Regge Pole Models for kaon-nucleon scattering. Nuc. Phys. B9, 549, (1969).

(17) G. Dass and C. Froggatt. Regge Pole Model for vector meson production; the reaction $KN \rightarrow K^* N$. Nuc. Phys. B10, 151, (1969).

(18) A. Citron, W. Galbraith, T.F. Kycia, B.A. Leontic, R.H. Phillips, A. Rousset and P.H. Sharp. Structure in the Pion-Proton total cross-section between 2 and 7 GeV/c. Phys. Rev., 144, 1101, (1966).

(19) Berkeley Particle Data Group. "Review of Particle Properties" UCRL-8030 (August 1970).

(20) R.W. Bland. Single Pion production in the K^+P channel from 860 to 1360 MeV/c. UCRL-18131 (thesis), 1968.

(21) J.D. Jackson. Remarks on the Phenomenological

analysis of resonances. Nuovo Cimento, 34, 1644, (1964).

(22) T.A. Filippas, V.P. Henri, B. Jongejans, M. Krammer, J.M. Perreau, S. Focardi, A. Minguzzi-Ranzi, L. Monari, G. Saltini and P. Serra. Study of the reactions $K^+P \rightarrow K\pi N$ at 735 and 785 MeV/c. Nuovo Cimento, 51A, 1053, (1967). This paper also contains references to all the earlier experiments reporting the Kappa meson.

(23) A.T. Goshaw, A.R. Erwin, W.D. Walker and A. Weinberg. A search for the Kappa meson. Phys. Letters, 22, 347, (1966).

(24) P. Sallström, G. Otter and G. Ekspong. The reaction $K^+P \rightarrow KN\pi$ in all three final change states at 3 GeV/c. Nuovo Cimento, 49, 348, (1967).

(25) P.M. Dauber, P.E. Schlein, W.A. Slater, D.H. Stark and H.K. Ticho. Analysis of the $K^-P \rightarrow \Sigma^-\pi^+$ reaction from 1.7 to 2.0 GeV/c. Phys. Letters, 23, 154, (1966).

(26) F. Muller et al (Saclay). Data unpublished by private communication with J. Danysz.

(27) C.G. Wohl, F.T. Solmitz and M.L. Stevenson. Y^*'s with spin $\frac{7}{2}$. Phys. Rev. Letters, 17, 107; (1966).

(28) P. Eberhard and M. Pripstein. Technique for eliminating interference effects and biases from overlapping resonances. Phys. Rev. Letters, 10, 351, (1963).

(29) S.M. Deen. Generalised Partial Wave Analysis. RPP/H/68, (Rutherford Laboratory Preprint).

(30) P.J. Litchfield. Private Communication.

(31) Y. Goldschmidt-Clermont, V.P. Henri, B. Jongejans, A. Moisseer, F. Muller, J.M. Perreau, A. Prokes, V. Yarba, W. De Baere, J. Debaisieux, P. Dufour, F. Grard, J. Heughebaert, L. Pape, P. Peeters, F. Verbeure and R. Windmolders. Two body channels in the interaction of 3, 3.5 and 5 GeV/c positive kaons on hydrogen: possibility of Regge Pole exchange. Nuovo Cimento, 46, 539, (1966).

(32) K. Gottfried and J.D. Jackson. On the connection between production mechanism and decay of resonances at high energy. Nuovo Cimento, 33, 309, (1964). The general expression for the decay distribution for any spin may be found in this reference.

(33) L.R. Price, N. Barash-Schmidt, O. Benary, R.W. Bland, A.H. Rosenfeld and C.G. Wohl. A compilation of K^+N reactions. UCRL-20000, (1969).

(34) G. Höhler, J. Baacke and G. Eisenbeiss. The parameters of the Regge Pole model for πN charge exchange scattering. Phys. Letters, 22, 203, (1966).

(35) L. Stodolsky and J.J. Sakurai. Vector Meson Exchange Model for Isobar Production. Phys. Rev. Letters, 11, 90, (1963).

(36) W.A. Smith. K9 Beam Handbook. (1967). This document, available from R.H.E.L., contains details and operating conditions of all K9 beam line components.

(37) For details and write-ups of all CERN programs mentioned in this thesis contact in the first instance: Service d'Information Scientifique, CERN, 1211 Genève 23, Switzerland.

Further Publications:

Other papers published by the author conjointly with the Imperial College - (C.E.N.) Saclay - Collège de France - Westfield College collaboration are listed below:

1. K^+P elastic scattering in the intermediate momentum range region (2.1 to 2.7 GeV/c). Nuc. Phys. B14, 161, (1969).
2. The reaction $K^+P \rightarrow NK\pi$ in the momentum range 2.1 to 2.7 GeV/c. Report to the Lund International Conference (1969).
3. The reaction $K^+P \rightarrow NK\pi\pi$ in the momentum range 2.1 to 2.7 GeV/c. Report to the Lund International Conference (1969).

More detailed papers, based on the full data set, are expected to appear early in 1971.

ACKNOWLEDGEMENTS

The field of high energy nuclear physics has become one in which exceedingly large scale experiments are carried out over long periods of time on very expensive pieces of apparatus. As such, some would claim that the topic becomes less suitable for the subject of Ph.D. theses. Certainly the whole scale of operations makes acknowledgements a particularly difficult task.

For these reasons I hope that the individuals concerned will not object if I express general thanks to everyone from accelerator crews at the Rutherford Laboratory to the scanning, measuring and book-keeping staff at Imperial College.

I am indebted to Professor C.C. Butler for extending to me the research facilities of the physics department and to the Science Research Council and Imperial College for financial support during my stay there.

My many colleagues in the collaboration, both English and French, must be given extra thanks for help and advice, especially to Dr. D.B. Miller for proof-reading this document. Naturally, remaining errors are solely my responsibility.

I acknowledge the help of Dr. G.V. Dass for producing the predictions of the Dass and Froggatt Regge pole model at the beam momenta used in this experiment.

Last, but by no means least, many thanks to my wife Barbara for reading the illegible and typing this thesis.